springer tracts in advanced robotics 65

David Ribas
Pere Ridao
José Neira

Underwater SLAM for Structured Environments Using an Imaging Sonar

Springer

Springer Tracts in Advanced Robotics

Volume 65

Editors: Bruno Siciliano · Oussama Khatib · Frans Groen

David Ribas, Pere Ridao, and José Neira

Underwater SLAM for Structured Environments Using an Imaging Sonar

Springer

Professor Bruno Siciliano, Dipartimento di Informatica e Sistemistica, Università di Napoli Federico II, Via Claudio 21, 80125 Napoli, Italy, E-mail: siciliano@unina.it

Professor Oussama Khatib, Artificial Intelligence Laboratory, Department of Computer Science, Stanford University, Stanford, CA 94305-9010, USA, E-mail: khatib@cs.stanford.edu

Professor Frans Groen, Department of Computer Science, Universiteit van Amsterdam, Kruislaan 403, 1098 SJ Amsterdam, The Netherlands, E-mail: groen@science.uva.nl

Editors

Dr. David Ribas
Researcher
Centre d'Investigació en Robòtica Submarina,
Parc Científic i Tecnològic de
la Universitat de Girona,
Pic de Peguera (la Creueta)
17003 Girona, Spain
E-mail: dribas@eia.udg.edu

Dr. José Neira
Associate Professor
Grupo de Robótica y Tiempo Real,
Dept. Informática e Ingeniería de
Sistemas,
Centro Politécnico Superior,
Universidad de Zaragoza
50018 Zaragoza, Spain
E-mail: jneira@unizar.es

Dr. Pere Ridao
Associate Professor
Centre d'Investigació en Robòtica Submarina,
Parc Científic i Tecnològic de
la Universitat de Girona,
Pic de Peguera (la Creueta)
17003 Girona, Spain
E-mail: pere@eia.udg.edu

ISBN 978-3-642-14039-6 e-ISBN 978-3-642-14040-2

DOI 10.1007/978-3-642-14040-2

Springer Tracts in Advanced Robotics ISSN 1610-7438

Library of Congress Control Number: 2010929358

© 2010 Springer-Verlag Berlin Heidelberg

This work is subject to copyright. All rights are reserved, whether the whole or part of the material is concerned, specifically the rights of translation, reprinting, reuse of illustrations, recitation, broadcasting, reproduction on microfilm or in any other way, and storage in data banks. Duplication of this publication or parts thereof is permitted only under the provisions of the German Copyright Law of September 9, 1965, in its current version, and permission for use must always be obtained from Springer. Violations are liable for prosecution under the German Copyright Law.

The use of general descriptive names, registered names, trademarks, etc. in this publication does not imply, even in the absence of a specific statement, that such names are exempt from the relevant protective laws and regulations and therefore free for general use.

Typeset & Cover Design: Scientific Publishing Services Pvt. Ltd., Chennai, India.

Printed on acid-free paper

5 4 3 2 1 0

springer.com

Editorial Advisory Board

Oliver Brock, TU Berlin, Germany
Herman Bruyninckx, KU Leuven, Belgium
Raja Chatila, LAAS, France
Henrik Christensen, Georgia Tech, USA
Peter Corke, Queensland Univ. Technology, Australia
Paolo Dario, Scuola S. Anna Pisa, Italy
Rüdiger Dillmann, Univ. Karlsruhe, Germany
Ken Goldberg, UC Berkeley, USA
John Hollerbach, Univ. Utah, USA
Makoto Kaneko, Osaka Univ., Japan
Lydia Kavraki, Rice Univ., USA
Vijay Kumar, Univ. Pennsylvania, USA
Sukhan Lee, Sungkyunkwan Univ., Korea
Frank Park, Seoul National Univ., Korea
Tim Salcudean, Univ. British Columbia, Canada
Roland Siegwart, ETH Zurich, Switzerland
Gaurav Sukhatme, Univ. Southern California, USA
Sebastian Thrun, Stanford Univ., USA
Yangsheng Xu, Chinese Univ. Hong Kong, PRC
Shin'ichi Yuta, Tsukuba Univ., Japan

STAR (Springer Tracts in Advanced Robotics) has been promoted under the auspices of EURON (European Robotics Research Network)

For Cristina and my parents.

Foreword

Robotics is undergoing a major transformation in scope and dimension. From a largely dominant industrial focus, robotics is rapidly expanding into human environments and vigorously engaged in its new challenges. Interacting with, assisting, serving, and exploring with humans, the emerging robots will increasingly touch people and their lives.

Beyond its impact on physical robots, the body of knowledge robotics has produced is revealing a much wider range of applications reaching across diverse research areas and scientific disciplines, such as: biomechanics, haptics, neurosciences, virtual simulation, animation, surgery, and sensor networks among others. In return, the challenges of the new emerging areas are proving an abundant source of stimulation and insights for the field of robotics. It is indeed at the intersection of disciplines that the most striking advances happen.

The *Springer Tracts in Advanced Robotics (STAR)* is devoted to bringing to the research community the latest advances in the robotics field on the basis of their significance and quality. Through a wide and timely dissemination of critical research developments in robotics, our objective with this series is to promote more exchanges and collaborations among the researchers in the community and contribute to further advancements in this rapidly growing field.

The monograph written by David Ribas, Pere Ridao and Jose Neira is based on the first author's doctoral thesis under the supervision of his co-authors. Different approaches aimed at solving the localization problem for Autonomous Underwater Vehicles (AUVs) are proposed. Technology aspects concerned with the vehicle's mechanics, actuators, sensors and modes of operation are also discussed and, remarkably, all the theoretical results have been implemented and validated on real environments.

The second contribution to the series on underwater vehicles in the face of several ones devoted to SLAM, this volume constitutes a fine addition to STAR!

Naples, Italy
March 2010

Bruno Siciliano
STAR Editor

Preface

This book is a revised version of the doctoral dissertation presented by D. Ribas of the Department of Computer Engineering at the University of Girona. The main purpose of this work is to present different techniques developed with the objective of providing a solution to the localization problem for Autonomous Underwater Vehicles (AUVs) operating in structured environments. It describes different methods for map based localization as well as a novel approach for Simultaneous Localization And Mapping (SLAM) which may be relevant for researchers and students in the field of underwater robotics. This work is structured in seven chapters. Chapter 1, which presents the goals and objectives of the thesis, is followed by three introductory chapters. Chapter 2 reviews the state of the art in SLAM focusing on those approaches developed for underwater environments, and Chapters 3 and 4 introduce the underwater vehicle and the sonar used throughout the elaboration of this work. The main contributions of this thesis are developed in Chapters 5 and 6, which progressively introduce different approaches for map based localization leading to the development of a full SLAM solution. All the techniques presented here are endorsed with results from real environments. Finally, Chapter 7 concludes the work by summarizing the contributions and describing possible future research.

Girona, Spain, David Ribas
December 2008 Author

Acknowledgements

I would like to express my gratitude to the people who have supported me during the elaboration of this PhD thesis. First and foremost to my two advisors, Pere Ridao and José Neira, for encouraging me and for giving me innumerable helpful comments and suggestions during this research. I also thank the members of the Underwater Robotics Lab for their camaraderie and willingness to help whenever necessary. For similar reasons my gratitude also extends to the other members of the Computer Vision and Robotics Group and of the department of Computer Engineering at the University of Girona, and to the Robotics and Real Time Group at the University of Zaragoza. I cannot finish these acknowledgements without mentioning my beloved parents, family and friends and the most important person in my life, Cristina, who with her love and encouragement has been my principal support during these years.

Contents

Acronyms

AUV	Autonomous Underwater Vehicle
CIRS	Centre d'Investigació en Robòtica Submarina
CML	Concurrent Mapping and Localization
CPE-SLAM	Constant Pose Estimation SLAM
CSS	Co-operating Statistical Snake
CTS	Constant Time SLAM
DCRO	Deferred Reference Counting Octree
DGPS	Differential Global Positioning System
DOF	Degree Of Freedom
DSM	Decoupled Stochastic Mapping
DVL	Doppler Velocity Log
EIF	Extended Information Filter
EKF	Extended Kalman Filter
FOG	Fiber Optic Gyro
GESMA	Groupe d'Etudes Sous-Marines de l'Atlantique
GPF	Geometrical Projection Filter
GPS	Global Positioning System
HRA	High Resolution Array
IC	Individual Compatibility
INS	Inertial Navigation System
JC	Joint Compatibility
LS	Least Squares
MRF	Markov Random Field
MRU	Motion Reference Unit
MSIS	Mechanical scanning imaging sonar
NN	Nearest Neighbor
NUWC	Naval Undersea Warfare Center
RLG	Ring Laser Gyro
RANSAC	RANdom SAmple Consensus
ROV	Remotely Operated Vehicle
RTS	Rauch-Tung-Striebel

SAS	Synthetic Aperture Sonar
SAUC-E	Student Autonomous Underwater Challenge - Europe
SBL	Short Base Line
SLAM	Simultaneous Localization And Mapping
TMS	Tether Management System
USBL	Ultra Short Baseline
UUV	Unmanned Underwater Vehicle

Chapter 1
Introduction

More than 70% of the earth's surface is covered by water. Oceans and seas host an incredibly rich biodiversity, influence short and long term climate and have a high impact not only on the economy, but on the life and evolution of human society as a whole. Exploring this large body of water is a matter of the utmost importance, not only because it represents a vast source of natural resources, but also because its study may help us understand how this complex ecosystem works.

Remotely Operated Vehicles (ROVs) are among the best tools used to undertake this mission, making possible the exploration of the deepest regions while avoiding risk to human lives. The first ROVs were developed in the 1960s to perform rescue and recovery operations. The technology, however, was soon extended to other uses. Many applications of ROV technology can be found in the oil and gas industries, where it is not uncommon to find tasks exceeding the reach of human divers. In fact, ROVs have become an essential tool without which the exploitation of offshore oil fields would not have been possible. Their missions range from the surveying of operation areas to the deployment, inspection and maintenance of undersea structures such as oil rigs or pipelines [60]. These vehicles have also played an important role in the scientific community, enabling the ocean to be studied in many different ways. Now the sea floor can be mapped with bathymetric sensors while image mosaicking techniques make the generation of large visual maps possible [38]. Moreover, zones of geological or biological interest can be explored and sampled, from oceanic ridges to the deepest trenches. Archeologists and historians now have access to sunken remains and shipwrecks [35]. ROVs can also be found in military missions, cleaning the path of ships in mine hunting operations or assisting in inspection or salvage tasks.

Missions involving the use of ROVs are complex. These vehicles are generally linked to a ship on the surface by means of an umbilical cable or *tether* which provides power and communications. In this way, operators on the ship can control the vehicle and receive feedback from the onboard sensors. Although this link enables ROVs to be operated over a long time period, the infrastructure requirements are high as are the costs. Campaigns may take place far from the coast, involving a ship of considerable dimensions with its corresponding crew and specialized ROV operators for many weeks. Furthermore, the ship has to be equipped with a crane for the

D. Ribas et al.: Underwater SLAM for Structured Environments, STAR 65, pp. 1–6.
springerlink.com © Springer-Verlag Berlin Heidelberg 2010

deployment and recovery operation, as well as with other elements including sufficient tether for the desired operational depth and even a Tether Management System (TMS) for those operations at greater depths.

In recent years, efforts have been made to provide these vehicles with a greater degree of autonomy. The objective is to remove the link with the surface ship to expand the vehicle's capabilities and, at the same time, reduce the operational costs. This is achieved by equipping the submersible with its own power source, generally batteries, and giving it the capacity to determine its actions based on inputs from its own sensors and a pre-defined mission plan. The result of this research is the so called Autonomous Underwater Vehicles (AUVs) which nowadays have already succeeded in performing different types of tasks, in particular those related with the collection of sensor data or the production of detailed maps of portions of the seafloor [103]. There are also a few designs for AUVs capable of performing undersea intervention operations. However, this research is still in its early stage and these vehicles cannot be considered as operational.

The development of AUVs has offered numerous advantages but has also presented new challenges. One of the most significant examples is the problem of underwater navigation or, in other words, how to determine the vehicle's position within the environment so it can take the correct actions to successfully accomplish the mission. Traditionally, the problem has been addressed in various ways, none of which are totally adequate. The positional error growth associated with dead reckoning based on Inertial Navigation Systems (INS) and/or Doppler Velocity Logs (DVL) make their use impractical for long term navigation [67, 99]. In order to avoid this problem, data from a Global Positioning System (GPS) receiver can be used to provide navigation resets but, due to the null coverage in underwater environments, this can only be done when on the surface. Alternatively, artificial beacons may be employed for long term underwater positioning. Many configurations are available for these beacon systems, such as Long Base Line (LBL), Short Base Line (SBL) or Ultra Short Baseline (USBL) (see Figure 1.1) [54, 56, 86]. Unfortunately, there are numerous missions in which these solutions are unfeasible. The need for prior beacon deployment, the high cost and the constraints in the working volume of the AUV are the principal disadvantages. However, there are other ways to achieve localization of an AUV without the need of external hardware. Map matching techniques use information from onboard sensors to provide ground-fixed, feature-relative localization given an *a priori* map of the environment [79]. Variants of the method can be found for gravitational anomaly and magnetic field maps [84, 127]. Even so, its main drawback is that an up-to-date map of sufficient resolution will not be available for many operating areas. So, again, a self-contained system would be preferable , with no need for previous knowledge of the terrain or external devices to obtain a reliable localization of the vehicle.

Simultaneous Mapping and Localization (SLAM), a research topic which has attracted a great deal of attention in the research community for almost two decades, may be the solution to the navigation problem. This is a method by which autonomous vehicles can build a map within an unknown environment while keeping track of their current position. This process is carried out using only the vehicle's

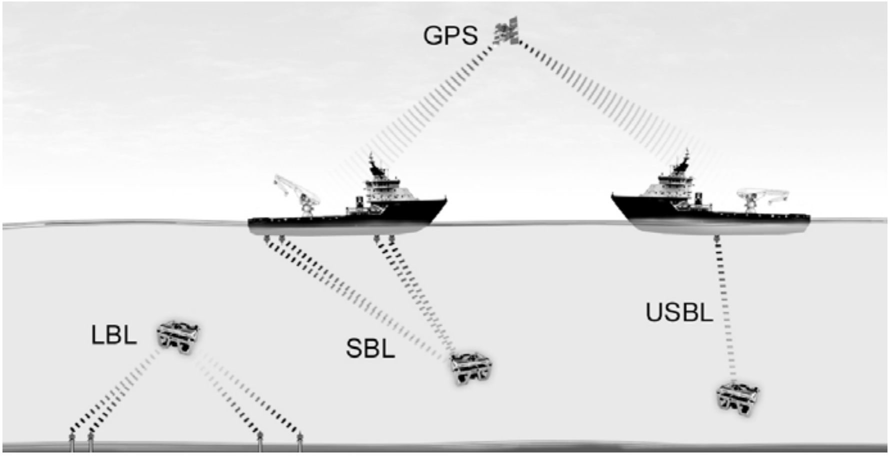

Fig. 1.1 Typical configurations for AUV localization using LBL, SBL and USBL.

sensors for the perception of the surrounding environment and/or its own state and hence can be considered as a self-contained system. This thesis is concerned with the application of SLAM techniques to the field of autonomous underwater navigation. Next, some background on motivation and applicability will be provided, as well as a description of the outline and objectives of the thesis .

1.1 Antecedents

The research presented in this thesis has been carried out in the Underwater Robotics Laboratory of the Computer Vision and Robotics Group of the University of Girona. This group has been doing research in underwater robotics since 1992. The main contribution over the past few years is the development of three Unmanned Underwater Vehicles (UUV). The first prototype, called GARBI, was developed in collaboration with the Polytechnic University of Catalonia. This vehicle was initially conceived as a ROV, but after successive modifications over the years, the vehicle evolved into its final configuration as an AUV in 2005. The second prototype, URIS (1999), was fully developed at the University of Girona and was designed as an small AUV for testing in laboratory conditions. The most recent vehicle is the Ictineu (2006), an AUV which brings together the broad sensorial capabilities of the GARBI and the small form factor of the URIS, which make this vehicle a perfect research platform for testing in both laboratory and real application environments.

The research efforts in the Underwater Robotics Laboratory have been oriented to the development of the diverse disciplines related with the operation of autonomous vehicles. An example can be found in the work done in control architectures, which has led to the creation of the O^2CA^2 control architecture [15], but also in the recent advances that we have made towards a control mission system [13]. Parallel work has also been done in the identification of the dynamic/kinematic models of the vehicles [112] which has made the development of research tools such as the Neptune simulator possible [111]. With respect to the application domain, preliminary work was carried out on the use of ROV technology for inspection of hydroelectric dams using image mosaics [5]. Later, the topic was readdressed using AUVs in the context of a research project supported by the Spanish commission MYCT, made in collaboration with the University of the Balearic Islands and the Polytechnic University of Catalonia. The objective of the project was to develop the capacity of AUVs for their use in industrial applications such as the inspection of hydroelectric dams, harbours and underwater cables and pipes.

The achievements in these research lines and application domains have resulted in an increase in the capabilities of our vehicles as well as further demands in terms of navigation requirements. The work done during the elaboration of this thesis has contributed to the beginning of a new research line whose objective is to improve the navigation capabilities of our vehicles. Our knowledge of this new topic has been complemented by collaboration with the Robotics and Real Time Group of the University of Zaragoza. This group has long experience in sensor perception and navigation systems and has been a referent in SLAM research since its origins, having made numerous relevant contributions to the field. One consequence of this relationship has been the co-tutoring of this thesis.

1.2 Goal of the Thesis

As mentioned in the antecedents, the goal of this thesis is the study and development of navigation systems for AUVs, with special attention to the application of SLAM techniques as a self-contained system which requires neither previous knowledge of the scenario nor the use of absolute positioning systems such as GPS, LBL or USBL. Moreover, and consistent with the application domains presented, the system is designed for use in structured environments found in many industrial scenarios, specifically those containing manmade structures in the form of rectilinear walls as, for example, in harbours, breakwaters, marinas, canal systems, etc. Although most previous work done in this field has focused on open sea and coastal applications, obtaining an accurate positioning in other scenarios would notably increase AUV capabilities. For instance, an AUV could use a harbour as an outpost for oceanography research if it is able to localize itself and navigate with sufficient accuracy to safely perform the leaving and returning operations [49]. Maintenance and inspection of underwater structures [65, 83] and even surveillance of marine installations are examples of other applications that can benefit from such a system.

Focusing on such scenarios will offer several advantages. For instance, one of the most critical issues when operating in underwater environments is the shortage of reliable landmarks to use in the map. Although the quantity of landmarks will depend on each application scenario, walls usually produce strong sonar returns which are much more constant and reliable than natural targets. Moreover, walls are usually vertical structures and therefore a planar map will be sufficient in most cases.

1.2.1 Objectives

After reviewing the research antecedents and describing the problem, the goal of this thesis is stated. The general purpose is summarized as:

> *"The development of a SLAM approach for an AUV to achieve localization in man-made structured underwater environments using a mechanically scanned imaging sonar as principal sensor"*

The term "man-made structured environment" should be understood as an environment containing artificial, previously existing structures characteristic of the scenarios for the applications at hand and where no additional elements have been introduced to serve as landmarks for the SLAM framework. This goal was selected in order to start a new research line on autonomous navigation, but also as the next logical step given the antecedents of the group and the research projects in which it is involved. Moreover, SLAM is one of the most active topics in robotics research and, although a large number of works have already been presented, there are still very few approaches applied to the field of underwater robotics. The application of SLAM algorithms in AUVs was certainly the most important purpose of this dissertation. For this reason, it was a priority to perform the experimentation with real data from a robot in the objective scenario as a premise to demonstrate the research advances achieved.

The goal of this thesis can be divided into the following more specific objectives:

Underwater localization with an *a priori* map. Exploring and designing different approaches to perform underwater localization for an AUV equipped with mechanically scanned imaging sonar operating in a structured scenario whose map is previously known. The interest in this topic is focused on exploring the use of Kalman filters and data association algorithms for underwater localization.

Feature extraction. Development of a feature extraction method capable of dealing with the particular complexities of a mechanically scanned sonar. This method should be able to detect the presence of walls in the environment as line features in the acoustic data, as well as to estimate the uncertainty of this observation. The detection of the features will rely on the use of a robust data association algorithm, while the estimate of the observed feature will be based on the imprint left by the landmark in the acoustic data.

Underwater SLAM. Developing a SLAM framework based on the stochastic map approach [115] using the above-mentioned feature extraction method and the experience gained during the development of the localization techniques. The purpose of this SLAM system is to localize a vehicle within a structured environment typical in previously commented applications.

Experimentation with an AUV. Evaluation of the proposed localization and SLAM systems with real experiments using an AUV. The feasibility and limitations of these approaches must be experimentally tested with the available systems and resources.

1.3 Outline of the Thesis

The contents of this thesis can be divided into three parts. The first part overviews the SLAM problem (Chapter 2), paying special attention to its application in underwater environments; introduces the Ictineu AUV (Chapter 3), a research vehicle developed during the elaboration of this thesis; and describes the operating principles of a mechanically scanned imaging sonar as well as the issues related with their application to the problem (Chapter 4). The second part presents three different localization algorithms (Chapter 5) as an introduction to some of the techniques and solutions employed later in the proposed SLAM algorithm (Chapter 6). Experimental results endorse the different proposals. Finally, the last part of the document summarizes the contributions and comments on further work (Chapter 7). A brief description of each chapter is presented below.

Chapter 2: *State of the Art.* This chapter presents the field of "Simultaneous Localization and Mapping", relates the history and development of the problem and overviews the most remarkable works performed on underwater environments. A discussion and the aims of this work can be found at the end of the chapter.

Chapter 3: *The Ictineu Autonomous Underwater Vehicle.* This chapter introduces the Ictineu AUV, the research platform developed during the elaboration of this thesis which was used to test the proposed SLAM framework. The main features of the vehicle are described, including many mechanical aspects, the equipped sensors and its software architecture.

Chaper 4: *Understanding Mechanically Scanned Imaging Sonars.* This chapter describes the basic operating principles of the sonar sensor which was chosen to perform SLAM. Some hints are provided about the interpretation of sonar images. Moreover, many issues that need to be addressed before using the sensor are identified.

Chapter 5: *Localization with an a priori Map.* This chapter describes three different approaches for localization with previous knowledge of the scenario. This chapter should be understood as an exploration of some of the techniques that will then be developed in the SLAM approach. Experimental results are included for each of the methods presented.

Chapter 6: *Simultaneous Localization and Mapping.* This chapter proposes a SLAM algorithm for AUVs equipped with a mechanically scanned imaging sonar operating in manmade environments. Details are provided about a novel method for extracting line features and their uncertainty from acoustic images as well as about the implemented Kalman filter framework. At the end of the chapter, experimental results including a SLAM executed with real data obtained in an application scenario with the Ictineu AUV are presented.

Chapter 7: *Conclusion.* This chapter concludes the thesis by summarizing the work and points out contributions and future work. It also comments on the research evolution and the publications accomplished during this research project.

Appendices: These chapters incorporate additional information on some of the topics introduced in the thesis.

Chapter 2
State of the Art

2.1 The SLAM Problem

Simultaneous Localization and Mapping (SLAM), also referred to as Concurrent Mapping and Localization (CML), is a fundamental problem in mobile robotics that has been the focus of substantial amount of research work in recent years [30, 2]. The objective of SLAM is to make it possible for a moving robot starting at an unknown location without previous knowledge of the environment to build a map using its onboard sensors while, at the same time, using this same map to compute the robot's location. Although performing these two tasks simultaneously may seem complex, the essentials behind SLAM are indeed quite simple. Figure 2.1 illustrates the basics of the process. A moving vehicle will inherently accumulate errors in its position estimate as a consequence of the noise introduced in the dead-reckoning and/or the inaccuracies in the use of a prediction model. Moreover, errors will also affect the map building process. The sensor that perceives the environment is mounted in the vehicle and therefore its position uncertainty will be incorporated when new information is added to the map. As a result, the vehicle will eventually get lost and the map will become unusable (Figure 2.1(a)). A system performing SLAM, however, is able to attenuate and even contain this uncertainty growth by means of the reiterated observation of the elements stored in the map. Figure 2.1(b) represents the situation where a new measurement from the robot is likely to correspond to an entity already incorporated in the map. Then, a data association process should be carried out to determine the correct matching. When this process is positive, this information is used to update the estimates of both the vehicle's position and the map. Adding more information results in a better estimate and hence a reduction of the uncertainty in the problem (Figure 2.1(c)).

2.2 History

In the 1980s and early 1990s, navigation and mapping were treated as separate problems. The work done in the field of mapping was broadly divided into topological

D. Ribas et al.: Underwater SLAM for Structured Environments, STAR 65, pp. 7–21.
springerlink.com © Springer-Verlag Berlin Heidelberg 2010

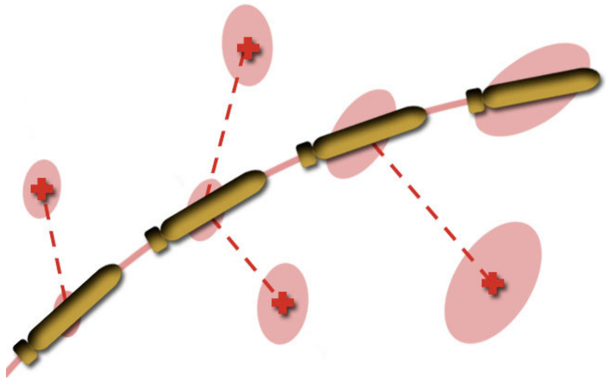

(a) Uncertainty growth in the map landmarks and vehicle locations.

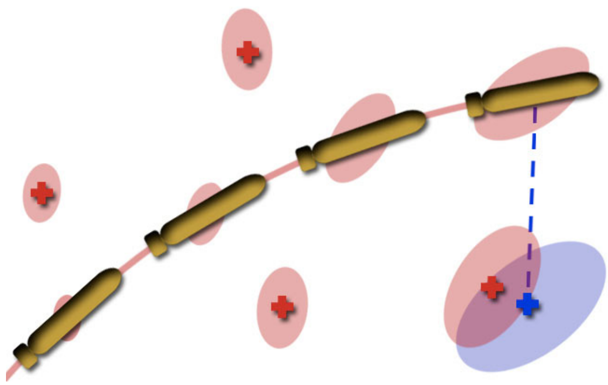

(b) The new measurement (blue) is a re-observation of a landmark in the map.

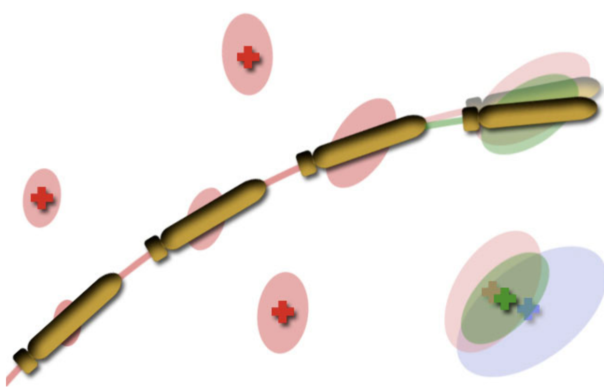

(c) Incorporating the new information results in a better estimate (green) of both map and vehicle positions.

Fig. 2.1 The SLAM problem.

[66, 20] and metric approaches, using either occupancy grids [32, 88] or a geometric description of the environment [19]. On the other hand, the work done on localization explored map/scan matching techniques [77, 22] and the use of geometrical landmarks in Kalman filters [69]. The success in these research strands created the proper environment for the birth and development of the SLAM problem. According to Durrant-Whyte and Bailey [30], its origins can be dated back to 1986 when many discussions about the application of estimation theories to mapping and localization problems took place during the IEEE Robotics and Automation Conference held in San Francisco, California. Over the subsequent few years, the seminal works by Smith and Cheeseman [116] and Durrant-Whyte [29] were presented, setting the statistical basis for the description of spatial relationships between landmarks and the manipulation of geometric uncertainty. It was not, however, until some years later that the developments in this new research line culminated in the publication of the notable paper by Smith et al. [115]. This paper showed that a consistent full solution of the SLAM problem would require a joint state containing the position of the vehicle and the features in the map to represent all the correlations that appear as a consequence of vehicle error which is common to all the relative landmark measurements obtained during the creation of the map. This implies that a map containing a large number of landmarks would require a huge state vector and hence a considerable computational cost to perform the estimation. This work, however, did not analyze the convergence properties of the problem. In fact, at the time, it was generally assumed that the map errors would not converge but would grow without bound. These two reasons, the computational complexity and the lack of knowledge about convergence, caused SLAM research to come to a standstill and, as a result, efforts were again focused on dealing with mapping and localization as separate problems.

It was not until the later 1990s when the convergence properties where finally elucidated [31, 23]. The correlations between landmark estimates increase monotonically with the number of observations made, which means that the knowledge of their relative positions improves and never diverges and, hence, a better map is obtained regardless of the vehicle's errors [26]. This breakthrough revived interest in the SLAM problem. In fact, over the last decade this field has experienced a substantial expansion and researchers have focused on many different lines of research from dealing with computational complexity [52, 72] to data association techniques [90]. Different solutions to the probabilistic SLAM problem have also been proposed as alternatives to the traditional implementations of the stochastic map with extended Kalman filters (EKF) [125]. Some other efficient strategies using Gaussian uncertainty models include postponement [64], decoupled stochastic mapping [71], the compressed filter [52], sequential map joining [117] and the constrained local submap filter [131]. Alternatively, other implementations such as Information Filters and particularly, its non-linear version, the extended information filter (EIF), have been used recently in order to reduce the computational cost [126]. Like the EKF, the EIF represents the uncertainty with a Gaussian. However, its main difference is the use of an alternative parametric representation to characterize the belief, which leads to slightly different equations and approximately sparse matrices that offer better computational efficiency. In spite of their popularity, the convergence of systems modeled under a Gaussianity assumption have only been demonstrated for the linear case, while non-linear systems have been shown to be inconsistent as a consequence of linearization errors [17].

The issues related with the representation of non-Gaussian probability distributions have been addressed with the use of particle filters [124, 87]. This technique uses a finite number of sample states drawn from the estimate, called particles, to represent the uncertainty distribution. The greater the number of particles, the better the description of the uncertainty. Luckily, the number of particles can be adapted to the suspected complexity of the estimate in order to obtain computationally efficient algorithms. The FastSLAM, introduced in [87], is one of the most remarkable implementations of this typology of probabilistic filters. In contrast to feature based techniques, the Constant Pose Estimation (CPE) SLAM [77, 53] is a method that makes use of dense sensor data, maintaining a network of local constraints between the robot's positions and producing the map through optimization. Its main advantage is that such a representation scales well with the map area because it generally represents only the local constraints. In parallel to the evolution of the probabilistic methodologies, the domains of application have also experienced a significant expansion. They have not been limited to dealing only with indoor environments of increasing complexity [16, 92, 6, 25]. SLAM systems have also been successfully deployed to work in challenging outdoor scenarios [52, 21], in the air [62] and even at sea [94, 132, 123]. These achievements evidence how intensive research has led to the definition and understanding of the main working principles of the SLAM problem. However, although it can be considered solved for small/medium environments, there are still some open issues. The optimization of computational burdens, consistency, data association, the definition of better map representations or the deployment of SLAM systems in new and challenging application domains are examples of problems that will probably be intensively studied in the near future.

2.3 The Use of Sonars for SLAM

Even though laser scanners are expensive, they are probably one of the most popular sensorial choices in either indoor or outdoor applications [124, 92]. This is mainly because they provide high quality dense data with good angular precision. Another popular alternative is the use of one or more cameras to obtain visual information (e.g. color, shape or texture) from the environment [25, 41, 21]. On the other hand, acoustic sensors have usually been considered one of the cheapest but less reliable sensorial options for performing SLAM. Even when operating in highly structured environments, sonars produce measurements with poor angular resolution and ghost returns appear as a result of specular reflections [70]. Many remarkable works have dealt with these limitations. For instance, in [74, 75], the indetermination in bearing measurements from an air sonar were addressed by using batches of range-only data acquired from multiple vantage points. The work presented in [117] went even further with the implementation of a voting procedure which made it possible to discriminate different types of features and reject spurious measurements. Works like these demonstrate that, despite their poor precision, air sonars can be used in SLAM, but the fact is that there are still few examples of air sonar systems performing SLAM in large areas. In underwater environments, however, the situation is the opposite. Laser based sensors are impractical because of the attenuation and dispersion of the light in water, while, for similar reasons the use of cameras is limited to applications where the vehicle navigates in clear water and very near to the seafloor. This leaves acoustic devices as one of the best options for underwater sensing. The excellent propagation of sound in water makes it possible for an acoustic wave to travel many thousands of meters without the signal losing significant energy. So it is not unusual to find sonars capable of measuring at long ranges even in turbid water conditions. Generally, the sonars equipping underwater vehicles are devices technologically more advanced than those equipping their indoor/outdoor counterparts. Sophisticated designs of the transducer heads and the use of beam forming techniques enable narrow beams to be obtained which can produce really precise bearing measurements. Moreover, in contrast with the confined spaces found in indoor applications, the open spaces in underwater scenarios usually produce more reliable data. Active sonars (i.e. sonars which can both transmit an acoustic signal and receive its reflected echo) are the most appropiate for SLAM because of their capacity to extract information from the environment. They can be classified into two categories depending on whether they produce only a set of range and bearing measurements or an acoustic image of the scene. Among those in the first category, the most commonly used are (Figure 2.2):

Echo sounder: This is one of the simplest and least expensive systems for measuring range. The echo sounder operates by emitting a pulse from its transducer. When this pulse reflects off a surface, it returns to the sensor head and the time of flight can be measured and therefore the distance estimated. These kinds of devices are usually mounted in a down-looking position to find the altitude of the vehicle with respect to the seabed.

Mechanically scanned profiler: This sensor is composed of a mechanically actuated transducer which can be sequentially oriented at different angles and produces a series of range measurements. Usually, the size of the scan sector can be selected from a few degrees to a complete 360° scan around the sensor, which is particularly interesting for obstacle detection tasks. When mounted in a down-looking position, they can also be employed to collect bathymetric data.

Multibeam echo sounder: This sensor is specifically designed to produce bathymetric maps of large areas of the seabed. It is composed of an array of hydrophones which can emit fan shaped beams towards the bottom and measure the range of a strip of points placed perpendicularly to the direction of the vehicle movement. These measurements can be produced at a high rate and resolution.

The sonars in the second category are capable of measuring the returning echo intensity values from particular places within the insonified area. These measurements can then be recomposed into an acoustic representation of the environment generally referred to as an acoustic image. The most common types of imaging sonars are (Figure 2.3):

Mechanically scanned imaging sonar: Similar to the mechanically scanned profiler, this device also has an actuated rotatory transducer which can emit fan-shaped beams at different orientations. It is usually placed in a vertical position so it can perform the scanning on the horizontal plane. These devices generally have a configurable scan sector and it is not unusual to find models which can perform full 360° scans, making them perfect for detecting objects around the vehicle. The main drawback is the slow refresh rate. The operation of this type of sonar has been of major importance during the elaboration of this thesis. A further description of mechanically scanned imaging sonars can be found in Chapter 4.

Electronically scanned imaging sonar: Also known as *multibeam imaging sonar* and *forward-looking imaging sonar*, this sonar is equipped with an array of hydrophones which allows, with the emission of a single pulse, the production of a complete acoustic image of the insonified area. This area is usually limited to a small sector in front of the sensor, but can be scanned at very high rates. Its main drawback is the cost which can be around ten times the price of a mechanically scanned unit.

Sidescan sonar: This sonar is designed for imaging large seabed areas. Its mode of operation is analogous to that of multibeam echo sounders, but oriented to imaging tasks. While the sonar is moved along a survey path (either mounted on a vehicle or towed by a ship), it emits fan shaped pulses down toward the seabed across a wide angle perpendicular to the direction of the movement, producing a strip of echo intensity measurements.

2.4 Underwater SLAM

This section presents an overview of the most relevant contributions to the application of SLAM techniques in underwater environments. This overview does not seek to be an exhaustive enumeration of all the publications in the field but will serve to identify the main protagonists, their approaches and, particularly, those projects involving the implementation of SLAM systems in realistic operating conditions. Later in this chapter, Table 2.1 provides a summary of the different aspects of the works discussed.

The first implementations of SLAM frameworks using real sensor data can be dated to the late 1990s. In September 1997, a test rig mounted on the side of a converted U.S. navy freighter was used to acquire a data set as part of a collaborative project between the Naval Undersea Warfare Center (NUWC) and the Groupe d'Etudes Sous-Marines de l'Atlantique (GESMA). The test rig was equipped with a complete sensor suite which included a custom developed sonar, the High Resolution Array (HRA) forward looking imaging sonar, as well as other typical AUV systems such as an INS, a DVL, a Differential GPS (DGPS) receiver and a sidescan sonar. The acquired data set was later used to test two SLAM approaches. The first one [11] presented a simplified EKF implementation in which independent filters

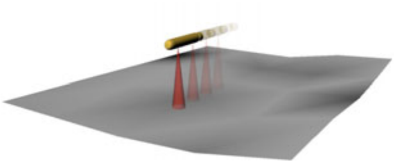

(a) Echo sounder.

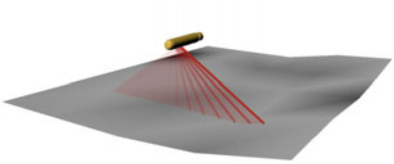

(b) Mechanically scanned profiler.

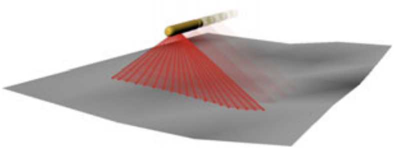

(c) Multibeam echo sounder.

Fig. 2.2 Range sonar typology.

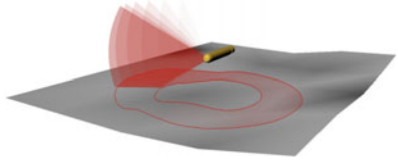

(a) Mechanically scanned imaging sonar.

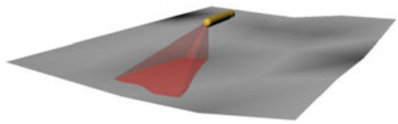

(b) Electronically scanned imaging sonar.

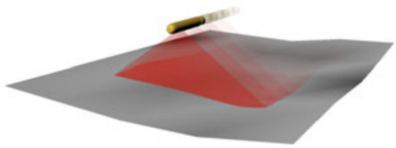

(c) Sidescan sonar.

Fig. 2.3 Image sonar typology.

were initialized with every new landmark extracted from the HRA acoustic images. The state vector of each of these filters contains the estimate of the vehicle and the corresponding landmark. Although an improved vehicle estimate can be periodically obtained by fusing the estimates from all the independent filters, the landmark estimates remain decoupled and hence the correlations are ignored. A key aspect of this work is the procedure to obtain the landmarks. First, the acoustic image is segmented to extract the different objects. Then, a set of characteristics (perimeter, area, area-to-perimeter ratio and radial signature) is obtained for each object to produce a description that, in conjunction with a pre-defined similarity metric, makes the data association process possible. In the results section, the estimated trajectories were represented together with the DGPS measurements as ground truth. There were, however, no uncertainty bounds represented. The second work using this same data set was made in collaboration with MIT researchers [68]. They presented an EKF based framework which produced a full stochastic map and hence correlations were taken into account. In this approach, the measurements from the dead-reckoning sensors were included in the process to improve the quality of the estimation. Moreover, point landmarks corresponding to the centroids of the objects were extracted from the acoustic data and used to build the map. The data association process was carried out by applying a Nearest Neighbor (NN) gating among compatible landmarks. Unlike the previously presented work, the error plots were represented within uncertainty bounds, demonstrating the correct operation of the system. Among these introductory works, it is also worth mentioning [71], where the Decoupled Stochastic Mapping (DSM), a computationally efficient approximation to large-scale SLAM, was presented. This proposal reduces the computational burden by dividing the environment into multiple overlapping submap regions, each with its own stochastic map. To assess the performance of the approach, experiments were carried out in simulation, but also with real data obtained in a water tank using a mechanically scanned sonar mounted on a robotic positioning system.

During the same period in which these works were carried out, the first steps towards underwater SLAM were also taken at the University of Sydney. This time, the chosen test platform was Oberon, a small research underwater vehicle equipped with a Tritech SeaKing mechanically scanned imaging sonar as its principal sensor for the perception of map features. Initial experiments took place in a swimming pool with many artificial landmarks placed at known positions [93]. Again, point features were selected to represent the observation of these objects in the resulting map. This setup provided the means to test a SLAM framework called the Geometrical Projection Filter or GPF, an approach which estimates the relationships between individual landmarks rather than estimating the location of landmarks in global coordinates. Later, new experiments took place in real natural terrain along the coast of Sydney, Australia [132].This time, a classical EKF implementation of the stochastic map was the core of the SLAM system. Once more, artificial landmarks were deployed in the area to produce a set of reliable point features and although a few natural landmarks were detected, many of them were found too unstable to be incorporated into the map.

A third focus of research on underwater SLAM appeared soon afterwards at Heriot-Watt University [121, 118]. Following the path opened by [11], part of the efforts in this case revolved around the study and development of techniques to characterize the landmarks from acoustic images. In addition to the point coordinates, a vector of landmark characteristics (including size, perimeter, compactness, maximum dimension, centroid and invariant moments) was introduced to improve the data association process [118]. To validate the proposal, experiments were carried out in three distinct environments. First, a data set was obtained in a water tank at the Ocean System Laboratory with a Tritech SeaKing sonar mounted on a planar Cartesian robot using two cylinders as targets. Second, a Seabat 6012 multibeam imaging sonar carried by two divers was operated among the legs of a pier at the Northern Lighthouse Board in Oban, Scotland. And third, a data set was acquired during an open sea trial with a concept electronically scanned sonar mounted on the Ocean Explorer AUV from the Florida Atlantic University. These experiments demonstrated that landmark descriptors are especially useful with real non-artificial data, but that they are much less reliable in situations where landmarks have similar descriptors (e.g. the pier legs). It is worth noting that in this work, SLAM was performed using only an appropriate vehicle model and the sonar data without control inputs or dead-reckoning information.

During the following years, works of the above mentioned groups alternated with contributions from new researchers. In [94], a SLAM framework was proposed to simplify the operation of LBLs by enabling on-the-fly calibration of submerged transponders using range-only measurements. The input of the system is the time of flight between a transceiver mounted on the vehicle and a transponder lying on the seabed whose location is undetermined. Assuming that the altitude of the vehicle is known, the range measurement constrains the possible transponder location to a 2D circle on the seabed. When measurements are obtained from different vehicle positions, the intersection of their circles makes it possible to determe the position of the transponder. Of course, solving this problem involves finding the location of many transponders as well as a sequence of position states. This is done by using a non-linear least-squares optimization algorithm. The data set used to test the approach was produced during the 2002 GOATS experiments, a collaboration between MIT and the NATO SACLANT Underwater Research Center which took place near the coast of Italy. A network of four small LBL transponders was deployed and surveyed with a high precision DGPS system to establish the ground truth. Then, the Caribou AUV, an Odyssey III class vehicle equipped with a transceiver, was operated within the area using an EKF based system for navigation. The EKF integrated compass, Doppler velocity and LBL data with *a priori* knowledge of the transponder locations. To validate the proposal, a comparison between the EKF estimated trajectory and that obtained with the range-only SLAM is shown. Moreover, the estimated transponder positions are placed within reasonable error bounds when compared with the surveyed ones.

A different approach to solve the range-only problem is taken in [98] where the authors, using the same 2002 GOATS data set, present an algorithm that imposes geometric constraints on the acoustic measurements to reject outliers. Then, a voting scheme implemented with a two-dimensional accumulator similar to that used in a Hough transform [58] is responsible for estimating the initial LBL beacon positions. Once their approximate location is obtained, a conventional EKF refines the estimates of both vehicle and beacon positions as new measurements arrive. When represented against the ground truth, the final estimation of the vehicle's path and the position of the transponders show a significant improvement with respect to the results presented in [94]. The data collected during the 2002 GOATS experiment is used again in [95]. This time, the MIT Synthetic Aperture Sonar (SAS) carried in the nose of the Caribou AUV during the trials acted as the primary sensor for landmark detection. The paper presents an implementation of the method previously described in [73], the Constant Time SLAM (CTS). The CTS algorithm is a consistent and convergent method for updating and creating a set of local maps while determining their best global location estimate. This offers computation independent of the workspace size at the cost of producing a suboptimal solution. The detection and tracking of features from the SAS data was performed automatically using the technique described in [113]. Data association was performed manually. To evaluate the method, the estimated trajectory resulting from the CTS algorithm is compared with the solution from a full covariance SLAM along with the ground truth from the AUV's navigation system.

In another line of research, imagery from sidescan sonar was used to deal with the underwater SLAM problem [120]. Again, the data set employed in this work was the result of a GOATS campaign, in particular from its year 2000 edition. The method relies on a classical EKF implementation of the stochastic map whose estimated trajectory is then smoothed with a Rauch-Tung-Striebel (RTS) filter. In [122], the same approach was tested in simulation and with real data obtained during the BP 2002 experiments carried out by the SACLANT in La Spezia, Italy, with a Remus AUV. In both works, the stochastic map stores the location of landmarks extracted from the sidescan sonar images. This landmark extraction is performed manually along with the data association process. In [123], the work was extended by addressing the problem of automatic extraction and association of landmark observations. The automatic extraction technique uses a Markov Random Field (MRF) model to detect candidates [106]. After removing those candidates with dimensions outside an acceptable range, a Co-operating Statistical Snake (CSS) is employed to extract the object highlighting and shadow regions. For the data association task, the Joint Compatibility (JC) test [90] is improved using the height of the landmark as an additional descriptor. Since no ground truth is available for validation, the performance of the proposal can only be appreciated by comparing the sidescan mosaics created using the navigation data with those generated using the estimated trajectory from the SLAM system. In the different tests, the resulting mosaic from the SLAM system generally offers a higher visual quality and the trajectories are smoother.

The estimation of the vehicle's motion using image mosaicking techniques has many points in common with the problem of underwater SLAM [89, 45, 48]. Among the first approaches which applied such techniques in the form of a SLAM system we can find work done at Stanford University [40], where a mosaic based navigation framework based on an augmented-state Kalman filter using trajectory states was demonstrated. A few years later, similar work was done here by the Computer Vision and Robotics Group at the University of Girona [46]. The number of published works presenting underwater visual SLAM systems with real data is still limited. In 2004, researchers from the University of Sydney presented a SLAM system capable of fusing information from sonar and vision systems to provide estimates of the vehicle's motion and generate image mosaics containing a gross tridimensional model of the scenario [130]. The data set for this work was acquired with the Oberon vehicle during a trial on the Great Barrier Reef in Australia. A camera mounted in a down-looking position was able to capture clear images of the coral reefs over which the vehicle travelled. Simultaneously, a pencil beam scanning sonar mounted above the camera produced a set of range measurements which were used to generate profiles of the terrain directly below the vehicle. The landmarks to be initialized in the stochastic map were extracted from the sonar measurements. For each range measurement, a high contrast visual feature was identified in the image within the area insonified by the sonar. The 3D position of the feature was then incorporated in a EKF framework and tracked using the Lucas and Kanade feature tracking technique [78] to provide the SLAM algorithm bearing only observations of the feature positions. Again, no positioning systems were available for ground truth validation. Therefore, the performance of the system could only be examined by studying the fidelity of the tridimensional mosaic. Despite the reduced dimensions of the resulting terrain model, a significant correspondence between the bumps in the model and the coral structures could be appreciated.

This same year (2004), a second proposal for visual underwater SLAM was presented as the result of a joint work between researchers at MIT and the Woods Hole Oceanographic Institution [34]. This proposal consisted of an augmented state EKF which stored the history of the vehicle's positions where a set of camera images were obtained. Then, pairwise image based registration was carried out to determine the correspondences between consecutive images and hence provided relative measurements between positions. In addition, the measurements from other sensors (heading, depth, velocity, etc.) were also incorporated as observations of the current state of the vehicle. It is worth noting that the system is only capable of detecting correspondences between consecutive images and that correspondences between cross-track images are established manually. The experimental results endorsing the proposal were produced from a data set collected at the Stellwagen Bank National Marine Sanctuary by the SeaBED scientific AUV. Although the experiment was much longer, only a sequence of 100 images taken along a 100 meter trail was used. The resulting vehicle trajectory was compared with the one obtained with dead-reckoning. As expected, the error increased at a lower rate in the SLAM solution, being bounded in those places were cross-track image links occur. Soon afterwards, in 2005, the same research group presented an evolution of the algorithm for visual underwater SLAM [35]. A data set obtained during a survey of the RMS Titanic wreck by the Hercules deep-sea ROV served as the testbed for a SLAM framework based on the use of the EIF instead of the traditional EKF approach. The sparsity of the solutions from an EIF led to computationally efficient SLAM algorithms and made storing a larger number of elements in the state possible. This is demonstrated in the work at hand with a state vector containing 866 robot states, each corresponding to the acquisition of one of the images from the data-set. A second enhancement of the proposal is that the search for correspondences is no longer restricted to consecutive images, since the system is capable of determining the regions where correspondences with other images can occur.

This same year, [114] proposed a method to improve bathymetric mapping using SLAM. The solution consisted of generating a set of submaps from small bathymetric patches created over short periods of time. In a similar way to that of the visual underwater SLAM algorithms presented, estimates of previously visited vehicle positions are retained in the state of an EKF to serve as anchor points for these submaps. Then, these patches are registered to generate relative position measurements between delayed states. It is worth mentioning that during the creation of the submaps, an accumulation of navigation errors occurs which affects the position of the range measurements. To minimize their effect, the authors propose a method to identify the quantity of internal errors in the submap to determine the point at which to break the current map and start a new one. Similar criteria are applied to ensure that the submap contains enough 3D information to make the registration process possible. In the experimental part of the work, the Jason ROV, equipped with an SM2000 multibeam echo sounder from Kongsberg-Mesotech Ltd. and many other typical navigation sensors, performed a 12 hour survey over a hydrothermal vent site. The resulting data set was used to generate a bathymetric map of the zone using both dead-reckoning and SLAM estimated trajectories. Using measurements from an LBL system as ground truth, it is possible to observe a better alignement of the SLAM estimated positions than those estimated by dead-reckoning. Moreover, the bathymetric map resulting from SLAM presents significantly fewer registration errors and greater detail.

In 2006, a SLAM system running on the Tri-Dog 1 AUV was successfully deployed during sea experiments carried out at the Tagari vent area of Kagoshima Bay in Japan [82]. The system took advantage of bubble plumes present in the area as well as two sonar reflectors specifically deployed to serve as landmarks. A mechanically scanned profiling sonar was the primary sensor for landmark detection. The sonar was set to scan horizontally around the vehicle to map the positions of the plumes and reflectors in the form of point landmarks. Moreover, other dead-reckoning sensors were also used. The SLAM framework, whose description and preliminary water tank tests were presented in [81], runs a particle filter which estimates the vehicle state while simultaneously a map builder is responsible for incorporating newly detected landmarks into the map. A third element, the motion controller, generates the control signals necessary to drive the vehicle through a sequence of waypoints which define the autonomous mission. Although the system effectively builds a map and simultaneously uses its information to localize the AUV, it is not able to update the map nor does it take into account the uncertainty of the vehicle's position while initializing the features in the map. The experimental part of the work presents several trajectories obtained during various dives as well as an example of an image mosaic composed using only the SLAM estimated positions. There is, however, no ground truth to validate the results.

During 2007, one more approach on underwater SLAM has appeared. [36] presents the DepthX, an AUV specially designed for exploring *cenotes* (i.e. sinkholes) in Mexico. Equipped with an array of 56 narrow beam sonar transducers, the vehicle is capable of acquiring a constellation of range measurements all around it and therefore perceive tridimensional structures from the environment. In additon, dead-reckoning sensors assist the navigation. In this work, the core of the SLAM system is a Rao-Blackwellized particle filter in which each particle represents the vehicle's position and the map [51]. The map is stored within a 3D evidence grid which uses the Deferred Reference Counting Octree (DCRO) data structure to reduce the memory requirements [37]. This paper presents two experiments in which the SLAM system has been tested. The first was performed in a large cylindrical water tank (11.6 meters deep and 16.8 meters in diameter) using the dead-reckoning sensors for real time navigation. Then, the same data-set was used in a localization algorithm together with a previous map of the tank to produce a ground truth trajectory. This trajectory serves to validate the SLAM system when, finally, an offline version is executed. The second experiment consisted of a dive performed in the La Pilita cenote with a real time version of the SLAM algorithm running on the DepthX vehicle. Due to the lack of ground truth, it was not possible to make strong assertions about the accuracy of the system. However, the vehicle succeeded in creating a map of the cenote and its navigation was accurate enough to return the vehicle to the starting location after the test.

Table 2.1 Summary of selected works on underwater SLAM

Reference	Principal sensor	Scenario	Filtering	Map	Feature extraction	Data association	Ground truth
[11]	Imaging sonar (electr.)	Natural (sea)	EKF (decoupled)	Landmark (point)	Automatic	Automatic	Yes
[93]	Imaging sonar (mech.)	Artificial (pool)	EKF (GPF)	Landmark (point)	Automatic	Automatic	Yes
[121]	Imaging sonar (mech.) Imaging sonar (electr.)	Artificial (tank) Artificial (pier)	EKF	Landmark (point)	Automatic	Automatic	Yes No
[118]	Imaging sonar (mech.) Imaging sonar (electr.) Imaging sonar (electr.)	Artificial (tank) Artificial (pier) Natural (sea)	EKF	Landmark (point)	Automatic	Automatic	Yes No No
[68]	Imaging sonar (mech.) Imaging sonar (electr.)	Artificial (tank) Natural (sea)	EKF	Landmark (point)	Automatic	Automatic	Yes Yes
[132]	Imaging sonar (mech.) Imaging sonar (mech.)	Artificial (pool) Mixed (reef)	EKF	Landmark (point)	Automatic	Automatic	Yes No
[71]	Imaging sonar (mech.)	Artificial (tank)	EKF (DSM)	Landmark (point)	Automatic	Automatic	Yes
[123]	Sidescan sonar	Natural (sea)	EKF	Landmark (point)	Automatic	Automatic	No
[94]	LBL (range only)	Artificial (sea)	LS optimization	Landmark (point)	Automatic	Solved	Yes
[120]	Sidescan sonar	Natural (sea)	EKF/RTS	Landmark (point)	Manual	Manual	No
[95]	Imaging sonar (SAS)	Natural (sea)	Undefined (CTS)	Landmark (point)	Automatic	Manual	Yes
[98]	LBL (range only)	Artificial (sea)	EKF	Landmark (point)	Automatic	Solved	Yes
[122]	Sidescan sonar	Natural (sea)	EKF/RTS	Landmark (point)	Manual	Manual	No
[34]	Camera	Natural (sea)	EKF	Vehicle poses	Automatic	Mixed	No
[130]	Camera and profiler	Natural (reef)	EKF	Landmark (point)	Automatic	Automatic	No
[35]	Camera	Artificial (wreck)	IF	Vehicle poses	Automatic	Automatic	No
[114]	Multibeam echo sounder	Natural (sea)	EKF	Bathymetric sub-maps	–	Automatic	Yes
[82]	Profiler (mech.)	Mixed (sea)	PF	Landmark (point)	Automatic	Automatic	No
[36]	56 pencil beams	Artificial (tank) Natural (cenote)	PF	Evidence grid	–	Automatic	Yes No

2.5 Discussion

This chapter has introduced the SLAM problem, its history and, in particular, a selection of the most representative works carried out so far towards a solution for underwater environments. Autonomous navigation of underwater vehicles has been a subject of great interest for years with an abundant published bibliography on many different topics, from dead-reckoning to terrain aided navigation. However, underwater SLAM is still in its initial phase and a relatively limited number of approaches have been presented. As has been shown in Section 2.4, the majority of underwater SLAM approaches have some points in common. For instance, among the different sensorial options, imaging sonars seem to be the most common choice, probably because of their high capability to explore large areas in search of features. Although cameras can produce rich information, their use is restricted to a more local domain and, in some situations, they may suffer visibility problems. Profilers and range sensors in general are less suitable for feature extraction and using their raw data (e.g. for scan matching) usually requires accumulating measurements in order to produce a sufficient representation of the scenario. The use of imaging sonars seems to be evenly distributed between those scanned mechanically and those scanned electronically. However, a direct relationship between electronically scanned sonars and those SLAM examples performed with AUVs in real environments can be observed . On the other hand, mechanically scanned devices are usually employed during tests performed under lab conditions. Independently of cost considerations, this may be related to the different scanning rates of the devices. Electronically scanned sonars can produce images almost instantaneously and the distortions due to the vehicle's motion usually fall within the range resolution of the sonar and so their effect can be ignored. The use of mechanically scanned sonars, with a much slower scanning rate, is usually limited to platforms which are static or moving at low velocities or in those situations where a suitable dynamics model and sufficient dead-reckoning sensors are available.

Another remarkable aspect of the SLAM approaches studied is the predominance of Kalman filters over other estimation techniques such as information filters or particle filters. Although the latter have gained importance during recent years, the number of implementations is still low. Moreover, the majority of the proposed systems implement variants of the classical stochastic map in which point features are used as landmarks. These features generally correspond to the centroids of objects which appear as high echo-intensity zones in the acoustic images. Extracting these kinds of features from the seabed is difficult for many reasons. For instance, they have variable sizes and their shapes can change depending on the sensor's vantage point. Of course, this makes the landmarks less reliable and could induce errors in the estimation of their centroids. Another typical problem of the underwater SLAM is the landmark shortage. The sea bottom is generally flat and it can be quite difficult to find landmarks capable of producing distinguishable features in the images. For this reason, it is not uncommon to find applications in which reliable artificial features are deployed to improve the performance of the system. Among alternative map representations, we can find maps composed of camera images. These maps contain rich visual data and in some cases tridimensional information is also incorporated. Although at this point there are still few published works, the interest in image mosaicking techniques and their possible applications will probably foster future works. On the other hand, two approaches using dense range data have also been presented. These systems produce very detailed maps. However, their main drawback is that their use remains restricted to areas where it is possible to extract sufficient 3D information to ensure the success of the registration process.

With respect to the validation of the SLAM proposals, it is worth mentioning that in half of the reported SLAM examples ground truth is not available, while an important part of the remaining half corresponds to those tests carried out in lab conditions. Obtaining reliable ground truth in real scenario operations is very complex. It usually requires the deployment and calibration of additional acoustic localization systems such as LBL or USBL. Nevertheless, these systems can only provide ground truth for the vehicle trajectory and validating mapping results is even more difficult, since previous maps of the area rarely exist.

2.6 Aims of This Work

As pointed out in the previous chapter, the work carried out for this thesis has pursued the goal of developing a SLAM system for AUVs operating in manmade environments. Among the sensorial options available, the mechanical scanned imaging sonar has been chosen because of its versatility but also for its relative low cost, particularly, when compared with electronically scanned ones. This approach has both advantages and disadvantages. For example, navigating through this kind of environment guarantees the presence of underwater structures from which it is possible to extract reliable features. An advantage of mechanical over electronically scanned sonars is that their perception area is not limited to the front of the vehicle. In fact, they can continuously rotate 360° around the vehicle, which is perfect for those situations where a limited number of landmarks exist. On the other hand, using a mechanically scanned sonar mounted on a moving vehicle requires dealing with motion induced distortions in the acoustic data. The effect is particularly problematical because the structures found in the application at hand are generally walls which appear as linear shapes in the acoustic images. In the presence of distortions, lines can experience significant deformations that may preclude their correct identification, contrary to what occurs when working with point landmarks, which in the worst case will simply be incorrectly located.

Chapter 3
Design and Development of the Ictineu AUV

This chapter describes the Ictineu AUV (Figure 3.1), the research vehicle of the Computer Vision and Robotics Research group at the University of Girona that constitutes the experimental platform of this thesis.

In 2006, the Defence Science and Technology Lab (DSTL), the Heriot-Watt University and the National Oceanographic Centre of Southampton organized the first Student Autonomous Underwater Challenge - Europe (SAUC-E) [27], European-wide competition for students to foster research and development in underwater technology. Ictineu AUV was originally conceived as an entry for the SAUC-E competition by a team of students collaborating with the Underwater Robotics Laboratory [129, 109]. This author, who was team leader during the competition, became involved in the hardware design and construction phase as well as in the development of the sonar based localization system (described in Section 5.2). Although the competition determined many of the vehicle's specifications, Ictineu was also designed taking into account its posterior use as an experimental platform for various research projects in our laboratory. The experience gained by the group in the previous development of vehicles such as the Garbi AUV, made it possible to build a low-cost vehicle of reduced weight (52 Kg) and dimensions (74 x 46.5 x 52.4 cm) with remarkable sensorial capabilities and easy maintenance.

3.1 Mechanical Aspects

The Ictineu AUV was conceived around a typical open frame design. This configuration has been widely adopted by commercial ROVs because of its simplicity, robustness and reduced cost. Although the hydrodynamics of open frame vehicles is known to be less efficient than that of closed hull type vehicles, the former are suitable for applications not requiring movements at high velocities or traveling long distances. The robot chassis is made of Delrin, a plastic engineering material that is lightweight, durable and resistant to liquids. Another aspect of the design is the modular conception of its components which simplifies the upgrading of the vehicle and makes it easier to carry out maintenance tasks. Some of the modules (the

D. Ribas et al.: Underwater SLAM for Structured Environments, STAR 65, pp. 23–35.
springerlink.com © Springer-Verlag Berlin Heidelberg 2010

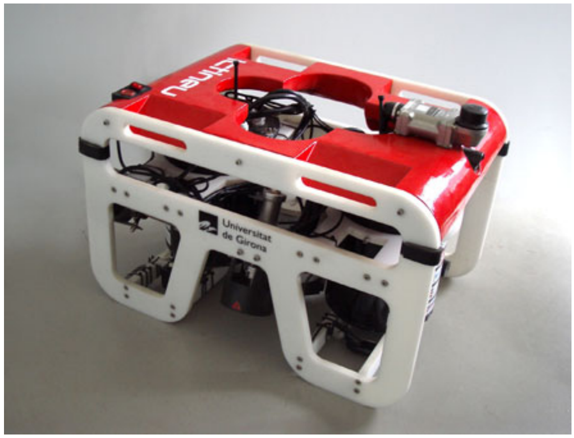

Fig. 3.1 The Ictineu AUV, a research vehicle of the Underwater Robotics Laboratory of the University of Girona.

thrusters and the majority of the sensors) are watertight and are therefore mounted directly onto the vehicle chassis. In addition, two cylindrical pressure vessels made of aluminum house the power and computer modules while a smaller one made of Delrin contains the Motion Reference Unit (MRU). Their end caps are sealed with conventional O-ring closures while the electrical connections with other hulls or external sensors are made with plastic cable glands sealed with epoxy resin. Four thrusters propel the Ictineu. Two of them, mounted horizontally, can propel the vehicle in the surge Degree Of Freedom (DOF), as well as change the heading (yaw DOF). The two vertical thrusters are positioned in a particular slanted distribution that makes it possible not only to control the movement in the heave DOF but also to produce small lateral movements in the sway DOF. Therefore, the prototype is a fully actuated vehicle in four DOF (surge, sway, heave and yaw), while being passively stable in roll and pitch as its meta-centre is above the centre of gravity. This stability is the result of an accurate distribution of the heavier elements at the lower part of the chassis combined with the effect of technical foam placed in the top which, with its 10.5 liters volume and a weight of 0.6 Kg, provides the Ictineu with a slightly positive buoyancy.

3.2 Tethered/Untethered Modes of Operation

The Ictineu can operate either as a ROV (tethered mode) or as an AUV (untethered mode). An optional 30 meter umbilical cable can be connected to the two principal hulls to supply power and communications to the vehicle. This mode of operation is very useful not only to operate the Ictineu as a ROV but also while working under laboratory conditions as it allows testing/developing the vehicle's software over long time periods. An external 1200 VA power supply, derived from 230 V AC mains or a power generator, feeds about 24 V DC to the vehicle. Moreover, a standard Ethernet connection is embedded in the umbilical allowing direct data transmission with the onboard computers. This 100 Mbps connection makes it possible not only

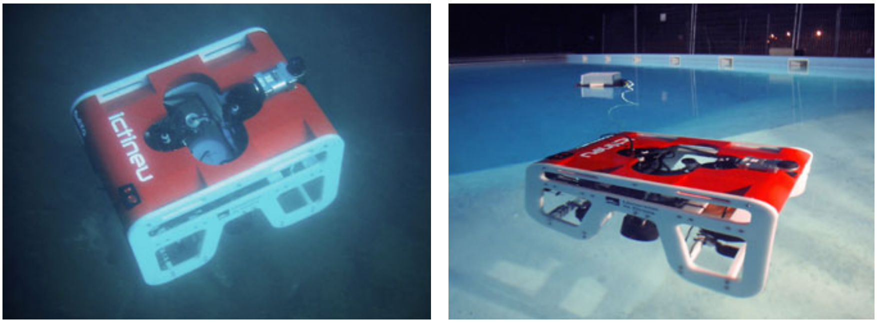

(a) Untethered mode. (b) Equipped with a buoy.

Fig. 3.2 Different configurations of the Ictineu AUV.

to remotely operate the vehicle but also to transmit real time video streams from the vehicle's cameras. When working in full AUV mode, the umbilical cable is removed and the connectors in the hulls are sealed with plugs. Being untethered, the vehicle relies on batteries to power all the systems and therefore has a limited running time but a longer range of operation. Unfortunately, communications with the vehicle are not possible in this setup. Recently, a third mode of operation has been developed. A buoy, connected to the Ictineu through a 25 meter Ethernet cable and equipped with a 802.11g Wi-Fi access point, enables communication with the vehicle while still providing a high level of autonomy. In addition, the buoy is also equipped with its own batteries for power supply and a DGPS receiver which provides the position of the buoy and hence the approximate location of the vehicle in the global reference frame.

3.3 Power Module

The power module (see Figure 3.3) contains the four power drivers for the thrusters as well as a pack of 2 cheap, sealed 12V 12Ah lead acid batteries that can provide the Ictineu with over 1 hour of running time. A DC-DC converter is included to provide stabilized voltage to the rest of the components. Finally, a simple relay circuit commutes between the internal and the external power supplies when the umbilical cable is connected. If necessary, it is also possible to recharge the batteries with the external power from the umbilical cable.

3.4 Computer Module

Two PCs, one for control and one for image and sonar processing connected through a 100 MBs switch, form the core of the robot's hardware. An image of the complete power module can be seen in Figure 3.4. The control PC is an AMD GEODE-300MHz powered by a 50 W power supply module. The PC104 stack also incorporates an A/D and digital I/O card with 8 analogue input channels, 4 analogue output

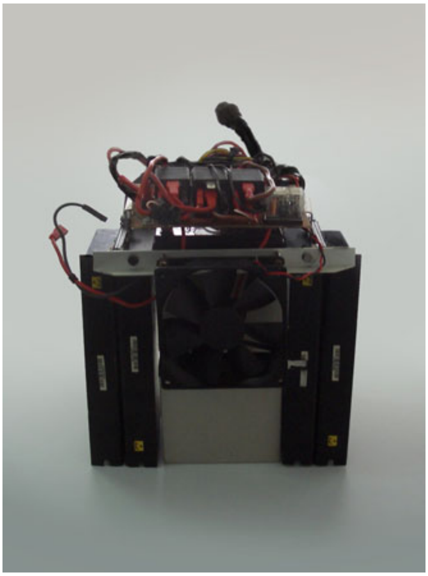

Fig. 3.3 Power module

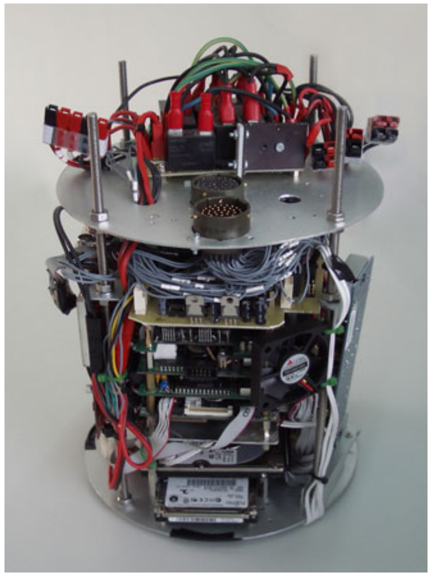

Fig. 3.4 Computer module

channels and 24 digital I/O. The mini-ITX computer is a Via C3 1 GHz Pentium clone and is used to process the data from the imaging sonar and the cameras. A cheap PCTV110 from Pinnacle is used for image processing.

3.5 Actuators

Since the Ictineu AUV is not an intervention robot, the actuator suite is basically limited to the 4 thrusters necessary to operate the vehicle. However, with the objective of taking part in the SAUC-E competition, an additional actuator, a marker dropper, was incorporated.

3.5.1 Thrusters

Each one of the thrusters mounted in the Ictineu vehicle (Figure 3.5) is able to produce around 14.7/14.2 N of forward/backward thrust. They were built with 250 W Maxon DC motors equipped with planetary gears and are enclosed in stainless steel housings with O-ring sealed end caps. The rotation is transmitted to a three-bladed brass propeller by means of a stainless steel shaft mounted through a rubber lip seal. Although lip seals do not withstand high pressures, their simplicity and reduced cost make them a good choice for vehicles operating in shallow waters.

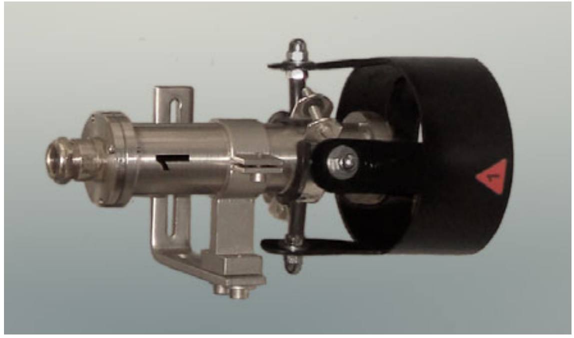

Fig. 3.5 One thruster from the Ictineu.

3.5.2 Marker Dropper

One of the missions proposed for the SAUC-E competition consisted of locating a circular target lying on the bottom of the tank and hitting it with a marker dropped from the vehicle. An electromagnetically actuated release mechanism with a 3-shot magazine was designed for this purpose and mounted in the rear part of the vehicle.

3.6 Sensor Suite

One of the main objectives the team had in mind while designing the Ictineu was to provide the vehicle with a complete sensor suite. Taking the set-up in the Garbi AUV as a starting point, the new suite was created by adding new sensors to correct some limitations of the old prototype. Moreover, as the Ictineu was started from scratch, it was possible to improve the distribution of the acoustic sensors within the vehicle frame in order to avoid dead zones and improve their overall performance.

3.6.1 Miniking Imaging Sonar

The Tritech MiniKing is a small compact mechanically scanned imaging sonar (MSIS) designed for use in underwater applications such as obstacle avoidance and target recognition for both AUVs and ROVs. This sonar can perform scans in a 2D plane by rotating a fan-shaped sonar beam through a series of small angle steps. It can be programmed to cover variable length sectors from a few degrees to full 360° scans. A characteristic fan-shaped beam with a vertical aperture angle of 40° and a narrow horizontal aperture of 3° allows a sonar image to be formed with enough information about the surrounding environment to recognize sizes, shapes and surface reflecting characteristics of a target at distances of up to 100 meters. The sensor is mounted on the upper front part of the Ictineu AUV to provide a clear view and avoid occlusions in the resulting data. Its capacity to sense the environment in which the vehicle is operating makes the Miniking one of the most important sensors aboard the Ictineu and represents a valuable potential for underwater localization and SLAM. This has made the Miniking one of the principal objects of study

Fig. 3.6 The Tritech Miniking imaging sonar.

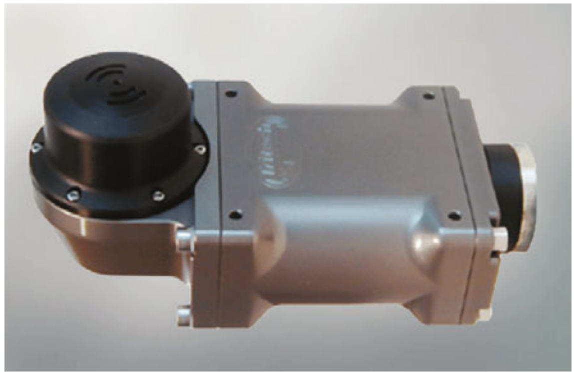

throughout the elaboration of this thesis. A more detailed description of the operation of MSISs in general and of the Miniking sensor in particular can be found in Chapter 4.

3.6.2 Doppler Velocity Log

The SonTek Argonaut DVL is a sensor specially designed for ROV/AUV applications which measures ocean currents, vehicle speed over ground, and altimetry using a precise 3-axis measurement system based on the Doppler shift effect (see Figure 3.7). Moreover, it has the capacity to analyze the quality of the measurements and produce a status value, which makes discarding erroneous data possible. This system operates at a frequency of 1500 kHz and has a range of about 15 m. Its three acoustic transducers are slanted 25° off the housing vertical axis and are equally spaced at 120° relative azimuth angles. In our particular configuration, the device is also equipped with additional sensors:

Compass: Outputs the sensor heading (angle with respect to magnetic north).
Tilt sensors: Measures the roll (rotation about the X axis) and pitch (rotation about the Y axis) angles.
Pressure sensor: Provides depth data by means of water column pressure measurements.
Temperature sensor: Provides water temperature for internal sound speed calculations, improving the measurements from the acoustic device.

Although some of these sensors could individually produce measurements at a higher frequency, the resulting Argonaut DVL output rate is of about 1.5 Hz because of the limitations of the acoustic device. However, the inclusion of all this equipment converts the Argonaut DVL into a very versatile sensor which, together with its compact size, low power consumption and depth ratings of about 200 meters, makes it especially suited for underwater vehicle navigation.

Fig. 3.7 Sontek Argonaut DVL

Fig. 3.8 Xsens MTi MRU

3.6.3 Motion Reference Unit

The Xsens MTi sensor (Figure 3.8) is a gyro-enhanced low cost miniature Motion Reference Unit (MRU) which provides 3D orientation (attitude and heading), 3D rate of turn (rate gyro) as well as 3D acceleration measurements. Although the sensor is able to provide data at a higher rate, the system gathers measurements from the MTi at a rate of 10 Hz. In order to produce drift-free angular measurements, the sensor also measures the directions of gravity and magnetic north. Our particular device configuration has 17 m/s^2 full scale in acceleration measurements, which is far from the smaller accelerations that the Ictineu actually experiences. For this reason we do not usually rely on its acceleration estimates. On the other hand, the angular measurements are much more reliable and, as they are outputted at a higher rate than the data from the DVL sensor, they have been chosen as the main source for the vehicle's attitude estimation.

3.6.4 Cameras

Ictineu is equipped with two cameras. The first is a forward-looking colour camera mounted on the front of the vehicle and intended for target detection and tracking, inspection of underwater structures and to provide visual feedback when the vehicle is operated in ROV mode. The second camera is a downward-looking black and white camera placed in the lower part of the vehicle. This camera is mainly used to capture images of the seabed for research on image mosaicking.

3.6.5 Hydrophone

The last task to be completed in the SAUC-E mission consisted of surfacing within a designated zone marked by means of an active acoustic device. In order to detect this acoustic signal, an external hydrophone was mounted on the front of the vehicle while all the signal processing circuitry, which was specifically designed for the task, was mounted inside one of the main pressure vessels.

3.6.6 Safety Sensors

There are several minor sensors whose purpose is to ensure the safety of the vehicle. The majority of these sensors are mounted inside the different pressure vessels and are designed to measure temperature and pressure, and to detect water leakage. The activation of any of these sensors indicates that some problem is occurring inside the pressure vessels and therefore an alarm is raised to prevent irreparable damage. There is also an acoustic range finder mounted on the front part of the vehicle. The purpose of this device is to provide a simple way to determine the presence of an obstacle close to the vehicle and thus avoid collisions without having to analyze complex data from the imaging sonar.

3.7 The O^2CA^2 Software Architecture

The software architecture has the task of guaranteeing the AUV's functionality. The real-time POSIX together with the ACE/TAO CORBA-RT ORB have been extensively used to develop the architecture as a set of distributed objects with soft real time capabilities. These objects are distributed between the two onboard PCs and, when operating in tethered mode, the external PC. The architecture is composed of a base system and a set of objects customized for each particular robot, which makes it possible to share the same software architecture with all the vehicles in the lab. There are classes providing soft real-time capabilities to allow for a periodic execution of tasks such as the controllers or the sensors. Another important part of the base systems are the loggers. A logger system is used to log data from sensors, actuators or any other object component. Loggers do not execute in real time; they are background processes which receive the data from real time objects. Their role consists of packing the data and saving them in files. It is worth noting that, although loggers do not run in real time, the data has a time-stamp corresponding to the gather time. Moreover, all the computers in the network are synchronized by means of the NTP (Network Time Protocol) and hence, all the data coming from different sensors can be time related. The software architecture is divided between the three modules as represented in Figure 3.9: the Robot interface module, perception module and control module.

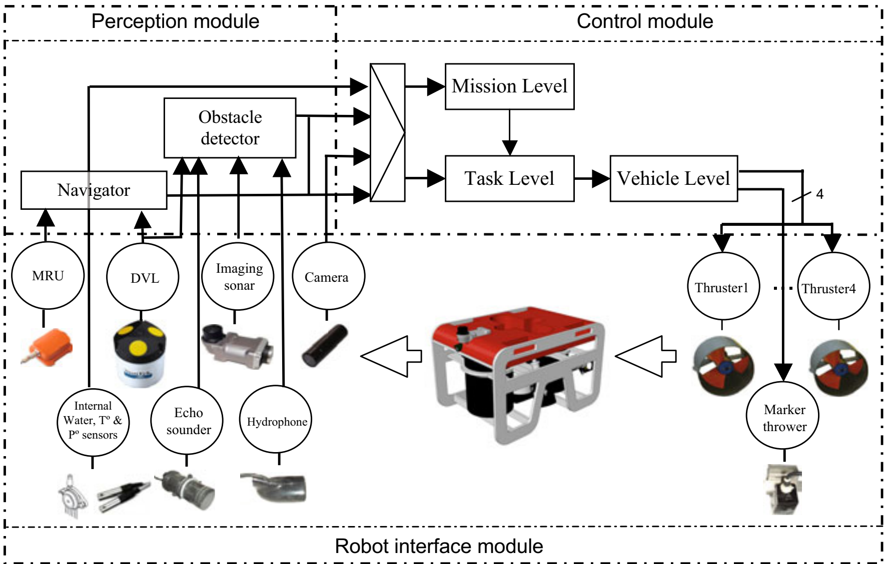

Fig. 3.9 Schematic of the Ictineu AUV software architecture.

3.7.1 Robot Interface Module

This is the only module containing software objects that dialog with the hardware. There are basically two types of objects: sensor objects responsible for reading data from sensors and actuator objects responsible for sending commands to the actuators. Sensor objects for the Ictineu AUV include a DVL, an imaging sonar, a MRU, two cameras, a depth sensor, and an echo sounder. There are also objects for the safety sensors such as water leakage detectors and internal temperature and pressure sensors that allow for the monitoring of conditions within the pressure vessels. Actuator objects for the Ictineu include the thrusters and the marker thrower.

3.7.2 Perception Module

This module contains two basic components, the *Navigator* and the *Obstacle Detector*. The *Navigator* object has the goal of estimating the position of the robot. To accomplish this task, there is an interface called the *Navigation Sensor* from which all the localization sensors (DVL, MRU, depth sensor) inherit. This interface provides all these sensors with a set of methods to return the position, velocity and acceleration in the 6 DOF together with an estimation of the quality of these measurements. The *Navigator* can be dynamically connected to any *Navigation Sensor*, fusing the data to obtain more accurate position, velocity and acceleration estimates. Furthermore, the *Navigator* can also access the imaging sonar to implement the navigation method specifically designed for the SAUC-E competition described in

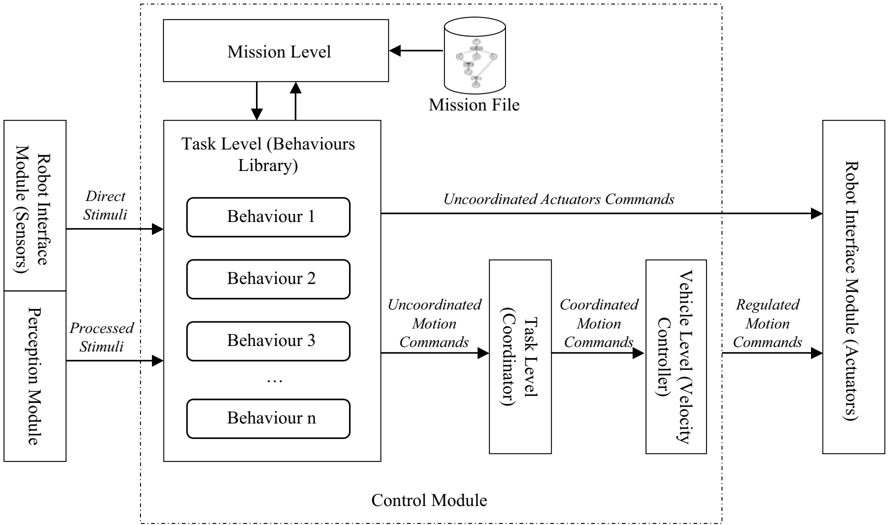

Fig. 3.10 Schematic of the Ictineu AUV control architecture.

Section 5.2. The control module uses the navigation data provided by the *Navigator* keeping the behaviours independent of the physical sensors being used for the localization. The *Obstacle Detector* uses the same philosophy to provide obstacle positions in the world fixed frame. The *Obstacle Detector* is also used to detect the distance between the vehicle and the bottom of the pool. Detecting frontal obstacles is possible using the echo sounder or the imaging sonar and the pool bottom obstacles can be detected with the DVL sensor.

3.7.3 Control Module

The control module receives sensor inputs from the perception module and sends command outputs to the actuators residing in the robot's interface module (Figure. 3.10) [13]. Since tasks and behaviours are words interpreted in different ways by different authors in the literature, we describe how they are defined within our project:

- A behaviour is a function that maps the sensor input space (stimuli) onto a velocity set point (behaviour response) for the robot's low level controller. The behaviour response is chosen in a way that drives the robot towards its corresponding goal. In this way, the goal corresponding to the *KeepDepth* behaviour is considered to be achieved when the robot is within an interval around the desired depth.
- A task is a set of behaviours that are enabled together to achieve a more complex goal. For instance, *KeepDepth* and *MoveTo2D* can work together to allow for planar navigation.

The control module follows the principles of the hybrid control architecture organized in three layers: vehicle level, task level and mission level.

3.7.3.1 Vehicle Level

The vehicle level is composed of a MIMO PID velocity controller for each DOF. This object reads the vehicle's velocity from the *Navigator* object and receives the velocity setpoints from the *Coordinator* object. This level also includes a simple control allocator strategy based on the pseudo inverse of the thruster configuration matrix [42].

3.7.3.2 Task Level

The Task level is a conventional behavioural layer [1] including a library of behaviours that can run alone or in parallel. Each behaviour has a particular goal. The input of a behaviour can be taken from any object of the software architecture (sensors, perception module...). The output, called behaviour response, contains:

- Velocity setpoints for every DOF normalized between -1 and 1.
- Activation level for every DOF normalized between 0 and 1 indicating how important it is for the behaviour to take control of the robot.
- Blocking term (boolean) stating if the behaviour must block the execution thread of the mission level.

To initialize a behaviour, apart from setting its particular parameters it is necessary to specify the following attributes:

Enable: Boolean variable that indicates if the behaviour is activated or not and if its output will be considered by the Coordinator.
Priority: Priority stating the relative importance of each behaviour.
TimeOut: The time out indicates when the behaviour will block the execution thread. If TimeOut< 0, the behaviour blocks the execution thread until its goal is fulfilled. If TimeOut$= 0$, the behaviour does not block the execution thread at all. If TimeOut> 0, the behaviour blocks the execution thread until TimeOut seconds elapse or until its goal is fulfilled.

During the execution of a mission, more than one behaviour can be enabled simultaneously. Hence, a coordinator module is used to fuse all the responses corresponding to the enabled behaviours into a single response to be sent to the velocity controller (vehicle level).

Each degree of freedom is considered separately since not all the behaviours act on all the DOF. To combine all the behaviour responses, the *Coordinator* sorts all the responses by their priority combining them two by two for every DOF, from the highest priority to the lowest. To combine the responses, the activation level and a k factor are used as follows:

$$s = \frac{a_1 s_1}{a_1 + a_2(1-a_1)^k} + \frac{a_2 s_2 (1-a_1)^k}{a_1 + a_2(1-a_1)^k}.$$

a_1, a_2 and s_1, s_2 correspond to the activation level and the desired setpoints for the highest priority and the least priority behaviour respectively, while s corresponds to the final coordinator response. The *Coordinator* output, after combining all active behaviours, is a vector as large as the number of the robot's DOFs where each value corresponds to a normalized velocity [100]. This coordination mechanism can be seen as a hybrid between the classical competition and cooperation methods. When the activation level of the behaviour with highest priority is zero, the coordinated response coincides with the output of the behaviour with the lowest priority. If the behaviour with the highest priority requests the control of the vehicle using an activation level equal to one, then the response of the behaviour with lower priority (non dominant behaviour) is totally subsumed and the coordinated response matches that of the behaviour with the highest priority (dominant behaviour). If both behaviours simultaneously request the vehicle control through an activation level greater than zero then both of them are merged using a weighted average operation with the weights depending on the specified activation levels. If equal activation levels are used, the dominant behaviour always has a stronger weight regulated by means of the exponent k. For details of this coordination mechanism the interested reader is referred to [12].

3.7.3.3 Mission Level

Finally, the upper layer (mission level) is responsible for the sequencing of the mission tasks, selecting for each mission phase the set of behaviours that must be enabled as well as their parameters.

The mission controller was built with a Petri network in which the sequence of tasks is defined. Since the vehicle can move in an unstructured environment, unexpected situations have to be taken into account by the mission designer. According to the network, some nodes will become active. Each node represents a behaviour that will be executed on the task controller. There is a library of behaviours that are used to define a mission. Each one has a simple goal such as move to point, keep depth, search a target, etc. Therefore, the mission controller has the job of defining the task the robot is accomplishing at each moment by activating or deactivating behaviours with the final goal of fulfilling the mission. The mission controller does not determine the actions that guide the robot, it only determines the active behaviours and their configuration which, through the task controller, will be coordinated to guide the robot.

In our Petri net, every place corresponds to one behaviour with a particular configuration. When a place has a token, this behaviour is enabled. When all places that go towards a transition are enabled, and their behaviours do not block the execution thread, the transition is ready to be fired. When a transition is fired, a token is removed from each of the input places of the transition and another token is generated in each output place of the same transition. The control mission algorithm starts on the initial state, checks fired transitions, applies the previously explained procedure, and repeats this process until it reaches the final state [100].

3.8 Summary and Further Work

As a research platform, the Ictineu AUV is subject to constant upgrades. These upgrades have the goal of either correcting and improving detected deficiencies or of extending the capabilities of the vehicle. Some of the imminent modifications are briefly described below.

Thruster upgrade: The thrusters currently mounted in the Ictineu AUV were developed in our lab years ago for a smaller vehicle. Although they are sufficient for operation under lab conditions, missions taking place in natural scenarios may require more thrusting power, especially in the presence of water currents, as well as a better capacity to withstand higher pressures for operations at greater depths. Recently, six new SeaBotix SBT150 thrusters have been acquired. Their reduced dimensions and weight together with a thrust of about 22 N make them a good choice for a small vehicle such as the Ictineu. At the time of writing this thesis, four of the thrusters have been mounted horizontally in a slanted distribution which makes performing movements in the surge and sway DOFs possible. Moreover, this particular distribution also provides redundancy to the system and therefore the vehicle is now able to operate even with a damaged thruster. The two remaining thrusters have been mounted vertically and actuate the heave DOF.

Absolute positioning: Recently, an Ultra Short Baseline (USBL) has been acquired by the lab. An USBL is a method of underwater acoustic positioning. This device consists of a transceiver, which is usually placed on the surface, on a pole under the ship, and a transponder/responder mounted on the AUV (see Figure 1.1). The device determines the position of the vehicle by calculating the range and angles obtained after the transmission and reply of an acoustic pulse between the transceiver and the transponder/responder. Our particular model can also provide communications by means of an acoustic modem incorporated in the package itself. Having a USBL opens the door to many applications where the availability of robot positioning is crucial. Moreover, the output of this device is precise enough (0.2 meters for the range and 0.25 degree for the angle) to be used as the ground truth to test SLAM algorithms. At the present time, software drivers have been developed and integrated into the vehicle's architecture, and a navigation filter is under development.

In this chapter the hardware and software elements which compose the Ictineu AUV have been described. In the short period of time since its creation, the vehicle has undergone extensive usage in many different research fields. Also, it has proved to be a very reliable platform, requiring only minor maintenance tasks. We expect this AUV to become a reference for all future prototypes developed in our laboratory.

Chapter 4
Understanding Mechanically Scanned Imaging Sonars

The purpose of this chapter is to give a brief introduction to the operational principles of MSISs by explaining the basics behind the acquisition of acoustic images as well as providing tools to understand and interpret the information they contain. Moreover, some hints about the principal issues associated with managing MSIS data are given at the end of the Chapter. Some of the figures and examples described here are adapted from the introductory document in [59]. A deeper study on sonars and their techniques can be found in [128].

4.1 Principles of Operation

An MSIS performs scans in a horizontal 2D plane by rotating a mechanically actuated transducer head at pre-set angular increments. For each one of the resulting angular positions, an acoustic fan shaped beam with a narrow horizontal and a wide vertical beamwidth is produced (Figure 4.1). When this emitted acoustic signal travels through the environment and collides with any object in its path, part of the energy transmitted as a mechanical wave returns to the transducer. Measuring the time of flight of the returning wave and assuming a known value for the speed of sound in water, it is possible to determine the range at which the signal was originated. In contrast with range-only sensors, imaging sonars also provide information regarding the intensity of the acoustic signal backscattered from the environment. During the measurement, the sonar transducer detects the water pressure changes produced by the acoustic wave and transforms them into an electrical current. If the signal returning to the transducer head is analyzed for a period of time it is possible to produce not one, but a series of echo intensity vs. range measurements. Generally, transducers are resonant, which means that they are designed to be sensitive at a particular frequency at which the sensor operates. For instance, the Tritech Miniking (see Section 3.6.1) has an operating frequency of 675 kHz, and will accept a return signal in the region of 0 to 80 dB (referenced at 1μPa). During the processing of a pulse, the signal is divided into small parts whose mean intensity value is determined and mapped into 8 bit values (0 will correspond to 0 dB and 255 to 80 dB).

D. Ribas et al.: Underwater SLAM for Structured Environments, STAR 65, pp. 37–46.
springerlink.com © Springer-Verlag Berlin Heidelberg 2010

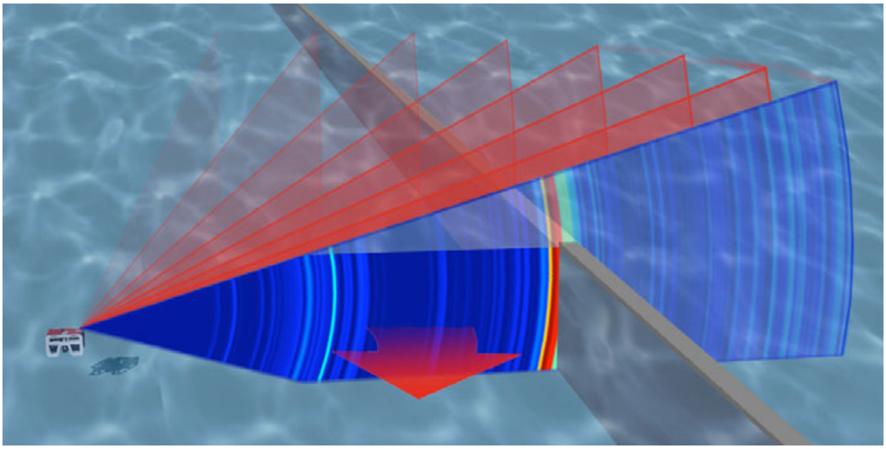

Fig. 4.1 Representation of the scanning process of an MSIS.

From now on, each one of these measured values will be referred to individually as a *bin*, while the set of bins obtained from a single emitted wave will be generally denominated as a *beam*. Therefore, when a transducer head oriented in a particular direction emits a pulse, a beam is produced. This beam is composed of a set of bins, each one representing the echo intensity returning from a specific place along the transducer axis.

Figure 4.2 shows an example of real data obtained by a Tritech's Miniking imaging sonar in a shallow water trial. The image has been generated by placing the polar measurements (set of bins) in a cartesian space and assigning colors to the measured intensities. In order to improve the visualization of the data, a sampling window can be defined between two fixed intensity values and then the colors remapped. In this way, it is possible to increase or decrease the contrast of the image, set the representation to be above low level noises, etc. The colors that fill the spaces between bins have been assigned through interpolation. It is worth noting that, although this kind of image appears in many sections of this document, its use is intended solely to simplify the interpretation of the sonar data and it is not used in any way in the methodologies to be presented. Likewise, the use of the term "acoustic image" generally refers to the set of acquired measurements and not to this particular representation.

4.2 Interpreting Sonar Images

In many cases, an acoustic image obtained in a particular scenario will closely resemble an optical image of the same place. In other cases, it may be substantially different and hence more difficult to analyze. To interpret the information contained in an acoustic image it is necessary to understand the process behind the generation of a beam. The diagram in Figure 4.3 will serve as a guide for the following

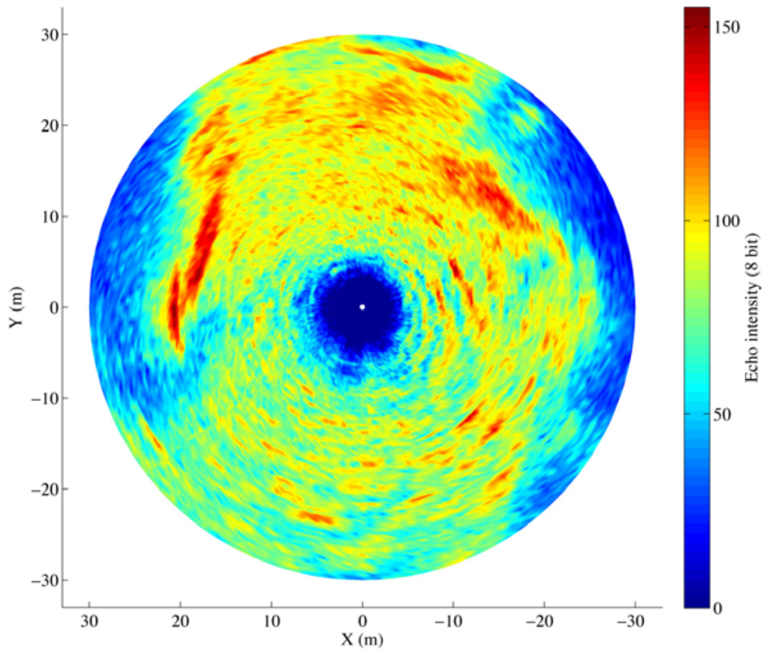

Fig. 4.2 Scan obtained in a shallow water scenario.

description. The process begins with the emission of a pulse from the transducer. During the first meters, the pulse travels through the water volume without impacting with any object. Therefore, no noticeable echo is produced and only some noise is returned to the sensor head. The first significant echo return is obtained when the arc-shaped pulse reaches the bottom. Because of the large incidence angle, only a small fraction of the mechanical energy is returned and hence the measured intensity value is small. However, as the acoustic signal advances and finds a protruding object, an increase in the measured intensity can be observed. Notice that behind the object there is a zone where the sound can not be reflected, thus no signal is returned. This is an acoustic shadow, usually identifiable as a leak of echo intensity after an object detection. Shadows are very useful when interpreting acoustic images, since their length provides information from which the height of insonified objects can be inferred. Figure 4.4 illustrates the scanning process for an IS operating in a scenario where two objects lie on the seabed. The image on the right represents the zones with different measured echo intensities that one would expect from an image obtained in such scenario. The largest area, in gray, corresponds to the low intensity returns from the bottom. The objects appear as high intensity zones and are represented in white. On the other hand, the absence of significant returning echoes is represented in a dark color. It is worth noting how the two objects cast shadows in a similar way to what one could expect from a light source placed in the sensor head. However, the interpretation of real acoustic data is not so

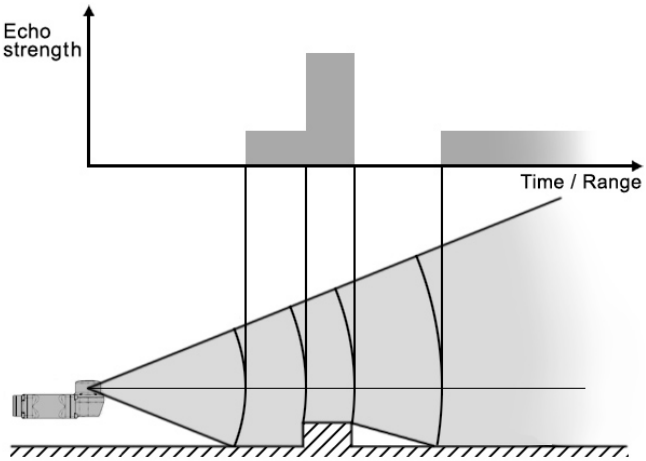

Fig. 4.3 Generation of an acoustic beam.

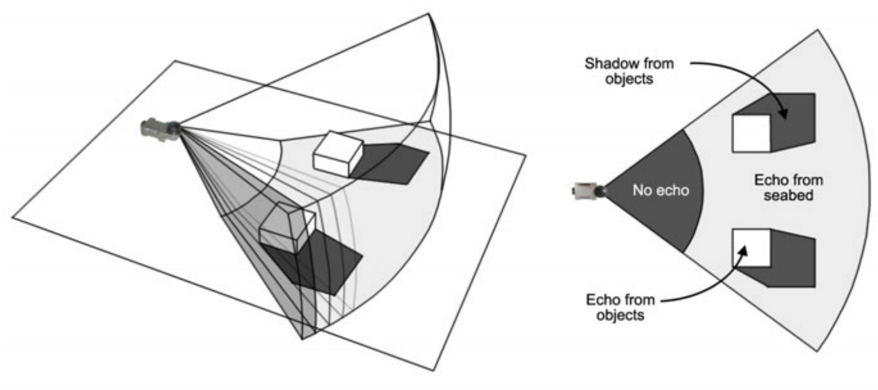

Fig. 4.4 Scanning a sector to produce a sonar image.

straightforward. First, a sonar image will always have a poor resolution due to the nature of the acoustic signals used to generate it. In addition, the materials composing the seabed will be a determining factor in obtaining information from a sonar. Generally, rough objects are better sonar targets because they return echoes in many different directions, whereas smooth surfaces may give a very strong reflection in one particular direction but almost none in any other. These characteristics become clear when examining the example image in Figure 4.2. Colour is assigned depending on the reception intensity level, so the zones in red represent high return areas, such as reefs or rocks; yellows and cyans represent medium/low return areas, such as the flat seabed and finally those in blue represent zones from which no echo is returned. Notice that, as previously stated, shadows are found behind the high intensity zones.

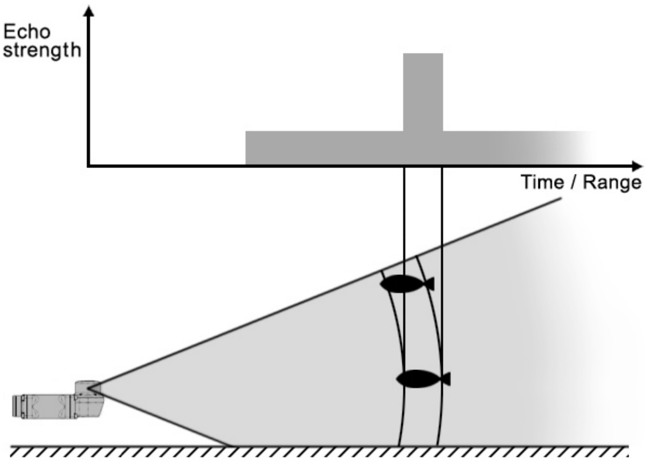

Fig. 4.5 Indetermination in the vertical position of the target.

It is also important to make clear that, although the sensor will reproduce in the acoustic image any tridimensional object present in the scene, it is not possible to determine its position in the vertical plane and therefore only a 2D representation of the environment is produced. This concept is illustrated in Figure 4.5, where two objects placed at the same distance from the transducer head, but at different heights above the seabed, produce the same acoustic return. This effect is a consequence of a wide vertical beamwidth. On the one hand, it increases the capacity of the sensor to detect objects, which is useful for some applications such as obstacle avoidance. However, it comes at the cost of introducing the indetermination in the vertical position. Moreover, errors can also affect the range measurements as a result of a wide beamwidth. As can be seen in the figure, although both objects are placed at the same radial distance from the sensor head, their linear distance along the horizontal is not the same. The resulting measured beam, however, suggests the contrary.

Another particular case is the presence of walls or other large objects in the trajectory of the emitted acoustic wave. Figure 4.6 represents this situation. Its main characteristic is that if the obstacle is large enough, the advance of the acoustic pulse is blocked and, depending on the nature of the obstacle, part of the mechanical energy is reflected back in the opposite direction. Likewise, as the reflected pulse moves across the environment and finds other objects, part of its energy is also returned, ricochetting again with the wall and returning to the sensor head where it is interpreted as if the reflection has never taken place. In other words, the wall acts as a mirror for the acoustic pulse and, as a result, phantoms and reflections not corresponding with real objects can appear. In the example figure, the reflected pulse impacts the sensor head and produces phantom measurements in the resulting beam. This effect is usually observed when operating in confined places (for instance, a water tank); however, it is less common in larger scenarios where the reflected wave can disperse more easily. The image in Figure 4.7, which corresponds

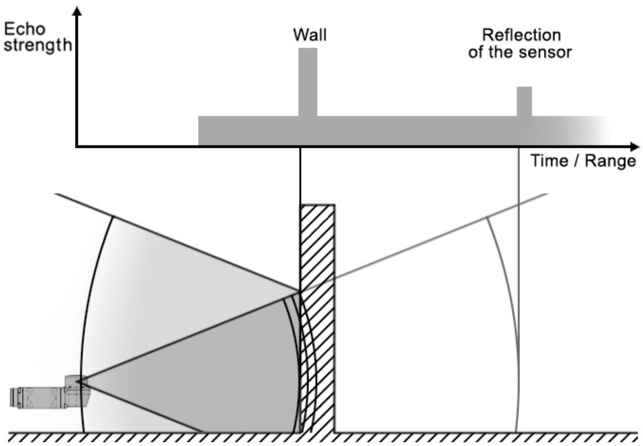

Fig. 4.6 Acoustic beam reflected by a wall.

to data obtained in a small water tank, illustrates this. Reflections are easily distinguishable as vertical lines at about 12 meters from the center of the image, while the real tank boundaries are placed at about 4 meters. Note also that the small high intensity shapes placed in between actually correspond to reflections produced by the vehicle carrying the MSIS.

4.3 Measurement Perturbations

Besides the phantoms, reflections and other acoustic artifacts present in the acoustic images, the measurements from the imaging sonar are also affected by noise. On the one hand, the background (or ambient) noise perturbing the sonar measurements is a result of the combined action of multiple sources which may exist in underwater environments: hydrostatic effects of waves or currents, seismic activity, non-homogeneous pressure distributions, ship traffic and even marine animals are only some examples. On the other hand, the perturbations may also come from the underwater vehicle itself, for instance in the form of vibrations from the thrusters or as a result of currents generated into the transducer. Noise can also be originated within the sensor itself. A clear example of this is the transient ringing which occurs at the transducer head as a result of the pulse being emitted through the housing (see the high intensity spot in the center of the scan in Figure 4.2). In addition, there are other effects, such as the attenuation suffered by the acoustic signal while travelling through the medium or the imprecision in the position of the measurements caused by the beam form which contribute to the degradation of the resulting data and complicate its interpretation.

It is worth noting that some of these perturbations are attenuated by the sensor itself. The transducer is generally designed to offer maximum sensitivity at a

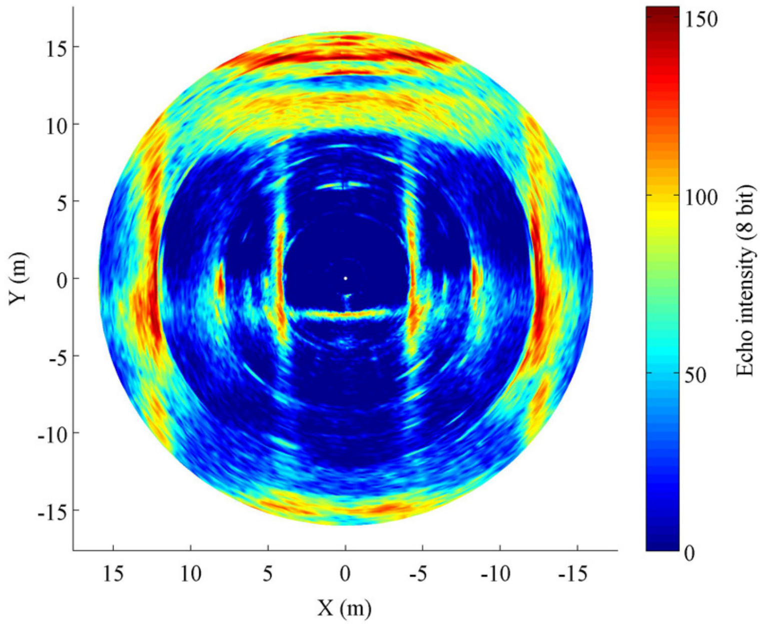

Fig. 4.7 Reflections on a scan obtained in a water tank.

particular frequency, which means that it has a lower sensitivity for noises outside this frequency. Moreover, most hardware performs some kind of signal extraction through filtering and thresholding to separate the signal from any noise. However, despite signal processing, it is impossible to completely remove the effect of noise in the measurements. In fact, according to the Central Limit Theorem, which states that the sum of a large number of independent random variables will be approximately normally distributed [110], we can assume that the resulting measurements will be perturbed by a Gaussian noise.

Therefore, a feature extraction algorithm will have to deal not only with these noisy measurements but also with the presence of phantoms, reflections and other sonar artifacts. This makes it necessary to establish an explicit representation model of the measurement precision, as well as robust mechanisms to deal with spurious data. Both aspects are considered in the following chapters.

4.4 Peculiarities of the MSISs

The basics for acoustic image interpretation have already been introduced. There are, however, some particular characteristics of the MSISs which, although habitually overlooked, should be taken into account to obtain optimal results.

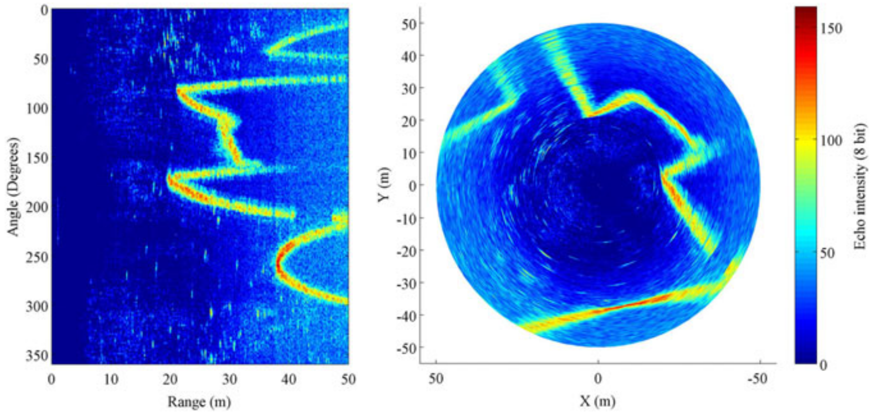

(a) Raw data represented in polar.

(b) The same data in cartesian.

Fig. 4.8 Different representations of MSIS data obtained in a marina.

4.4.1 Polar Sensor Representing a Cartesian Space

The acoustic data from an MSIS is usually represented as an image generated in a cartesian coordinate system because it is easier for a human observer to interpret the information it contains in this form. However, given the nature of the measurement process, the sensor is, in fact, a polar sensor. Figure 4.8 shows the raw polar data as it is obtained from the sensor and its corresponding representation in a cartesian space. One important consequence is that, with the increment of range, a loss in the measurement resolution occurs because the bins are more dispersed as a result of the angular aperture between consecutive beams. This effect, which is inherently represented in polar, will produce gaps between the beams in the cartesian image. To avoid this, different strategies can be carried out to fill the discontinuities in the image. However, it is recommended whenever possible to work with the raw polar measurements instead of using a cartesian image, since the change of representation may alter the original data.

4.4.2 Continuous Dataflow

The majority of the sensors typically used in localization and SLAM produce discrete amounts of information which can be treated as independent entities (e.g., images from cameras, scans from laser range finders or scans from sonar rings). This is possible because the measuring process of these sensors is very fast or even instantaneous. In the case of MSISs, the information is not gathered instantaneously but by means of a rotatory transducer head that needs a considerable amount of time to complete a turn. Since this rotation is continuous, the resulting data is not naturally split into separate subsets and hence is also continuous. A naive approach when working with MSIS data is to divide it into a sequence of independent 360° scan sectors. This is not an optimal procedure for many reasons. First, the division is totally arbitrary and serves no other purpose than providing a way to independently operate chunks of data. Second, the 360° scan sectors are produced at a very low rate. Finally, the first and the last beams in the scan are usually placed near each other but a considerable time lapse separates the instants in which they were obtained. As a result, when either the environment or the vehicle's position change, the generated acoustic image can eventually present a discontinuity. Better alternatives to manage continuous data include using data buffers, analyzing smaller scan sectors or even using the data beam to beam as soon as they are measured. Some examples of operating with data from MSISs will be the subject of further discussion in Chapters 5 and 6.

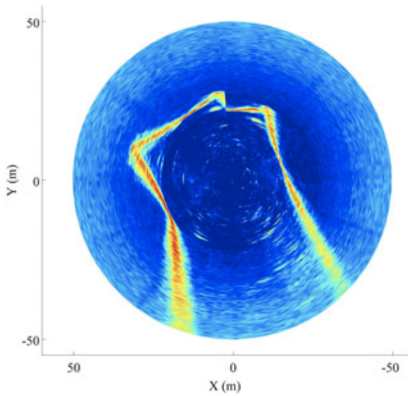

(a) Image generated from raw sensor data.

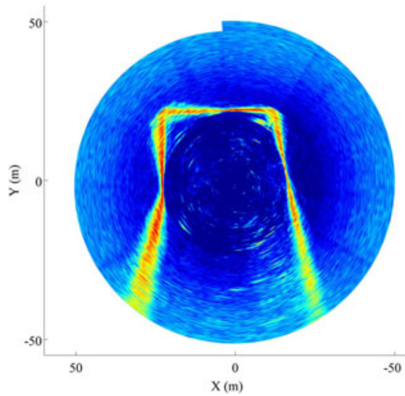

(b) Image after undistorting the data.

(c) Zenithal view of the real scenario.

Fig. 4.9 Effect of the vehicle motion on the acoustic images.

4.4.3 Motion Induced Distortions

As stated previously, an MSIS transducer head usually needs a considerable period of time to perform a 360° rotation. In the case of the Tritech Miniking imaging sonar, the minimum time necessary to complete a scan is about 6 seconds (mechanical limit); although, depending on the settings (in particular, the range), it can increase drastically (e.g., a 50 meter range setting requires about 15 seconds to complete a scan). This is an important issue that has to be taken into account when operating with an MSIS mounted on a submersible, since the resulting acoustic images can become distorted as a consequence of the vehicle's motion. Generally, this effect can be ignored for low velocities. For higher velocities, however, it is vital to have a suitable localization method (a dynamics model, dead-reckoning sensors, SLAM, etc.) to provide the necessary position feedback to un-distort the data. It is important to note that distortions are the consequence of the combined action of both translational and rotatory movements and that their influence may vary depending on the typology of the vehicle. For instance, survey vehicles (torpedoes, flat-fish vehicles, etc.), which generally move along straight paths at considerable speeds, will be more prone to suffer translational distortions. On the other hand, hovering vehicles, like the Ictineu, generally move at lower speeds but have the capability to perform quick rotations, being more sensitive to angular distortions. The image in Figure 4.9(a) shows a cartesian representation of the acoustic data obtained with the Ictineu vehicle during a test in a marina environment. Since the motion has been ignored during the generation of the image, an important distortion appears. Figure 4.9(b) presents the same dataset represented along the trajectory performed by the vehicle during the acquisition. As can be observed, when comparing it with the aerial image of the test scenario in Figure 4.9(c), the distortion in the second image is almost completely cancelled, obtaining a more accurate representation.

Chapter 5
Localization with an *a priori* Map

This chapter concerns the use of MSIS to solve the localization problem for an underwater vehicle navigating in a structured environment when an *a priori map* is available. The initial objective of this work was to develop a system to locate the Ictineu AUV within the square water tank which served as the theatre of operation during the SAUC-E competition. The availability of such a localization system made it possible to pre-define a series of waypoints to be followed by the vehicle and therefore optimize the exploration of the scenario in search of the various necessary targets to accomplish the proposed tasks. However, solving the navigation problem for an AUV moving in a water tank was not only useful for the SAUC-E competition. Further work has been undertaken to develop improved localization algorithms to work under laboratory conditions, since we believe that such a system opens the door to further advanced control experiments.

Section 5.1 reviews different strategies to perform data association in localization problems, while Sections 5.2 and 5.3 present two map-based localization methods developed for the competition. The first is a simple algorithm which determines the vehicle's position by means of a voting strategy, while the second relies on an EKF to merge the information from several sensors and the tank map. A third method, which combines several aspects of the two other algorithms to improve the estimation process, is presented in Section 5.4. The chapter concludes with a summary of the advantages of the different methods and some guidelines for further work.

5.1 Data Association and Localization

A key aspect of a localization system is solving the data association, i.e. finding the correspondences between the sensor measurements and the elements contained in the map. Many authors have studied this problem with the objective of improving localization systems, but also as a necessary step to obtain a robust SLAM solution capable of relocalizing the vehicle when it gets lost or suffers large odometry errors. A particularly difficult situation is the global localization problem, also known as the "kidnapped" robot problem, where no previous estimate of the vehicle's position is available and only the information from the onboard sensors can be used

D. Ribas et al.: Underwater SLAM for Structured Environments, STAR 65, pp. 47–75.
springerlink.com © Springer-Verlag Berlin Heidelberg 2010

to determine its position [22]. The techniques to perform this data association can be divided between those that analyze the pose space and those that analyze the correspondences between the measurements and the map.

In the first approach, a set of candidate vehicle positions is considered and rated according to the evidence presented by the sensor measurements. The hypothesis presenting a better consistency between the measurements and the map is the one that corresponds most closely to the vehicle's real position. Different methods are used to represent the space of possible vehicle positions. One example is the Monte Carlo localization [43, 126], which addresses the problem by sampling a set of random vehicle locations covering the entire area and computing the likelihood of each position. An alternative is using grid sampling, such as Markov localization [44, 9], where the map is represented as an occupancy grid in which each cell represents a particular vehicle position. The cost of this kind of algorithm is proportional to the size of the map (number of particles or cells in the grid).

In the second approach to the data association problem, the process consists of defining a set of hypotheses for the pairings between the sensor measurements and the features in the map. The hypothesis with the largest number of consistent matches should define the correct vehicle position. The cost of this method depends on the size of the correspondence tree. To limit the complexity of the search, different approaches have been developed such as the use of simple geometric constraints [50], the hypothesize and test technique [76], branch and bound algorithms [18], graph theory [3], random sampling [91] and voting [102].

In the context of the present work, different examples can be found for the localization of underwater vehicles operating in structured environments. In the Autonomous System Laboratory of the University of Hawaii, range measurements gathered with a set of fixed-bearing sonar beams were used to update a Kalman filter and estimate the position of the vehicle in a water tank [97]. Using this system, and thanks to its omni-directionality, Odin AUV can navigate keeping its relative orientation with respect to the walls of the water tank. A more elaborate system is described in [10] where a profiling sonar is used to track the walls of the water tank and hence the robot is allowed to change its heading freely. In a previous work, our team solved this problem using a coded pattern lying on the bottom of a water tank together with a real-time vision system able to provide accurate absolute position estimates at 12 Hz [14]. An example of a real application can be found in [65], where a localization system makes the autonomous inspection of a breakwater possible.

5.2 Voting-Based Localization Method

The localization system described here, was initially conceived as a method to determine the position of the Ictineu AUV within the SAUC-E water tank during the initialization phase of the Kalman filter-based localization algorithm presented in Section 5.3. However, preliminary tests showed its potential and we soon realized that it could become a localization system on its own. Moreover, the fact that this method was already required as part of the alternative algorithm together with the strict time constraints set by the competition prompted the team to finally implement it in the vehicle's software architecture while making the necessary minor changes to convert the method into a full localization algorithm. Due to its simplicity of operation and proven reliability, it became our final choice for positioning the vehicle during the competition.

5.2.1 Voting Algorithm

The method presented here determines the vehicle's position by exploring the correspondence between the measurements and the elements of the scenario using a voting-based strategy. This algorithm only requires an *a priori* map and the measurements from an MSIS, a compass and a pressure sensor to locate the vehicle within a particular environment. The map, the MSIS and the compass are used to determine the vehicle's heading and position in the horizontal plane while the pressure sensor is sufficient to estimate its vertical position, as the measurements provided by the sensor are directly related with the depth at which the vehicle is operating. For the purpose of this work, only square-shaped scenarios were taken into account to test the algorithm. However, there are no particular restrictions limiting the use of this algorithm to such scenarios and it is assumed that the algorithm would be able to work in more complex environments.

The acoustic image in Figure 5.1(a) illustrates the type of data we can expect when working in a water tank. Note that the range of the sensor has been set to approximately half of the longest tank dimension, which makes it possible to observe a great part of the tank from most of the vehicle's positions while avoiding the appearance of reflections in the image. The objects (walls) present in the vicinity of the sensor appear in the image as elongated zones populated with high intensity echo

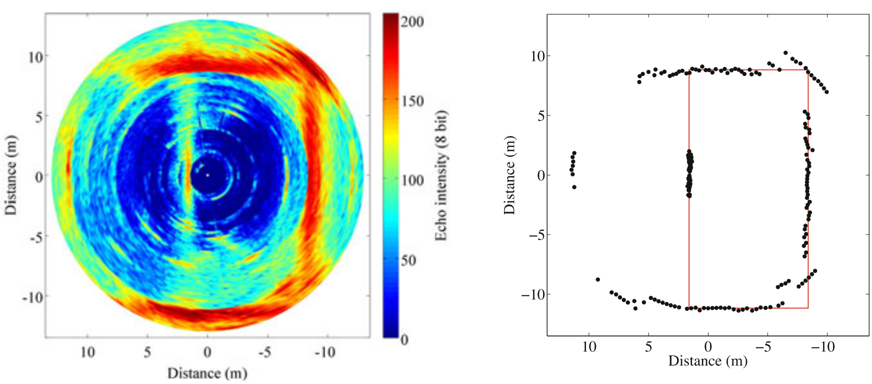

(a) Acoustic image obtained in the SAUC-E water tank during the competition.

(b) Resulting set of bins after selecting those with the highest intensity (tank walls in red).

Fig. 5.1 Selection of the most representative bins.

returns (shapes in red). In order to reduce the number of bins involved in the process and consequently, to improve the overall computational efficiency, only those bins which are the global maximum of each beam are selected. Moreover, a threshold is applied to select those with an intensity value high enough to correspond with the detection of a real object, discarding the less significant ones. In Figure 5.1(b) the selected bins appear as small black dots. For reference, the real water tank boundaries are represented by a rectangle in red. The majority of the selected bins are expected to match the real position of the water tank walls. Therefore, it is possible for a set of bins, regardless of ghosts and reflections in the acoustic data, to reach a consensus and determine the true position of the tank limits, and reciprocally localize the vehicle. In the present algorithm, this consensus is determined by means of an adapted version of the Hough transform [28, 4]. The classical implementation of the Hough transform is a voting algorithm for line feature extraction used in digital image processing. However, for this particular application, it has been modified to identify the position of the vehicle inside the water tank area.

The first step of the procedure is using the information from the *a priori* map to define a discretized space representing the environment (tessellation of the water tank area). The goal of this grid model of the water tank is to accumulate evidence regarding the actual vehicle position in the form of votes. At the end of the voting process, the cell with the highest number of votes will be chosen as the most likely to correspond with the current vehicle position. The set of high intensity bins previously selected are responsible for determining where the votes should be assigned in the voting space. Assuming that the orientation of the water tank is known and that the vehicle is equipped with a compass, it is possible to obtain the angle between the vehicle and the tank. Furthermore, the position of any bin with respect to the vehicle's frame is totally determined by the range and bearing measurements provided by the sensor. Therefore, for each single bin and given all this information, a search for compatible vehicle locations is carried out. Every candidate position should accomplish two conditions. First, the bin associated with the position must overlap the boundaries of the tank at some point. Second, the vehicle must be placed within the limits of the tank. The compatible vehicle positions that meet the two conditions describe a particular L-shaped zone which can be easily determined. Figure 5.2(a) depicts a schematic representation of this process. In the voting space, each one of the cells corresponding to the described locus will receive one vote. If this is repeated for all the selected high intensity bins from a complete scan, the accumulation of votes will result in a voting space such as the one represented in Figure 5.2(b). In the example, the cell with the highest number of votes appears in dark red and matches the real vehicle position, as can be observed by comparing the result with the central point on the original scan in Figure 5.1(a).

5.2.2 Dealing with Continuous Acoustic Images

In order to determine the position of the vehicle, this algorithm needs to have a sufficient amount of information available. It is not unusual to find situations in which the vehicle's vantage point results in limited observation of the scenario. For this

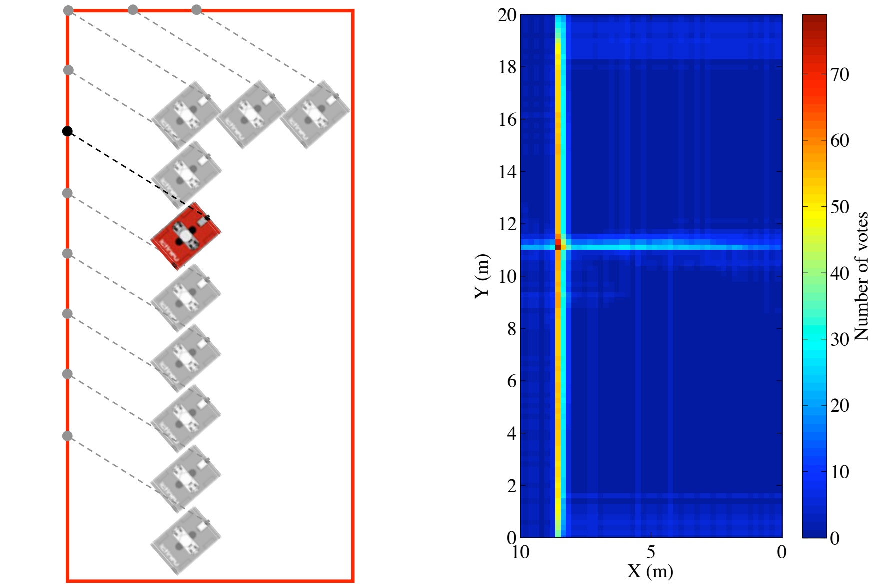

(a) Locus of all the possible vehicle positions assuming that the measured bin corresponds with a tank wall.

(b) Resulting voting space after assigning all the votes produced by a set of bins from a complete 360° scan.

Fig. 5.2 Voting process for vehicle localization.

reason, extracting high intensity bins from a 360° scan sector is usually a good approach. Another important aspect is the frequency at which these scan sectors are obtained. As stated in Chapter 4, the range setting of the sensor is one of the factors directly related with the amount of time necessary to produce a complete scan. A good option is to choose the shortest range possible (about half of the longest dimension of the tank). However, even when working at their shortest range configuration, MSISs usually need a considerable period of time to obtain a scan (e.g. the Miniking has a lower time limit of about 6 seconds). To summarize, using 360° scan sectors for the voting process is desirable but usually obtaining such scans takes a lot of time and, as a result, the vehicle position estimates can only be produced at a low frequency. In order to overcome this disadvantage, a simple modification has been implemented in the algorithm: the new beams produced by the sensor are accumulated by means of a data buffer so, at any moment, the information from the most recent 360° scan can be recalled to produce a new voting and determine the actual position of the vehicle. As new areas are explored with each beam arrival, new bins are added to the data buffer. Simultaneously, older bins falling outside the considered scan sector are removed. In other words, instead of interpreting the sonar measurements as a discrete sequence of consecutive“acoustic images”, they are treated as a continuous dataflow from which it is possible to instantaneously, and at any desired frequency, recover the most recent “snapshot” of the environment.

5.2.3 Managing Compass Errors

Another important modification of the present algorithm is a method to adapt the voting process to possible angular errors. As mentioned before, a compass is used to determine the current vehicle orientation with respect to the water tank. However, one should expect magnetic disturbances to affect the sensor when the vehicle navigates through scenarios where the presence of ferro-magnetic elements is not uncommon (e.g. wire meshes inside the concrete walls of a water tank). An error in the estimation of this angle will be transmitted to the localization process as an incorrect allocation of the votes in the voting space. The example in Figure 5.3(a) represents a set of bins affected by this error (black dots), that are misaligned with respect to the real water tank position (red rectangle). The relative positions of three particular bins and the vehicle have been represented with dashed lines of different colors. In the scheme in Figure 5.3(b), the places that will receive the votes for each one of these three bins are represented with solid lines. Note that since all three bins correspond to the same wall on the right, the three vertical sections should overlap. However, instead of overlapping, the votes are spread over three parallel vertical zones as a result of the misalignment caused by the angular error. Figure 5.3(c) shows the resulting voting space after using all the selected bins, with the majority of the votes spread over a wide area. Of course, such a space cannot produce a reliable position estimate.

The strategy to address this issue is simple and effective. First, it is assumed that some angular error is affecting the entire set of voting bins. The exact value of this error is unknown but is assumed to be bounded. Then, instead of performing the voting in a single space, several spaces are taken into account. These spaces are identical except for the fact that different error values are used to correct the relative vehicle-map angular measurements employed during the voting in each space. As a result, a set of voting spaces with different error assumptions is obtained (those in Figures 5.2(b) and 5.3(c) can be taken as examples of the kind of spaces that are obtained). Next, a search for the vehicle position estimate is carried out, first by selecting the candidate with the maximum number of votes from each one of the different spaces and then choosing the overall most voted candidate (see Figure 5.4). The reason behind this process is simple. A great accumulation of votes implies that the bins are perfectly aligned with the boundaries of the water tank. Therefore, the voting space that contains the candidate position with the maximum number of votes has to be the one with the angular error assumption that best matches the discrepancy in the real system. For instance, the winning candidate position in Figure 5.3(c) has only 31 votes as a result of a bad angular error assumption that is not able to correct the misalignment in the voting bins. This contrasts with the space obtained in Figure 5.2(b), where a correct assumption in the error is able to produce a winner with 79 votes. It is worth noting that working with multiple voting spaces is computationally less efficient than performing the voting for all the error hypotheses in a single space. However, using a single space would offer a more dispersed solution as a consequence of placing votes with wrong hypotheses. Moreover, without the possibility of discriminating the effect of combined false assumptions from the

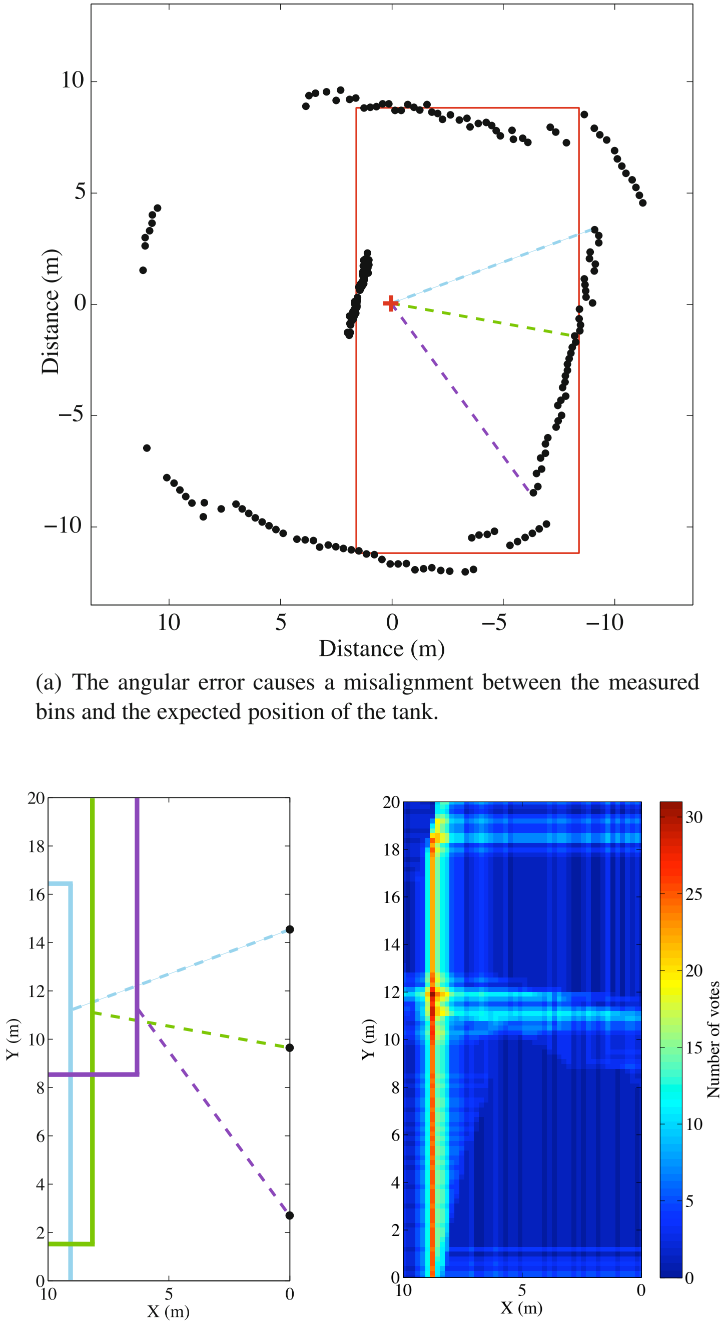

(a) The angular error causes a misalignment between the measured bins and the expected position of the tank.

(b) The effect of voting with misaligned bins.

(c) Resulting voting space after voting with misaligned data.

Fig. 5.3 Voting with an angular error.

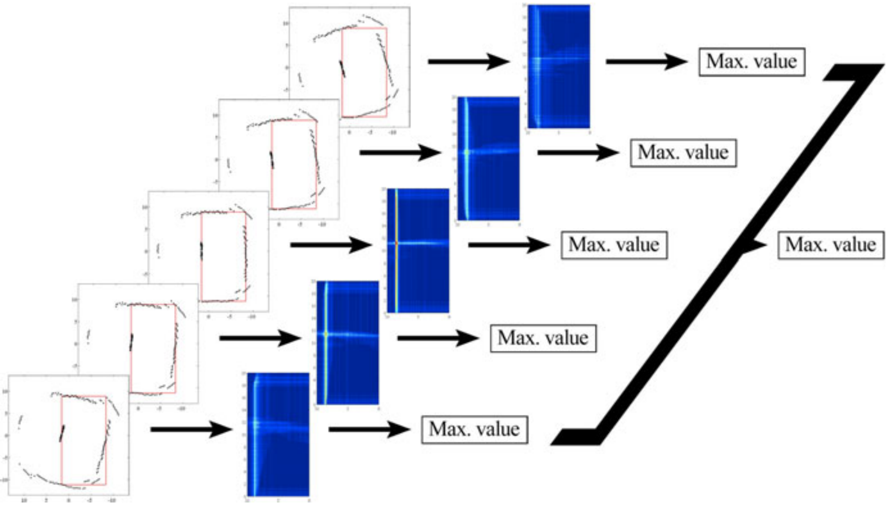

Fig. 5.4 Voting in multiple spaces with different angular error hypotheses.

accumulation of votes due to the correct hypothesis, this method would present a considerable risk of producing false position estimates.

5.2.4 Discretization of the Voting Space

One of the key issues while implementing the voting algorithm is to select a correct grid resolution when defining the discretized voting space. Choosing a large cell size will reduce the resolution of the space and hence the precision of the measured positions. On the other hand, choosing a smaller cell size increases the computational cost of the algorithm, especially when dealing with angular errors, as several voting spaces are used simultaneously. A good initial assumption is choosing a grid resolution comparable to the actual resolution of the acoustic images generated by the MSIS (distance between consecutive bins). However, there are situations where taking a smaller resolution will have some benefits. One of these situations is when the vehicle is moving at a high speed and the bins gathered during a 360° scan are obtained from significantly different positions. Consequently, when a voting is performed with those bins, their votes are placed according to the position of the vehicle at the moment when the measurement takes place. This is reflected in the voting space as a dispersion of the votes along the vehicle's path and produces an unpredictable outcome in the final position estimate. It is worth noting that the present algorithm cannot estimate the vehicle's motion during the acquisition of the bins and thus it is not possible to correct this issue in the voting process. However, if the resolution of the voting space is reduced, the uncertainty produced by this effect can be confined in a bigger cell size. Of course, position measurements will also have a lower resolution but will benefit from a steadier behavior.

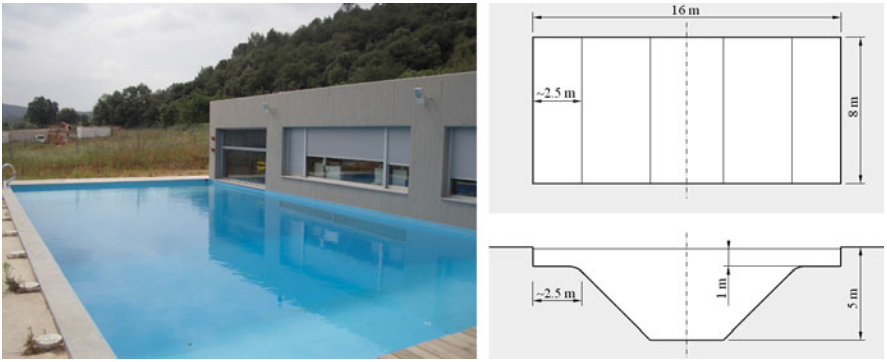

Fig. 5.5 CIRS water tank at the Unversity of Girona.

5.2.5 Experimental Results

In this section, two examples of the algorithm running in real environments are presented. The first corresponds to an experiment executed under laboratory conditions that will be used throughout this chapter as a benchmark to compare the different localization methods. The second corresponds to real data obtained during the final run of the SAUC-E competition.

5.2.5.1 CIRS Water Tank Test

This experiment took place in the water tank at the *Centre d'Investigació en Robòtica Submarina* (CIRS) at the University of Girona (Figure 5.5). Although the Garbi vehicle was used to obtain the dataset, it can be considered as equivalent to a set obtained with the Ictineu vehicle since both share compatible sensor suites. The dataset is formed by measurements from the MSIS and the DVL (which includes a compass and a pressure sensor, as explained in Section 3.6.2). The MSIS was set to a range of 10 m and a resolution of 0.1 m (100 bins per beam) and was able to produce a complete 360° scan sector in about 6.6 s (0.15 Hz). During the experiment, the vehicle was operated to perform a trajectory in the deepest part of the water tank. Starting from the center, it went to one side near to the water tank wall and then described a roughly square-shaped loop. The algorithm was set to perform votings with 360° scan sectors at a frequency of about 0.3 Hz (i.e. each time a new 180° scan sector was obtained). The chosen resolution of the discretized space was 0.1 m. Figure 5.6 shows the measured positions (red dots) and the resulting estimated trajectory (line in black). No ground truth was available to validate the results; however, they seem consistent with the actual path followed by the vehicle. Although the algorithm exhibits a high level of reliability, a single erroneous position measurement was obtained during the execution of the algorithm. This was mainly because of the sonar readings produced by the slanted walls limiting the deepest zone of the water tank. During the voting, the algorithm expects the selected bins to correspond

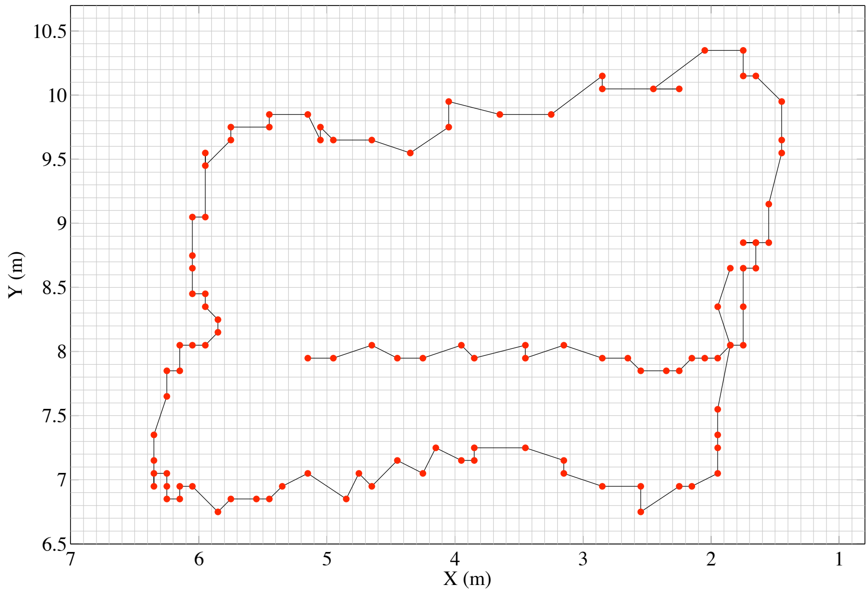

Fig. 5.6 Trajectory obtained with the voting-based localization algorithm for the experiment performed in the CIRS water tank.

with the outer limits of the water tank and, as no alternative strategy was defined for such measurements, they are erroneously assigned producing a false position estimate. Typically, the bins corresponding with the slanted walls represent a small portion of the total, so the correctly placed votes prevail and generally a correct position is produced. Nevertheless, erroneous position measurements are not an issue as they are infrequent and easily detected as outliers when their distance to previous position estimates is compared.

5.2.5.2 SAUC-E Final Run

The results presented in this section were produced with sensor data gathered by the Ictineu AUV during its performance in the SAUC-E 2006 competition final. The run took place in the water tank of the Underwater Stage at Pinewood Studios in Buckinghamshire (United Kingdom) and consisted of a sequence of tasks to be accomplished autonomously by the vehicle (Figure 5.7). First, the vehicle started from the release point and had to submerge and pass through a validation gate. Then, a cross target lying on the bottom of the tank had to be found and a marker dropped over it. A second target, an orange buoy, had to be located and impacted with the frame of the vehicle. Finally, the vehicle had to end the mission by surfacing at a designated recovery zone marked by an acoustic device. During the final run, the

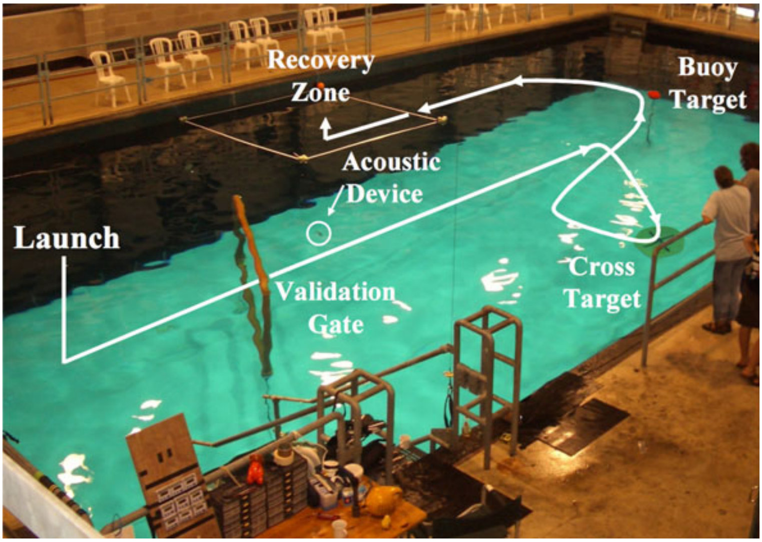

Fig. 5.7 Water tank at the Underwater Stage of Pinewood Studios with all the elements comprising the setup for the SAUCE competition.

Ictineu AUV attempted all four tasks. With two of them partially achieved and two more successfully completed, our team gained the final victory.

A version of the voting-based localization algorithm was implemented in the Ictineu AUV in order to provide position feedback to the software architecture during the competition. To reduce the cost of the algorithm and free resources for other tasks that were running simultaneously, the voting space grid resolution was set to 0.5 m. This decrease in precision did not represent any problem as the purpose of the localization system was to drive the vehicle to particular zones of the water tank rather than to position it in a precise spot. Moreover, the reduction in cost made it possible to increase the system's output rate to a frequency of 2 Hz. Unfortunately, it was not possible to record the trajectory estimation obtained by the algorithm during the execution of the mission. In spite of this, the data loggers were able to record the measurements from all the sensors and thus the estimated path could be post-processed. Figure 5.8 represents the resulting trajectory. It is worth noting that a voting space resolution of 20 cm had been used during the generation of this trajectory in order to represent more accurately the path actually followed by the vehicle during the run. In fact, it is sufficiently accurate to be able to observe how the vehicle moves through the validation gate, hovers over the cross target to release a marker, attempts to impact with the buoy and finally moves towards the recovery zone. For reference, the estimated trajectory can be compared with the one appearing in the video in [57], which corresponds to the actual run performed by the Ictineu during the final.

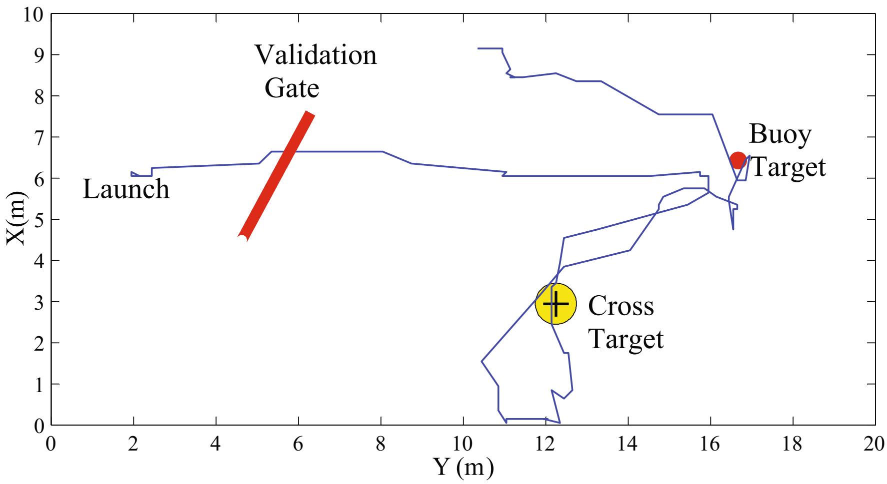

Fig. 5.8 Trajectory performed by the Ictineu AUV during the final run of the SAUC-E 2006.

5.3 EKF-Based Localization Method

This second proposal relies on an EKF to estimate a state vector containing the position and velocity of the vehicle. A simple kinematic model allows the state to be predicted at any moment while the information from different sensors is used to update it. In addition to the compass and the pressure sensor, a DVL sensor is incorporated to provide direct measurements of the vehicle's velocities. The MSIS together with an *a priori* map produce information regarding the absolute position of the vehicle within the environment. This approach defines the *a priori* map as a set of line features representing the planar objects present in the scenario (in the application at hand, the four vertical walls delimiting the water tank). Then, the readings from the MSIS are analyzed beam to beam in order to determine the bin with the highest echo-intensity return. Again, the assumption is made that this bin should correspond to a feature in the map. Therefore, after determining the bin-line feature correspondence, the discrepancy between their positions in the space is used to update the current vehicle position estimate.

5.3.1 Defining the Map

The *a priori* map of the environment $\mathscr{M}$ is defined as a set of n line features:

$$\mathscr{M} = \{\mathbf{l}_1, \mathbf{l}_2, \ldots, \mathbf{l}_n\}.$$

Each line describes the horizontal cross section of a vertical planar structure (e.g. walls of the water tank as seen from a zenithal point of view) and is represented by its *rho-theta* pair as:

$$\mathbf{l}_n = [\rho_n \, \theta_n]^T$$

which represents the perpendicular distance from a line feature to a common base reference B. The position of this base reference is arbitrary. However, placing it in one of the corners of the water tank – aligned with the direction of the walls– is usually a good choice, as the definition of line parameters would be straightforward. The origin is placed at the water level and the Z axis points downwards. In other words, anything placed below the water surface receives a positive value on its Z coordinate. It is worth noting that the β angle representing the orientation of the base reference B (i.e. orientation of the water tank) with respect to an earth fixed reference frame E must be known when working with a compass in order to integrate its measurements. This issue will be discussed in Sections 5.3.3 and 5.3.5. A representation of the map and the different reference frames can be seen in Figure 5.9

5.3.2 State Vector

The state vector contains information regarding the position and velocity of the vehicle at time k:

$$\mathbf{x}(k) = [x \; y \; z \; \psi \; u \; v \; w \; r]^T$$

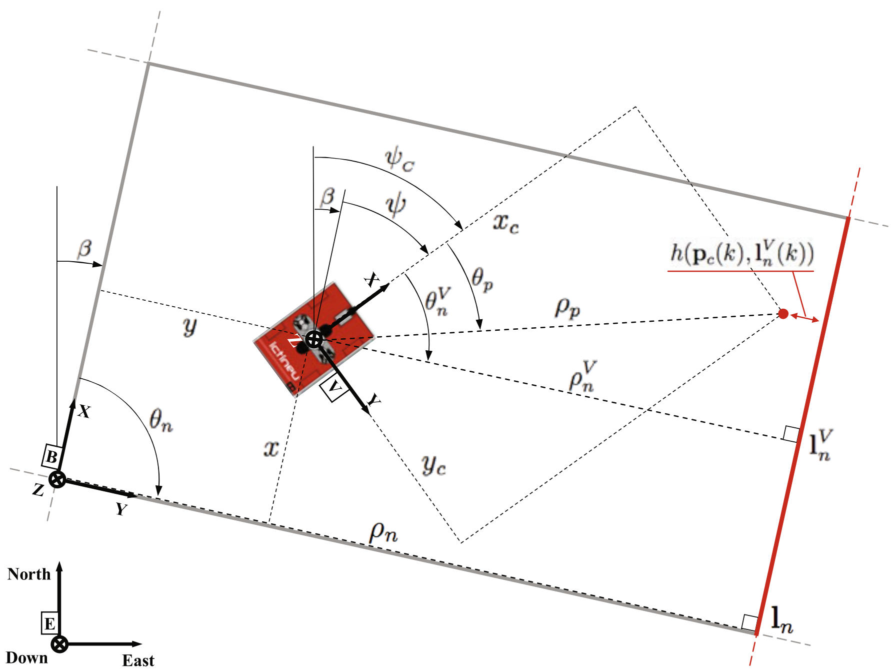

Fig. 5.9 Representation of the different elements involved in the localization method.

where, following the nomenclature proposed in [42], the vector $[x\ y\ z\ \psi]$ represents the position and heading of the vehicle in the local base reference B, while $[u\ v\ w\ r]$ are the corresponding linear and angular velocities represented on the vehicle's coordinate frame V.

Our vehicles are passively stable in *roll* and *pitch*. Although small angles ($< 2°$) can occur, their effect on the sonar readings can be ignored since the large vertical beamwidth (see Figure 4.5) makes it possible to detect objects which are not aligned with the axis of the beam. For this reason, their corresponding angles and velocites have not been included in the state vector.

5.3.3 Initializing the Filter

The initial value of the state vector $\mathbf{x}(0)$ should be estimated before starting the Kalman filter. As mentioned previously, the voting algorithm described in Section 5.2 was originally designed for this task. The process begisn with the obtention of a complete 360° scan with the MSIS and the corresponding angular measurements from the compass. After defining a voting space according to the *a priori* information of the scenario, this set of measurements is used to perform a vote. The winning candidate will determine the situation of the vehicle within the tank. Therefore, it can be used to initialize the estimated XY vehicle position in the state vector. As this value represents a measurement relative to a fixed base reference, some level of uncertainty has to be considered. One alternative for assigning this initial value is using a filter to estimate the position of the vehicle with the measurements that have been previously associated in the vote. However, the results obtained with this method tend to be optimistic. Here, a simpler alternative is chosen.

The uncertainty is set according to the precision of the voting process by taking into account the grid resolution used during the estimation of the initial position. Although taking this resolution to set the standard deviation of the position is a good approach, adopting a slightly larger value is usually recommended in order to cope with unexpected errors. Obtaining the initial values for the depth and the heading of the vehicle is much easier as these values can be directly measured with the outputs from the pressure sensor and compass. This time, the variance of this initial estimate will be determined by the sensor's accuracy. It should be noted that the vehicle heading ψ is referenced to the base reference B, while the angle measured from the compass is obtained with respect to magnetic north. Thus, the angle between the earth-fixed reference E and the base reference B must be taken into account when using the compass measurement to initialize the vehicle's heading. During the initialization phase, the vehicle is presumed to be static, as this makes the voting process for determining the vehicle position more reliable. Therefore, the velocities can be set to zero, along with their uncertainty, as a perfect knowledge of the variables can be assumed. The resulting estimate for the state vector at time 0 is:

$$\hat{\mathbf{x}}(0) = \begin{bmatrix} x_V \\ y_V \\ z_P \\ \psi_C - \beta \\ 0 \\ 0 \\ 0 \\ 0 \end{bmatrix}, \qquad \mathbf{P}(0) = \begin{bmatrix} \sigma_V^2 & 0 & 0 & 0 & 0 & 0 & 0 & 0 \\ 0 & \sigma_V^2 & 0 & 0 & 0 & 0 & 0 & 0 \\ 0 & 0 & \sigma_P^2 & 0 & 0 & 0 & 0 & 0 \\ 0 & 0 & 0 & \sigma_C^2 & 0 & 0 & 0 & 0 \\ 0 & 0 & 0 & 0 & 0 & 0 & 0 & 0 \\ 0 & 0 & 0 & 0 & 0 & 0 & 0 & 0 \\ 0 & 0 & 0 & 0 & 0 & 0 & 0 & 0 \\ 0 & 0 & 0 & 0 & 0 & 0 & 0 & 0 \end{bmatrix}$$

where the subindex V stands for the voting algorithm, P for pressure sensor, C for compass and β corresponds to the angle between north and the base reference B as represented in Figure 5.9.

5.3.4 System Model

A simple 4 DOF constant velocity kinematics model is used to predict how the state will evolve from time $k-1$ to time k:

$$\mathbf{x}(k) = f(\mathbf{x}(k-1), \mathbf{n}(k-1)),$$

$$\begin{bmatrix} x \\ y \\ z \\ \psi \\ u \\ v \\ w \\ r \end{bmatrix}_{(k)} = \begin{bmatrix} x + (uT + n_u\frac{T^2}{2})cos(\psi) - (vT + n_v\frac{T^2}{2})sin(\psi) \\ y + (uT + n_u\frac{T^2}{2})sin(\psi) + (vT + n_v\frac{T^2}{2})cos(\psi) \\ z + wT + n_w\frac{T^2}{2} \\ \psi + rT + n_r\frac{T^2}{2} \\ u + n_uT \\ v + n_vT \\ w + n_wT \\ r + n_rT \end{bmatrix}_{(k-1)} \tag{5.1}$$

where $\mathbf{n} = [n_u\ n_v\ n_w\ n_r]^T$ represents a vector of white Gaussian acceleration noises with zero mean. They are additive in the velocity terms and propagate through integration to the position. The covariance of the $\mathbf{n}$ vector is represented by the system noise matrix $\mathbf{Q}$:

$$E\left[\mathbf{n}(k)\right] = \mathbf{0}, \qquad E\left[\mathbf{n}(k)\mathbf{n}(j)^T\right] = \delta_{kj}\mathbf{Q}(k),$$

$$\mathbf{Q} = \begin{bmatrix} \sigma_{n_v}^2 & 0 & 0 & 0 \\ 0 & \sigma_{n_u}^2 & 0 & 0 \\ 0 & 0 & \sigma_{n_w}^2 & 0 \\ 0 & 0 & 0 & \sigma_{n_r}^2 \end{bmatrix}.$$

The model described in (5.1) is non-linear and therefore the prediction should be performed with the EKF equations (see Appendix A). This version of the filter linearizes the system model around the current estimate with the Jacobian matrices **F** and **W**:

$$\mathbf{F}(k) = \frac{\partial f}{\partial \mathbf{x}}(\hat{\mathbf{x}}(k),\mathbf{0}) = \begin{bmatrix} 1 & 0 & 0 & -\hat{u}T\sin\hat{\psi} - \hat{v}T\cos\hat{\psi} & T\cos\hat{\psi} & -T\sin\hat{\psi} & 0 & 0 \\ 0 & 1 & 0 & \hat{u}T\cos\hat{\psi} - \hat{v}T\sin\hat{\psi} & T\sin\hat{\psi} & T\cos\hat{\psi} & 0 & 0 \\ 0 & 0 & 1 & 0 & 0 & 0 & T & 0 \\ 0 & 0 & 0 & 1 & 0 & 0 & 0 & T \\ 0 & 0 & 0 & 0 & 1 & 0 & 0 & 0 \\ 0 & 0 & 0 & 0 & 0 & 1 & 0 & 0 \\ 0 & 0 & 0 & 0 & 0 & 0 & 1 & 0 \\ 0 & 0 & 0 & 0 & 0 & 0 & 0 & 1 \end{bmatrix},$$

$$\mathbf{W}(k) = \frac{\partial f}{\partial \mathbf{n}}(\hat{\mathbf{x}}(k),\mathbf{0}) = \begin{bmatrix} \frac{T^2}{2}\cos\hat{\psi} & \frac{-T^2}{2}\sin\hat{\psi} & 0 & 0 \\ \frac{T^2}{2}\sin\hat{\psi} & \frac{T^2}{2}\cos\hat{\psi} & 0 & 0 \\ 0 & 0 & \frac{T^2}{2} & 0 \\ 0 & 0 & 0 & \frac{T^2}{2} \\ T & 0 & 0 & 0 \\ 0 & T & 0 & 0 \\ 0 & 0 & T & 0 \\ 0 & 0 & 0 & T \end{bmatrix}.$$

5.3.5 Measurement Model

The vehicle is equipped with a number of sensors providing direct observations of particular elements of the state vector and hence a linear observation model can be used (see Appendix A). The general model for such measurements is written in the form:

$$\mathbf{z}(k) = \mathbf{H}\mathbf{x}(k|k-1) + \mathbf{m}(k)$$

where $\mathbf{z}$ is the measurement vector and $\mathbf{m}$ represents a vector of white Gaussian noises with zero mean affecting the observation process. The covariance of the $\mathbf{m}$ vector is represented by the measurement noise matrix $\mathbf{R}$:

$$E\left[\mathbf{m}(k)\right] = \mathbf{0}, \qquad E\left[\mathbf{m}(k)\mathbf{m}(j)^T\right] = \delta_{kj}\mathbf{R}(k).$$

The form of the observation matrix $\mathbf{H}$ changes according to the measurements obtained from the sensors. Different forms of the H matrix are presented below for each of the cases that can occur in our particular system:

Velocity: A DVL sensor produces velocity measurements in the 3DOF. Assuming a sensor coordinate frame coincident with the vehicle reference V, or at least a known transformation relating them, the velocity measurements can be taken as direct observations of the vehicle's velocities. Thus, the observation matrix $\mathbf{H}$ can be written as:

$$\mathbf{H}_D = \begin{bmatrix} 0 & 0 & 0 & 0 & 1 & 0 & 0 & 0 \\ 0 & 0 & 0 & 0 & 0 & 1 & 0 & 0 \\ 0 & 0 & 0 & 0 & 0 & 0 & 1 & 0 \end{bmatrix}, \tag{5.2}$$

and the covariance matrix of the measurement noise as:

$$\mathbf{R}_D = \begin{bmatrix} \sigma_{Du}^2 & \sigma_{Duv} & \sigma_{Duw} \\ \sigma_{Dvu} & \sigma_{Dv}^2 & \sigma_{Dvw} \\ \sigma_{Dwu} & \sigma_{Dwv} & \sigma_{Dw}^2 \end{bmatrix}.$$

Note that the covariance matrix is not diagonal. The reason behind these correlations is that the measurements provided by the DVL are not directly observed, but calculated from the projection of the vehicle's velocity onto the multiple beam axes of the sensor. More details on how to determine the measurement correlation can be found in Appendix B.

Depth: The measurements from a calibrated pressure sensor can be easily operated to obtain an estimation of the vehicle's depth (position in the Z axis). The resulting **H** matrix is:

$$\mathbf{H}_P = \begin{bmatrix} 0\ 0\ 1\ 0\ 0\ 0\ 0\ 0 \end{bmatrix}. \tag{5.3}$$

The variance of the depth measurement will be represented by:

$$\mathbf{R}_P = \sigma_P^2.$$

Heading: The compass measures the angle of the vehicle with respect to magnetic north. As the vehicle heading ψ in the state vector is referenced to the base frame B, the angle β (angle of the frame with respect to north) has to be subtracted from the compass reading to produce the measurement $\mathbf{z}_C$. The resulting angle can be used to update the state vector with the following **H** matrix:

$$\mathbf{H}_C = \begin{bmatrix} 0\ 0\ 0\ 1\ 0\ 0\ 0\ 0 \end{bmatrix}. \tag{5.4}$$

As the β angle is perfectly known as part of the *a priori* map, subtracting it from the compass measurement has no effect on the uncertainty. Therefore, the measurement noise $\mathbf{R}_C$ is represented by the variance of the compass:

$$\mathbf{R}_C = \sigma_C^2.$$

It is worth noting that, depending on the configuration of the system, different readings could happen simultaneously. For instance, the DVL sensor in the Ictineu vehicle (see description in Section 3.6.2) is also equipped with a compass and a pressure sensor. Therefore, each time a new output is produced by the device, not only should the velocities be updated but also the depth and heading estimates in the state vector. In order to deal with multiple measurements simultaneously, a composed form of the **H** matrix can be obtained by adding different rows from (5.2), (5.3) and (5.4):

$$\mathbf{H} = \begin{bmatrix} \mathbf{H}_D \\ \mathbf{H}_P \\ \mathbf{H}_C \end{bmatrix}, \qquad \mathbf{R} = \begin{bmatrix} \mathbf{R}_D & \mathbf{0} & \mathbf{0} \\ \mathbf{0} & \mathbf{R}_P & \mathbf{0} \\ \mathbf{0} & \mathbf{0} & \mathbf{R}_C \end{bmatrix}.$$

Another particularity of the system is that the DVL sensor is able to measure the velocity with respect to the ground as well as the relative velocity between the sensor and the water volume below. The first set of measurements is worthwhile as it represent a direct estimation of the movement of the vehicle with respect to a fixed reference. Unfortunately, some scenarios are particularly difficult (those in shallow water or where reverberations take place) and such velocity measurements are incorrect. On the other hand, water volume velocities do not seem to be so dependent on the environment as ground velocities. For this reason, although they are less accurate, they can be used to estimate the vehicle's motion. However, this can only be done in those situations where the water volume is static or, in other words, when no water currents are present. The Argonaut DVL has the capacity to determine the quality of the received signals automatically and provides a status value for the velocities. Accordingly, the measurements with a bad status are discarded before the update by removing the corresponding rows in (5.2).

5.3.6 Updating the Position Estimate

The process of estimating the vehicle's position from the integration of velocity measurements suffers from an inherent drift. To deal with this, the MSIS is used together with the *a priori* map $\mathscr{M}$ to correct the absolute vehicle position in the state estimate. This process is carried out each time a new single beam is obtained from the imaging sonar and begins with the selection of the bin with the maximum intensity value. This measurement represents a point in the space which is the most likely to evidence the presence of an object in the scene and, as a consequence, to correspond with a line feature in the *a priori* map. The information regarding the point-line pairing will be used to perform an update in the state estimate from the filter (see Figure 5.9).

The selected high intensity bin from the MSIS is produced in polar coordinates:

$$\mathbf{p}_p(k) = [\rho_p(k), \theta_p(k)]^T, \quad \mathbf{p}_p(k) = \hat{\mathbf{p}}_p(k) + \mathbf{u}(k)$$

where $\mathbf{u}$ is a zero mean white Gaussian noise affecting the sensor during measurement:

$$E\left[\mathbf{u}(k)\right] = \mathbf{0}, \qquad E\left[\mathbf{u}(k)\mathbf{u}(j)^T\right] = \delta_{kj}\mathbf{P}_p(k), \qquad \mathbf{P}_p(k) = \begin{bmatrix} \sigma^2_{\rho_p} & 0 \\ 0 & \sigma^2_{\theta_p} \end{bmatrix}.$$

To determine its correspondence with the line features composing the map, the first step is transforming the bin parametrization from polar to cartesian coordinates.

$$\begin{aligned} \hat{\mathbf{p}}_c(k) &= q(\hat{\mathbf{p}}_p(k)) \\ \begin{bmatrix} \hat{x}_c(k) \\ \hat{y}_c(k) \end{bmatrix} &= \begin{bmatrix} \hat{\rho}_p(k)\cos\hat{\theta}_p(k) \\ \hat{\rho}_p(k)\sin\hat{\theta}_p(k) \end{bmatrix}. \end{aligned}$$

The Jacobian of the non-linear q function is also obtained for further calculations concerning the measurement uncertainty.

$$\mathbf{J}_q = \frac{\partial q}{\partial \mathbf{p_p}}(\hat{\mathbf{p}}_p(k)) = \begin{bmatrix} \cos\hat{\theta}_p(k) & -\hat{\rho}_p(k)\sin\hat{\theta}_p(k) \\ \sin\hat{\theta}_p(k) & \hat{\rho}_p(k)\cos\hat{\theta}_p(k) \end{bmatrix}.$$

For the sake of simplicity, the sensor reference frame has been taken as coincident with the vehicle's reference frame V. Otherwise, the appropriate transformations (see Appendix C) should be carried out to represent the bin in cartesian coordinates in the V reference frame. The next step is to represent each one of the line features $\{\mathbf{l}_1, \mathbf{l}_2, \ldots, \mathbf{l}_n\}$ stored in the $\mathscr{M}$ map in the same V frame so they can be compared with the selected bin. The g function obtains the parameters for a line feature $\mathbf{l}_n$, originally defined in B, with respect to the position of the vehicle's frame stored in the current state estimate $\hat{\mathbf{x}}(k|k-1)$:

$$\begin{aligned} \hat{\mathbf{l}}_n^V(k) &= g(\mathbf{l}_n, \hat{\mathbf{x}}(k|k-1)), \\ \begin{bmatrix} \hat{\rho}_n^V \\ \hat{\theta}_n^V \end{bmatrix} &= \begin{bmatrix} \rho_n - \hat{x}\cos\theta_n - \hat{y}\sin\theta_n \\ \theta_n - \hat{\psi} \end{bmatrix}. \end{aligned}$$

As the map is assumed to be perfectly known, the uncertainty depends only on the vehicle state estimate $\hat{\mathbf{x}}$. Therefore, only the Jacobian of the g function with respect to the state is necessary:

$$\mathbf{J}_g = \frac{\partial g}{\partial \mathbf{x}}(\hat{\mathbf{x}}(k|k-1)) = \begin{bmatrix} -\cos\theta_n & -\sin\theta_n & 0 & 0 & 0 & 0 & 0 & 0 \\ 0 & 0 & 0 & -1 & 0 & 0 & 0 & 0 \end{bmatrix}.$$

With both the sonar return and the map in the same reference frame, an implicit non-linear measurement function h stating that the distance between them is zero and thus that the point belongs to the line can be defined (see Figure 5.9) [18]:

$$\begin{aligned} h(\mathbf{p}_c(k), \mathbf{l}_n^V(k)) &= \rho_n^V - x_c\cos\theta_n^V - y_c\sin\theta_n^V, \\ &= 0, \end{aligned}$$

with:

$$\begin{aligned} \mathbf{H}_1 &= \frac{\partial h}{\partial \mathbf{l}_n^V}(\hat{\mathbf{p}}_c(k), \hat{\mathbf{l}}_n^V(k)) = [1 \quad \hat{x}_c\sin\hat{\theta}_n^V - \hat{y}_c\cos\hat{\theta}_n^V], \\ \mathbf{H}_2 &= \frac{\partial h}{\partial \mathbf{p}_c}(\hat{\mathbf{p}}_c(k), \hat{\mathbf{l}}_n^V(k)) = [-\cos\hat{\theta}_n^V \quad \sin\hat{\theta}_n^V], \end{aligned}$$

where $\mathbf{H}_1$ and $\mathbf{H}_2$ are the Jacobians of the implicit measurement function h with respect to the selected bin and a particular line of the map.

Multiple hypotheses can be made relating the bin with the different n line features. To produce the update, one of them has to be chosen as valid. For this purpose, an Individual Compatibility (IC) test is performed for each hypothesis by means of the measurement equation presented as:

$$\begin{aligned} \mathbf{S} &= \mathbf{H}_1\mathbf{J}_g\mathbf{P}(k|k-1)\mathbf{J}_g^T\mathbf{H}_1^T + \mathbf{H}_2\mathbf{J}_q\mathbf{P}_p(k)\mathbf{J}_q^T\mathbf{H}_2^T, \\ D^2 &= h(\hat{\mathbf{p}}_c(k), \hat{\mathbf{l}}_n^V(k))^T\mathbf{S}^{-1}h(\hat{\mathbf{p}}_c(k), \hat{\mathbf{l}}_n^V(k)) < \chi^2_{d,\alpha}. \end{aligned} \tag{5.5}$$

Distance D^2 is the Mahalanobis distance [80]. The correspondence is accepted if the distance is less than $\chi^2_{d,\alpha}$, with α defined as the confidence level and $d = \dim(h)$. The Nearest Neighbor (NN) selection criterion determines that, among the pairings that satisfy (5.5), the one with the smallest Mahalanobis distance is chosen and the association hypothesis is accepted. If none of the pairings pass the test, the bin is considered as spurious and rejected. This association process ensures not only the correct association of the measurement but also allows the rejection of spurious data from the sonar image, such as those produced by multipath propagation or by the presence of other objects not represented in the map.

Having solved the data association, an update of the vehicle state estimate can be performed using the EKF equations for an implicit measurement function [18]:

$$
\begin{aligned}
\mathbf{K} &= \mathbf{P}(k|k-1)\mathbf{J}_g^T\mathbf{H}_1^T\mathbf{S}^{-1} \\
\hat{\mathbf{x}}(k) &= \hat{\mathbf{x}}(k|k-1) - \mathbf{K}\,h(\hat{\mathbf{p}}_c(k),\hat{\mathbf{l}}_n^V(k)) \\
\mathbf{P}(k) &= (\mathbf{I} - \mathbf{K}\mathbf{H}_1\mathbf{J}_g)\mathbf{P}(k|k-1)
\end{aligned}
$$

5.3.7 Experimental Results

This section presents results obtained with the EKF-based localization method for the CIRS water tank test previously presented in Section 5.2.5. In addition to the MSIS, compass and pressure sensor measurements already used in the previous method, the velocity measurements from the DVL were also employed. As mentioned in Section 3.6.2, the DVL can produce velocity measurements with respect to the ground and to the water. The reduced dimensions and the reflectivity of the concrete walls in the CIRS water tank make it a complex scenario in which to operate the DVL sensor. In consequence, a considerable number of measurements receive bad quality status and are rejected. Although bottom tracking velocities are generally more precise, water velocities are more reliable and the number of rejected measurements is lower. During this test, both velocity measurements were used to update the filter in order to obtain a better estimate. It is worth noting that using the water velocity measurements to estimate the vehicle movement is only possible when operating in scenarios were no currents exist and the water volume can be assumed as static. Otherwise, the system model should be adapted to account for the effect of water currents.

Figure 5.10 represents the trajectory obtained with the present EKF-based localization method (line in black). It can be observed that this trajectory is consistent with the one obtained with the previous method (line in red). For comparison purposes, the dead reckoning trajectory obtained by running the filter without performing the position updates with the MSIS measurements is also represented (dashed line in blue). As the position in the dead reckoning estimate is obtained only by integrating the velocity measurements, the process is inherently affected by drift. This effect is even more noticeable as a result of the important perturbations affecting the velocity measurements when operating in such an adverse scenario. On the other hand, when the MSIS measurements are contrasted with the *a priori* map and

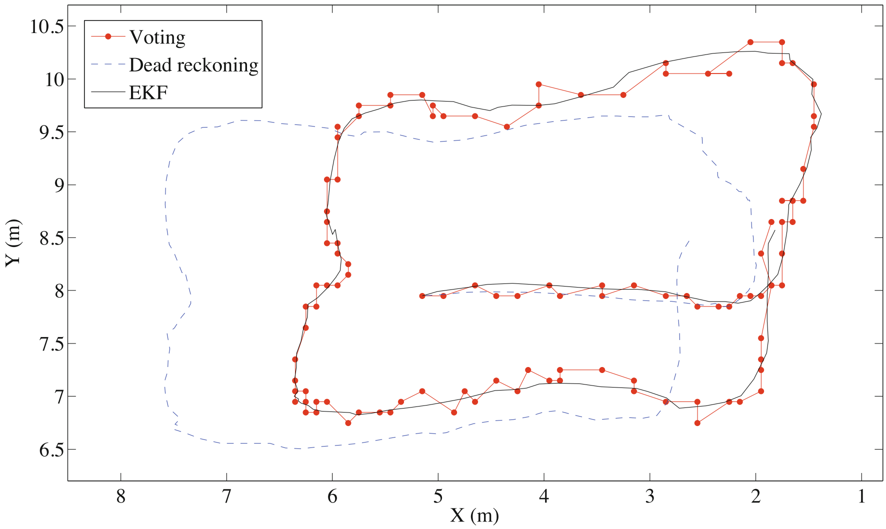

Fig. 5.10 Trajectory obtained with the EKF-based localization algorithm compared with trajectories obtained with other methods.

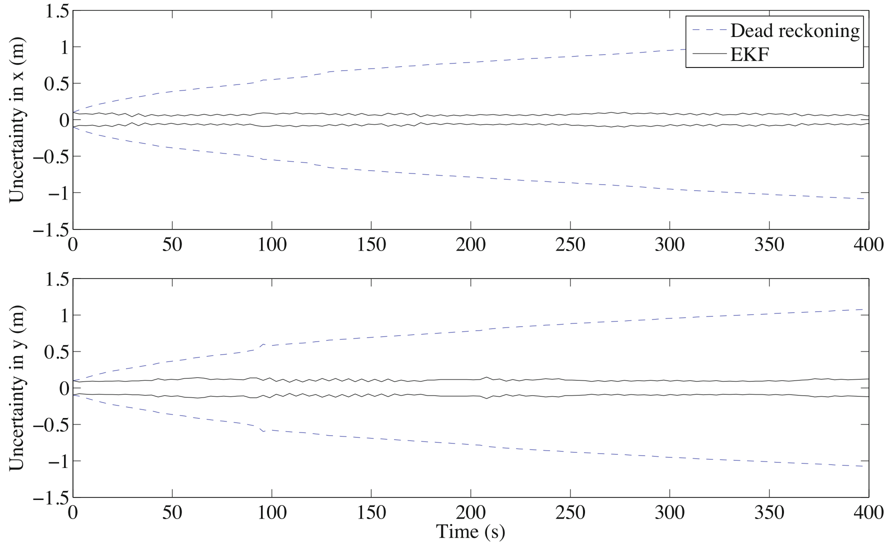

Fig. 5.11 Uncertainty of the estimated position in the B reference frame represented by its 2σ bounds.

used to update the estimate, information regarding the absolute position within the tank is incorporated and, as a result, the drift disappears. As shown in Figure 5.11, the effects of these updates are also reflected in the error plots of the position estimate. The represented 2σ bounds grow without limit in the dead reckoning estimate (dashed line in blue) as a result of the velocity error integration, while they remain constant when updated with the map (black line).

5.4 Hybrid Approach

This third approach to the localization problem is an attempt to merge the best from the two methods already presented. The main advantage of the voting-based localization is the capability of producing independent absolute measurements. This means that even when a position estimation fails, posterior votings can relocalize the vehicle since this is a global localization method that does not rely on position tracking. In contrast, the above mentioned EKF-based method corrects the position estimate in the filter by means of relative measurements between the vehicle and a wall from the *a priori* map and, since this correction relies on the current position estimate, errors can eventually cause the vehicle to get lost and force the system to re-initialize. This second method however, has its strongest point in the use of an EKF which allows the position estimate to be improved by integrating information from additional sensors and, at the same time, makes it possible to obtain position estimates at a higher rate with a fraction of the computational cost required for the voting algorithm.

The proposed hybrid method includes an EKF update with the measurements from a DVL, a compass and an adapted version of the presented voting algorithm. The benefits are twofold. First, the position estimate will now be corrected with absolute measurements, making it more reliable and avoiding eventual track losses. Second, the position estimates from the filter can be included in the voting process to avoid the dispersion of votes along the vehicle's trajectory while moving.

5.4.1 The Filter

The EKF used in this hybrid approach is equivalent to the one presented in Sections 5.3.2 to 5.3.5 and only differs in the process of updating the position estimate. Instead of using the procedure described in Section 5.3.6, this method uses the output from the adapted voting algorithm that will be presented in Section 5.4.2. The measurement $\mathbf{z}_V$ provided by this voting algorithm corresponds to the coordinates of the vehicle's position within the 2D map of the water tank. Since the measurements are obtained in the B reference frame, they can be directly integrated by means of the following linear measurement equation:

$$\mathbf{z}_V(k) = \mathbf{H}_V \mathbf{x}(k|k-1) + \mathbf{m}(k),$$

$$\mathbf{H}_V = \begin{bmatrix} 1\,0\,0\,0\,0\,0\,0\,0 \\ 0\,1\,0\,0\,0\,0\,0\,0 \end{bmatrix},$$

where $\mathbf{m}$ represents a vector of white Gaussian noises with zero mean affecting the measurement process. The covariance of the measurement is represented by $\mathbf{R}_V$:

$$E[\mathbf{m}(k)] = \mathbf{0}, \qquad E\left[\mathbf{m}(k)\mathbf{m}(j)^T\right] = \delta_{kj}\mathbf{R}_V(k).$$

Although the voting algorithm has proved to be quite reliable, there are still situations where reduced visibility, phantoms or reflections in the acoustic data can affect the process and cause errors in the resulting measurement. Since these values are direct observations of components in the state vector, integrating these erroneous measurements strongly affects the correctness of the estimate. To avoid this, we can determine if a given position measurement from the voting algorithm is consistent with the current predicted vehicle position estimate by means of the innovation term ν_V, which represents the discrepancy between them. Its value and covariance are:

$$\begin{aligned} \nu_V &= \mathbf{z}_V - \mathbf{H}_V\hat{\mathbf{x}}(k|k-1), \\ \mathbf{S}_V &= \mathbf{H}_V P(k|k-1)\mathbf{H}_V^T + \mathbf{R}_V. \end{aligned}$$

To determine the compatibility of the measurement, an IC test is performed. The measurement can be considered as corresponding to the current position estimate if the Mahalanobis distance D^2 satisfies:

$$D^2 = \nu_V^T \mathbf{S}_V^{-1} \nu_V < \chi^2_{d,\alpha},$$

where $d = \dim(\mathbf{H}_V)$ and α is the desired confidence level. All the measurements passing the IC test are then used to update the filter. Since the measurement model equation is linear, this can be done with the classic KF update equations that can be found in Appendix A.

5.4.2 Adapted Voting Algorithm

As mentioned in Section 4.4.3, distortions affecting the acoustic data could be differentiated between those resulting from rotations and displacements. In the method presented in Section 5.2, using the information from the compass to determine the relative orientation between the vehicle and the scenario implicitly takes into account rotations during the voting process and removes the effect of its distortion. On the other hand, distortions due to the displacement of the vehicle are ignored since it is assumed that the vehicle is stationary or moving very slowly. In the present method, such an assumption can be removed by integrating the position estimate from the EKF into the voting process. The process begins by tagging each new beam arriving from the MSIS with the current vehicle position in the state vector and storing them in the data buffer. Before producing a voting, a set of n selected high echo intensity bins from a 360° scan sector is obtained together with its corresponding set of vehicle positions $\{[x_1, y_1], \dots [x_n, y_n]\}$. This concept is shown graphically in Figure 5.12, where the position of the vehicle at the beginning of the scan (acquisition of the n bin) is described by $[x_n, y_n]$ and the current vehicle position (bin

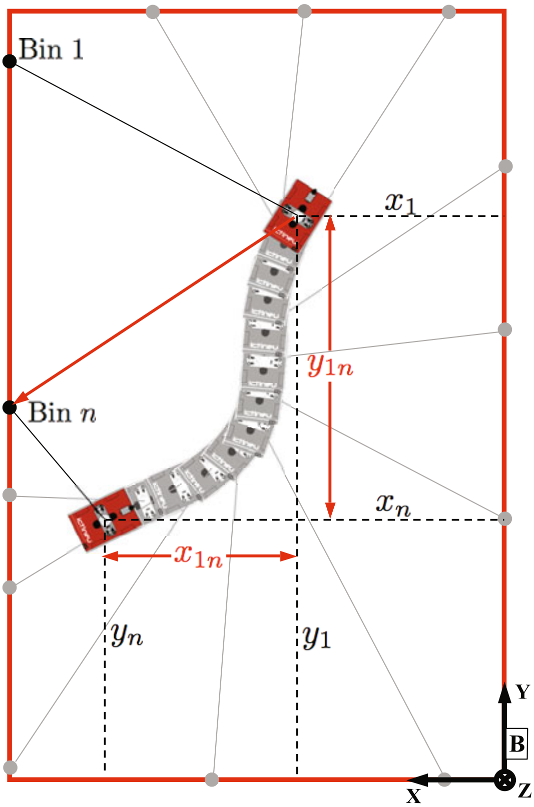

Fig. 5.12 Compensating the effect of motion during the voting process

number 1, the most recent) is represented by $[x_1, y_1]$. The voting method described in Section 5.2 places the votes in accordance with the position of the vehicle at the moment when the measurement of each particular bin took place. The vehicle's movement results in a dispersion of the votes along the performed trajectory which can produce a loose estimation of the real vehicle position (see Figure 5.13(a)). In the present method, this effect is compensated for by using the stored vehicle positions to determine the relative positions of the different bins and making them vote for the current location of the vehicle instead of voting for all the different positions along the trajectory (see Figure 5.13(b)). In the example in Figure 5.12, the difference between the current position and the position at which the n bin was obtained is represented by $[x_{1n}, y_{1n}]$. Composing the vehicle's referenced location of the n bin with this relative measurement makes it possible to determine the position of that same bin with respect to the current vehicle location (represented by a red arrow) and therefore the votes can be assigned accordingly. Transforming all the votes from the whole set of n bins so they can vote for a common vehicle position removes the effect of motion-induced distortions. Moreover, the resulting voting space presents

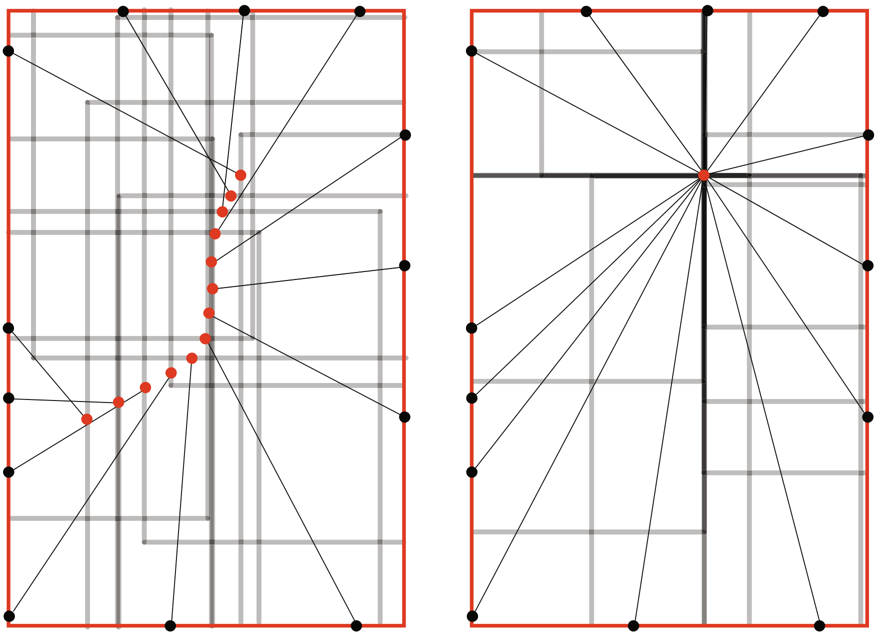

(a) Each bin places the votes according to its corresponding vehicle position.

(b) All the bins vote for the current vehicle position.

Fig. 5.13 Compensating the motion-induced dispersion of votes.

a better description of the real position because there is a more focused distribution of votes. Figure 5.14 shows two voting spaces generated with the voting algorithm from Section 5.2 (on the left) and the present one (on the right). Although both of them were generated from the same set of sonar measurements, it can be seen how the first one shows a sparse distribution of votes, making it difficult to discern the winning position, while the second one has a small cluster with a high concentration of votes which is easy to identify as the winner.

The winner is considered for the vehicle estimate and, as described in Section 5.4.1, this requires defining the uncertainty of the measured position. In contrast to the original method, this adapted voting does not suffer the effects of uncompensated vehicle motions; the process is only affected by the noise in the sensor measurements and their corresponding vehicle positions. Therefore, it is reasonable to assume the resulting output as Gaussian. In this particular implementation, the uncertainty value $\mathbf{R}_V$ is assigned according to the grid resolution in the voting space with the objective of reflecting the empirically observed precision of the method.

5.4.3 Experimental Results

Again, the CIRS water tank experiment is used to test this new proposal. Figure 5.15 represents the trajectory obtained with the current approach (black line), which

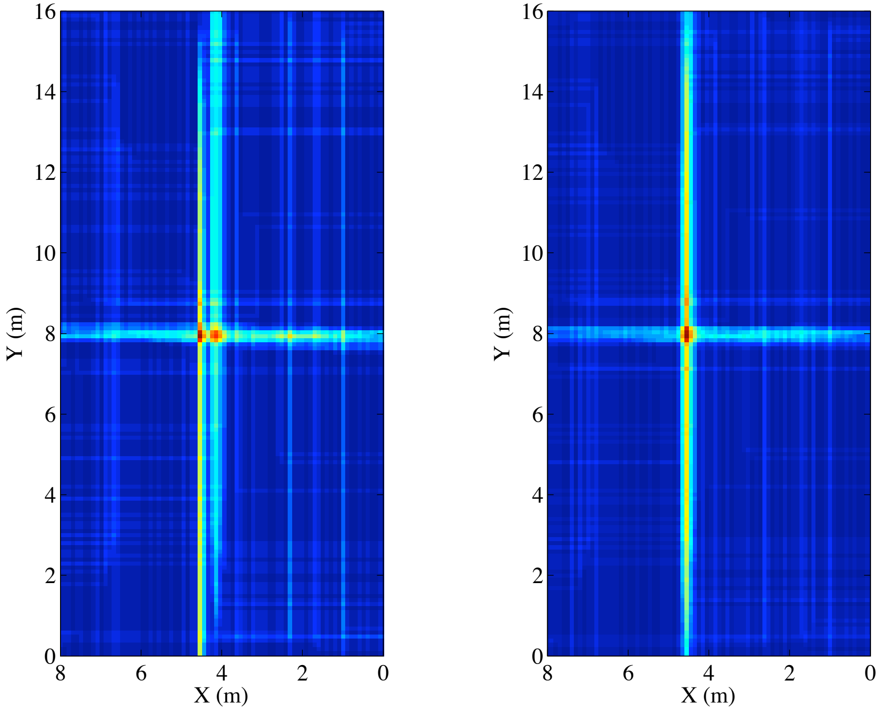

Fig. 5.14 Comparison between the original voting algorithm (left) and the adapted version (right).

strongly resembles the ones obtained with the previous methods: voting-based (line with dots in red) and EKF-based (green line). For comparison purposes the dead-reckoning trajectory (dashed line in blue) has also been included. The algorithm has been set to perform updates with the information from the adapted voting algorithm, which produces measurements at a frequency of about 0.3 Hz. These measurements are also represented in the figure (black crosses) so they can be compared with those obtained with the original voting algorithm (red dots). As can be seen, the measurements are quite similar, which is reasonable since the experiment was performed at a low velocity and the induced distortions were not important. In some parts of the trajectory, the improvement in the voting spaces obtained with the new method is considerable (see the example shown in Figure 5.14). However, in other zones, where perturbances affect the measurements from the DVL, the improvement is hardly appreciable. This is because the effect of the corrections performed during the voting process is dependent on the quality of the estimated trajectory. The side effects of performing absolute position updates are the elimination of the drift affecting the estimate done with the dead-reckoning sensors and the bounding of the vehicle position errors. Figure 5.16 represents the uncertainty of the estimated position error for the current method (in black) together with the uncertainty of the dead-reckoning error obtained by running the filter without the absolute position

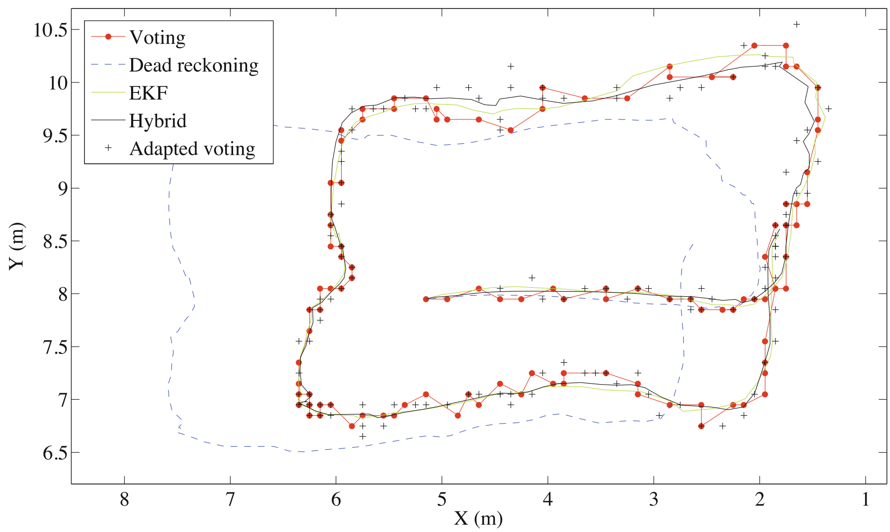

Fig. 5.15 Trajectory obtained with the hybrid localization algorithm compared with trajectories obtained with the other methods.

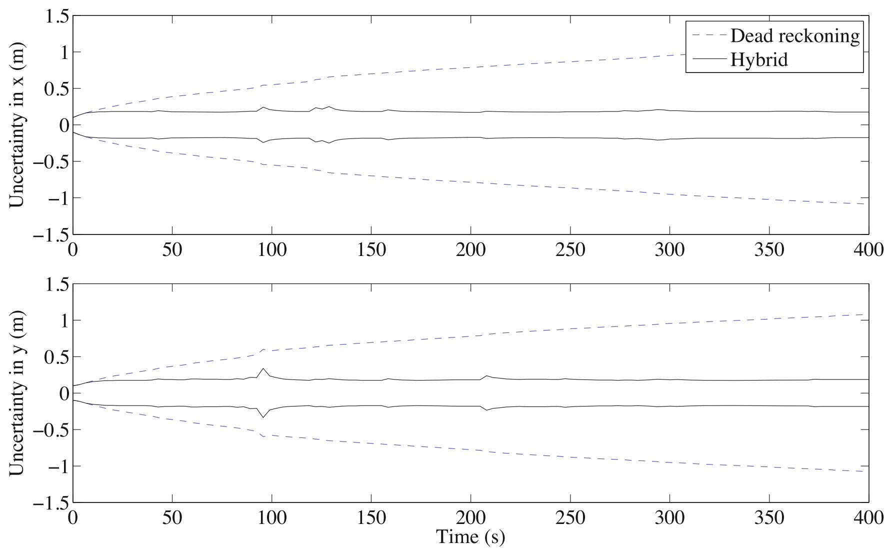

Fig. 5.16 Uncertainty of the estimated position in the B reference frame represented by its 2σ bounds.

updates (blue dashed line). As expected, the first one remains constant (except for small peaks produced by the absence of reliable DVL measurements) while the second shows the typical unbounded error growth.

5.5 Summary and Further Work

In this chapter, three different localization methods have been presented. The first, the voting-based algorithm, provides absolute position measurements and combines simplicity and reliability. Angular distortions affecting the acoustic data are reduced by integrating compass measurements. Distortions caused by displacements are ignored under the hypothesis that the vehicle is static or moving very slowly. Of course, the reliability of the method is affected when this hypothesis does not hold. One weak point of the method is that the computational cost is directly related to the resolution and frequency at which the measurements are obtained. During the SAUC-E competition, the version of the algorithm running in the vehicle was set to work at a low resolution in order to increase the measurement rate and fulfill the real time requirements. This is the only one of the three presented methods implemented in real time in the Ictineu software architecture and tested under working conditions.

The second method relies on an EKF for position estimation. Its strong point is the use of the filter itself, which makes it possible to constantly estimate the vehicle's state and merge information from different sensors. The MSIS data is treated beam to beam to produce corrections with the *a priori* map. As the vehicle's position is taken into account for each individual beam, the effect of distortions is implicitly corrected. The main disadvantage of this method is that using a single bin to perform the updates does not provide enough information to determine the absolute vehicle position and, therefore, if something fails (incorrect association, absence of measurements, etc), the vehicle can eventually get lost. In fact, this disadvantage is corrected in the third presented method. Again, an EKF is used but this time the algorithm relies on absolute position measurements obtained from a modified voting algorithm to perform the updates. The modified voting procedure uses the estimated position to remove the effect of motion in the acoustic data and thus to improve the reliability of the whole algorithm even when the vehicle is moving fast. Further work includes implementing this third method in the Ictineu software architecture so that it can be tested under real working conditions in the CIRS water tank.

One limitation common to all the algorithms is that, although the vehicle can move in 3D, only 2D maps are considered. This is not an issue if the elements composing the map correspond to vertical planes in the real scenario. However, the map will not be valid for a vehicle navigating at different depths since, in this situation, the position of the sensed non-vertical objects could change considerably with respect to their original description in the map. An illustrative example can be found in the CIRS water tank (see Figure 5.5). The different methods take into account only the outermost limits of the tank, composed of vertical walls, but ignore the presence of the two slanted walls placed near the center. This is sufficient to localize the vehicle because, as a consequence of the large vertical beamwidth of the MSIS, the limits are visible even when the vehicle is navigating at a few meters under the water. Moreover, the slanted walls appear in the acoustic data as zones with lower intensity values than those from the outer boundaries and therefore are generally discarded in the high intensity bin selection step. Removing this limitation in the description of the scenario, either by integrating 3D maps or by using a set of 2D maps defined for different working depths, would make it possible to use non-vertical structures to add more information to the system, thereby improving the quality of the measured position. In the CIRS water tank, for instance, it is not possible for the MSIS to detect the boundaries completely when the vehicle is navigating close to the bottom in the deepest zone of the tank. The slanted walls, however, appear in the acoustic data and, if a compatible map is defined, can be used to determine the vehicle's position.

Chapter 6
Simultaneous Localization and Mapping

In this chapter a SLAM framework for AUVs equipped with an MSIS operating in manmade structured environments is proposed. In the previous chapter, the use of techniques such as the Hough transform and the Kalman filter were studied in the context of a localization problem. Here, these techniques are further explored for their application in SLAM. The proposed approach is composed of two parts running simultaneously. The first is a line feature extraction algorithm which is responsible for managing both the measurements arriving from the MSIS and the vehicle position estimates from the SLAM system to search continuously for new features by means of a voting scheme. Eventually, when a new feature is detected, the algorithm also estimates its uncertainty parameters through an analysis of the imprint left in the acoustic images. The second part is a Kalman filter implementation which is the core of the proposed SLAM system. This filter merges the information from various sensors (DVL, compass and pressure sensor) and the observations from the feature extraction algorithm in order to estimate the vehicle's motion and to build and maintain a feature based map (see Figure 6.1 for a diagram of the complete system). In addition, the problems associated with large scenarios have also been addressed through the implementation of a local map building procedure. At the end of the chapter, two tests performed with real sensor data endorse the proposed SLAM approach. The first employs the dataset corresponding to the previously presented CIRS water tank test, while the second undertakes a more realistic application scenario with a dataset obtained in an abandoned marina.

6.1 Line Feature Extraction

There is extensive published bibliography on segmentation, classification, registration and feature extraction from acoustic images [24, 119, 105]. Generally, these works are focused on dealing with natural environments from which features corresponding to compact regions with high intensity backscatter are extracted. In most of the underwater SLAM approaches reviewed in Chapter 2, these regions are usually modeled as point landmarks. The process often requires dealing with significant

D. Ribas et al.: Underwater SLAM for Structured Environments, STAR 65, pp. 77–112.
springerlink.com © Springer-Verlag Berlin Heidelberg 2010

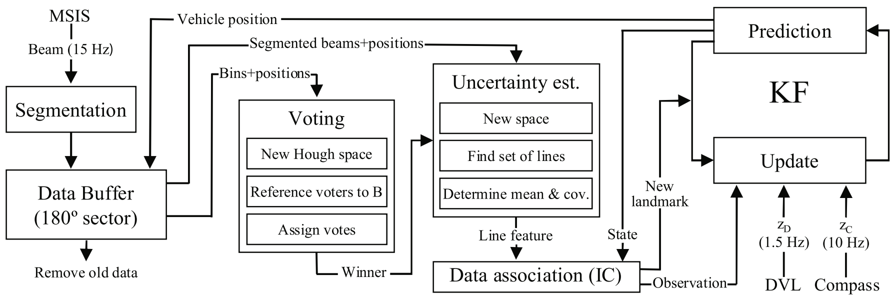

Fig. 6.1 Diagram of the proposed SLAM approach.

background noise and extracting supplementary characteristics regarding their size and shape [118] or even their associated shadows [105] to improve the discriminability. Nevertheless, working with landmarks extracted from acoustic data is not an easy task because their appearance may change substantially when observed from different vantage points. The problem for structured scenarios like the ones handled in this thesis is substantially different. As shown in Chapters 4 and 5, the cross-section of a sonar scan with walls and other planar structures results in line-shaped features in the acoustic images. The aspect of these features remains constant independently of the sensor position, although their visibility may change depending on the incidence angle of the emitted beam and many other factors such as water turbidity or the structure and materials of the reflecting surface. The resulting acoustic images rarely present shadows since the emitted wave cannot generally pass over the walls and the main part ricochets back to the scenario. Of course, this can cause phantom reflections, especially when operating in confined spaces. The sensorial choice for this work, the MSIS, also presents many differences with respect to the common approach based on electronically scanned sonars. As commented on previously, the MSIS produces scans at a much lower frequency, the data is continuous and is affected by motion-induced distortions. On the other hand, its visibility is not limited to a reduced scan sector, but can be extended to 360° around the vehicle. This is important because landmarks can be tracked for a longer period of time, being observable even when the vehicle has left them behind.

6.1.1 Classical Approaches for Line Feature Extraction

The use of line features has traditionally been related to the use of 2D laser scans in indoor environments. The extensive research carried out in this type of scenario has fostered the development of an abundance of methods for the estimation of lines from a cloud of point measurements. The most popular approaches include algorithms based on segmentation and grouping such as Split-and-Merge [101], iterative methods such as the RANdom SAmple Consensus (RANSAC) [39] and voting schemes such as the Hough transform [58] among others. It is also worth mentioning the methods based on the Least Squares (LS) minimization which, although not robust to spurious measurements, is an excellent option for refining lines previously obtained with other methods such as Hough or RANSAC.

The approach presented in this thesis relies on the Hough transform, although it has been substantially modified for the application at hand. This choice was motivated by the simplicity of adapting the system to operate with continuous data from the sensor as well as to integrate the necessary motion corrections. Moreover, the Hough transform offers the possibility of detecting other types of features in addition to lines, on the condition that an adequate parametric representation exists [4]. The particular approach implemented here is based on the work presented in [117]. This work demonstrated a SLAM system running a Hough-based feature extraction algorithm using measurements from a sonar ring mounted on an indoor robot. Although the algorithm proposed here has some similarities, the change in the application domain and the use of an MSIS represent important differences with respect to the original.

6.1.2 Hough-Based Feature Extraction Method for MSIS

This line feature extraction method has some points in common with the voting algorithm for the hybrid localization system presented in Section 5.4. The operation of this feature extraction algorithm is intimately related to the Kalman filter which, simultaneously, executes the SLAM. This is not only because it provides the filter with the landmark observations necessary to build and maintain the map, but also because the voting algorithm requires position estimates to deal with the motion induced distorions in the acoustic data. The segmentation of the acoustic data and the use of a buffer to accumulate information are other similarities with the previously introduced localization method. The different aspects of the algorithm are described in detail below.

6.1.2.1 Beam Segmentation

Objects present in the environment appear as high echo-amplitude returns in acoustic images (see the yellow to red zones in Figure 6.2(a)). Thus, only part of the information stored in each beam is useful for feature extraction. Therefore, a segmentation process is required in order to obtain the most significant information. This process consists of three steps performed beam to beam as the beams arrive from the sonar. First, only those bins with an intensity value over a threshold are selected and stored. This procedure separates the acoustic imprint left by an object in the image from the noisy background data (Figure 6.2(b)). As will be explained in Section 6.2, this imprint plays an important role in the estimation of the uncertainty for the features detected with the voting algorithm.

The second step is to select from the segmented data above the threshold value, those bins that are local maxima. These high intensity bins are the ones that most likely correspond to objects present in the scene. It is worth noting that this process is performed beam to beam and that as a result of the search for local maxima, one

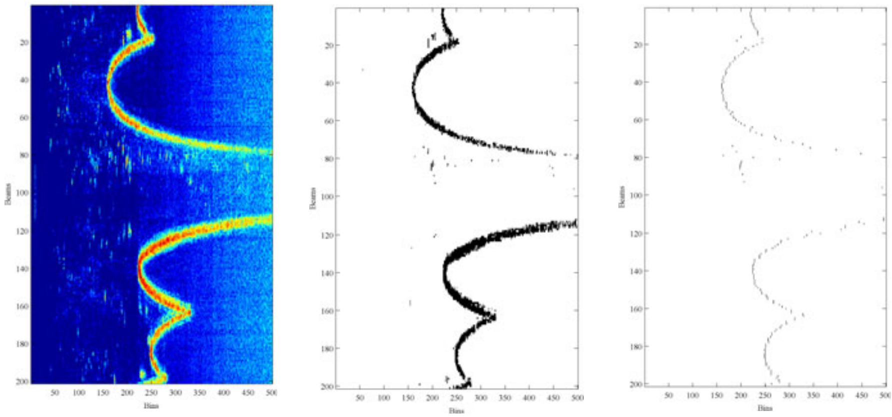

(a) (b) (c)

Fig. 6.2 Different phases of the acoustic data segmentation: (a) Raw polar sensor data. (b) Thresholded data. (c) Local maxima bins.

or more high intensity bins can be obtained per beam. The purpose of selecting multiple bins is to make detecting features possible when more than one wall intersects with a single beam. Structures composed of steps or ramps are examples of scenarios where this can happen (see Figure 6.12). Moreover, using this segmentation technique, it is also possible to extract features from ghost reflections. Although it has not been an object of study during this thesis, the invariance and persistence of these reflections suggest that they could be suitable to act as landmarks in a SLAM framework.

The last step of the segmentation process is to reject those bins which do not satisfy a "minimum distance between them" criterion. This means that if two bins which have been previously selected as local maxima are too close, they should correspond to the same object and are hence redundant. Then, the one with the lowest intensity value is discarded (see the resulting high intensity bins in Figure 6.2(c)).

6.1.2.2 Data Buffer

In order to deal with the stream of measurements produced by the continuous arrival of beams, a data buffer similar to that introduced in Section 5.2.2 is set up. This time, the buffer stores information on the beams for the most recent 180° scan sector. The choice of this sector size is not arbitrary. The feature extraction algorithm is constantly looking for new lines, which makes detecting a candidate as soon as it is fully represented in the scan possible. Since a 180° sector is the maximum sector that a single line can cover within a scan, there is no need to store more data. Whenever new beams corresponding to an unexplored zone are acquired with the MSIS, the stored information corresponding to old beams that fall outside the most recent 180° scan sector is discarded. When the segmentation process determines that a newly measured beam contains one or more high intensity bins that must take part in the voting, the following information is stored in the buffer:

1. The range and bearing for each of the selected bins (polar coordinates in the sensor reference frame). This information will be used in the voting.
2. The segmented beam obtained after applying the threshold value in the first step of the segmentation process. This will be used during the uncertainty estimation phase (Section 6.2).
3. The vehicle position estimate at the moment the beam was acquired. This estimate is obtained from the EKF-based SLAM which runs parallel to the feature extraction algorithm. Taking into account these position estimates during the voting compensates for the motion-induced distortions in the acoustic data.

6.1.2.3 Defining the Voting Space

The information stored in the data buffer is used periodically in a voting to look for possible candidate features. This is performed with a modified version of the classical implementation of the Hough transform for line extraction. This algorithm accumulates the information from the sensor data in a voting table which is a parameterized representation of all the possible feature locations. Those features that receive a great number of votes are those with a relevant set of compatible sensor measurements and thus the most likely to correspond to a real object in the environment. In our application, line features are described by two parameters, ρ^B and θ^B (perpendicular distance and orientation with respect to a base frame B). Hence, the resulting Hough space is a two-dimensional space where the voting process and the search for maxima can be done efficiently. The base reference frame B can be set arbitrarily. However, our choice for B is the current position of the sonar head at the moment the voting is performed. Since in this implementation the voting is triggered by the arrival of new beams from the sensor, the most recently stored position in the data buffer (corresponding to the last beam) defines the position of B. An advantage of choosing this base is that, when a line feature is detected after the voting, its parameters are already represented in the sensor coordinate frame and hence it can be integrated directly into the SLAM framework as an observation of one of the features already in the map, or incorporated as a new feature after being compounded with the current vehicle position.

It is worth noting that B is not a fixed coordinate frame. As the parametrization in the Hough space is performed in polar coordinates, setting the reference in a fixed position would produce a resolution loss with an increase in range. To avoid this, we need to re-situate B according to the vehicle's motion. Unfortunately, this requires recomputing the Hough space with each change in the position of B. Although it may seem a great deal of computation, the fact is that the number of bins involved in the voting is not large (less than 100 bins during the tests performed) and the calculations can be executed quite fast. Moreover, as will be explained in the next section, there are situations when recalculating the Hough space can be avoided. Another key issue is the quantization of the Hough space. In our case, we have observed that selecting

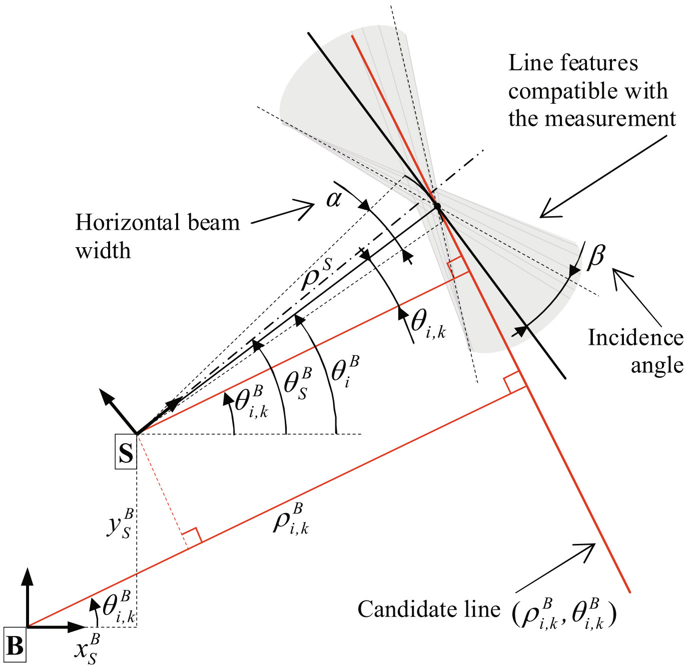

Fig. 6.3 Model of the sonar sensor for line features. B is the base reference frame and S is a reference frame attached to a beam.

the quantization equal to the angular and linear resolutions of our sensor (typically, 1.8° and 0.1 m) works well. A higher resolution does not necessarily increase the quality of the detection because the sonar resolution limits its precision. On the other hand, a lower resolution would produce a rough observation.

The general execution of the feature extraction process consists of several steps. First, with each beam arrival, the Hough space is referenced to the current sensor position as the new base frame B. Next, all the bins stored in the buffer are referenced to B so they can be used to vote in the space. It is worth noting that the stored beam positions are taken into account when transforming to B. Hence, the data is undistorted. Then, the votes corresponding to each bin are assigned to the candidate lines by means of a sonar model. Finally, a search for winning candidates is performed.

6.1.2.4 Sonar Model and Voting

Each bin represents the strength of the echo intensity return in a particular place within the insonified area. Due to the uncertainty produced by the horizontal beamwidth, a measurement cannot be assigned to a single point in the space. A common approach [70],[117], is to consider the measurement as an arc whose aperture represents the beamwidth uncertainty. Moreover, as a high intensity return is typically produced when the acoustic wave hits a surface perpendicularly, we can infer that all the surfaces tangent to the arc can explain the high intensity return. While this simple model is well suited for air sonar ranging systems, it is not able to explain the acoustic images gathered with an MSIS. A careful analysis of these images reveals that their object detection capability is not limited to the arc-tangent surfaces, but that those beams intersecting the surface within the limits defined by a certain maximum incidence angle also produce a discernible return. On the other hand, those beams with a shallower angle are completely reflected and do not perceive the surface. To obtain a better description of this situation, an extended model to describe the imaging sonar has been adopted (Figure 6.3). Basically, given a horizontal beamwidth angle α (in our sensor, $\alpha = 3°$) and an incidence angle β (generally, not less than 60°), the set of line features compatible with a particular bin is composed not only of these lines tangent to the arc defined by α, but also of all the lines which intersect the arc with an incidence angle smaller than $\pm\beta$. Before performing a voting, this set of lines must be determined for each bin stored in the data buffer.

This process will now be described using as reference the illustration in Figure 6.3. Let the reference frame S define the position of the transducer head at the moment a particular bin was obtained, with $[x_S^B, y_S^B, \theta_S^B]$ being the transformation which defines the position of S with respect to the chosen base reference B, and ρ^S the range at which the bin was measured from the sensor. Both the transformation and the range values can be obtained from the information in the data buffer. To emulate the effect of the horizontal beamwidth, a set of i values are taken at a given resolution within an aperture of $\pm\alpha/2$ around the direction in which the transducer is oriented, also referred to as θ_S^B:

$$\theta_S^B - \frac{\alpha}{2} \leq \theta_i^B \leq \theta_S^B + \frac{\alpha}{2}.$$

Each value θ_i^B represents the bearing parameter for a line tangent with the arc which models the horizontal beamwidth. As stated earlier, not only are the lines tangent to the arc candidates, but also those inside the maximum incidence angle limits of $\pm\beta$. For this reason, k values are taken at a given resolution for each value of θ_i^B and within an aperture of $\pm\beta$:

$$\theta_i^B - \beta \leq \theta_{i,k}^B \leq \theta_i^B + \beta.$$

The result of this operation are $i \times k$ different values of $\theta_{i,k}^B$. These are the bearings for a set of lines which are a representation of all the possible candidates compatible with the bin. The final step is to determine the range parameter $\rho_{i,k}^B$ corresponding to each one of the $\theta_{i,k}^B$ bearings obtained. Given the geometry of the problem, they are calculated as:

$$\rho_{i,k}^B = x_S^B \cos(\theta_{i,k}^B) + y_S^B \sin(\theta_{i,k}^B) + \rho^S \cos(\theta_{i,k}).$$

This set of lines can now be used to determine the cells in the voting space that should receive a single vote from this particular bin. It is assumed that the resolutions chosen during the generation of the $i \times k$ lines are sufficient to ensure a correct exploration of the grid cells and hence that the zone in the discretized space corresponding to the compatible candidates is correctly determined. This process is repeated for all the bins stored in the data buffer. Figure 6.4 shows what the set of voters looks like when assigned to the Hough space. Note that each selected cell of the space can only receive one vote from any particular bin and that those cells containing multiple votes therefore represent lines compatible with different individual bins.

Every time a new beam arrives, a new voting space is generated to look for winning line candidates. A winning line must only be detected once it has been completely observed (i.e., further beams cannot provide more votes to the candidate). In the voting space, the zone in which these winning lines can exist is completely determined by the subset of all the candidate lines contained in the most recent 180° scan sector that do not intersect with the last beam (shaded zones in Figure 6.4). Any line candidate with a sufficient number of votes found within this zone is declared a winner. Performing the detection in this way can ensure that the algorithm detects the lines as soon as they are completely visible. After a line detection, all the bins involved in the election of the selected candidate are removed from the buffer so that they do not interfere with the detection of further features.

It is worth mentioning that in order to reduce the computational cost of the process, some votings can be skipped. After each voting, it is possible to determine the cell with the largest number of votes and therefore to calculate the number of supplementary votes required to produce a winner. Since additional votes can only be obtained from newly measured bins, it is not necessary to perform more votings before the minimum required number of bins has been measured and introduced in the buffer.

6.2 Uncertainty Model for Line Features

At this point a method has been introduced to determine the position, in polar coordinates, of a candidate line feature extracted from acoustic data acquired with an MSIS. This information, however, is not sufficient for using the line as a landmark for the SLAM system. Although an estimate for the feature parameters has been produced, their values are discrete and their precision depends on the grid resolution of the Hough space. In addition, the line feature lacks an adequate uncertainty model, which makes it impossible to integrate the observation in the stochastic map. This section will introduce a novel method for producing estimates and their uncertainty for line features extracted from rich acoustic data.

6.2.1 Classical Approach

The subset of high intensity bins compatible with the observation of a particular line feature can be determined by analyzing the votes the line has received in the Hough

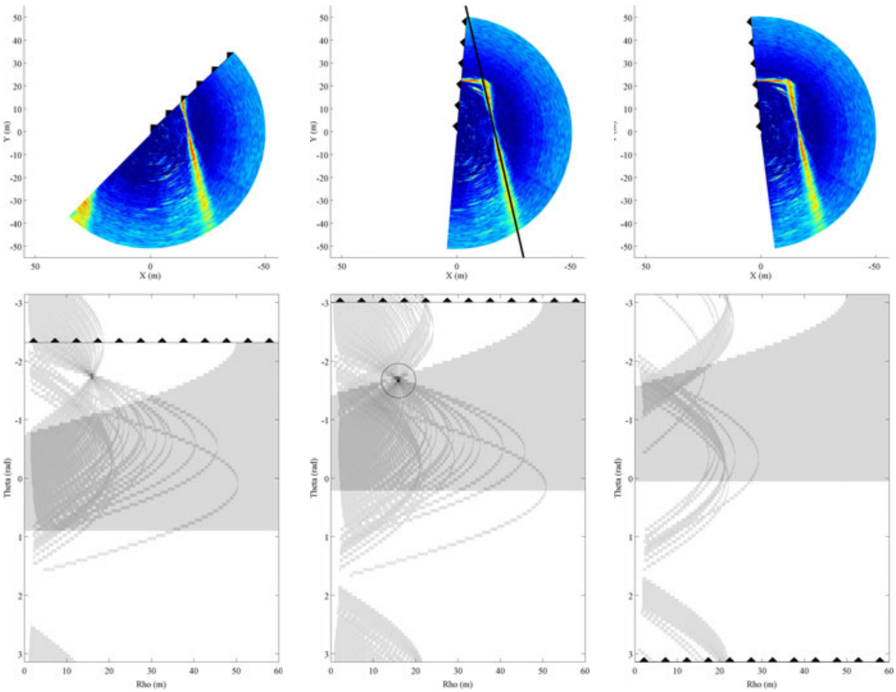

(a) (b) (c)

Fig. 6.4 Sequence representing the voting process. The scan sector stored in the buffer (top) is represented together with its corresponding voting space (bottom). The line with triangular shapes marks the position of the most recent beam. The darker cells in the voting space represent those candidates with a larger number of votes while the shaded zone represents those candidates which have received all the possible votes. (a) Part of the target line is still outside the sector scan and can receive more votes in the future. (b) The line can now be detected because it has been fully observed and more votes cannot be added. (c) Those votes corresponding to the detected line, as well as the old ones that fall outside the 180° scan sector, are removed from the Hough space so they cannot interfere with future line detections.

space. A common approach for incorporating new features into the stochastic map is to initialize the line feature using the parameters obtained in the Hough space and assigning large covariance values to them (non-informative prior). Then the information from the subset of bins associated with this line feature is used in the form of sensor measurements with the objective of refining the estimate of the feature [117, 108]. This method is well suited for laser scans and range measurements in general. However, from the author's point of view, this is not the most appropiate method for the estimation of features from the rich data produced by an MSIS since an important part of the information contained in the acoustic images is not taken into account. To optimize the voting in the Hough space, only a small group of selected high intensity bins are used, while neighboring bins with similar intensity values are discarded. Moreover, when a winner is selected, those bins associated with the line candidate are biased into being perfectly aligned, leaving slightly misaligned bins which may also correspond to the real feature outside the estimation process. On the other hand, the noise model assigned to the bins during the estimation of the line is generally based on assumptions regarding the sensor precision, but it ignores the fact that other external factors such as water turbidity, incidence angle or characteristics of the reflecting surface also determine the quality of the measurement. For all these reasons, this process usually leads to overoptimistic line estimates which may eventually result in inconsistent maps.

A variant of this method seeks to obtain less confident estimations by using only the two bins placed at the endpoints of the line feature instead of using the complete set of measurements. Although the desired effect is obtained, the resulting estimate does not match with the real uncertainty of the feature because of the small number of measurements involved and the inadequacy of the noise model. The method that will be presented in the next section takes a completely different approach. For a human observer analyzing an acoustic image it is fairly simple to discern the zone in which a particular feature will exist with high probability. This zone will not be defined by a few aligned bins but by a large set of bins which look like a blurry elongated shape. The aspect of this shape reflects the quality of the observation, not only depending on the sensor's performance but also on the environment's characteristics. The basic idea for the proposed method is, therefore, focusing on the appearance of the features in the acoustic images to determine their uncertainty model rather than relying solely on some particular measurements.

6.2.2 Estimating Feature Uncertainties from Acoustic Images

The process to estimate a feature's uncertainty is based on relating the probability of an object existing in a particular place with the measured intensities in the acoustic image representing the same location. There is a high probability that there will be an object in a zone where large intensity values have been measured (e.g. the red-yellow shapes in Figure 6.2(a)) while the probability in the zones with lower intensity measurements gradually decreases to zero (the blue zones in the figure). Given this situation, the process of applying a threshold to segment the acoustic data can be considered analogous to defining a particular confidence interval for a probability distribution. In other words, a line feature will fall inside the thresholded zone in the acoustic image with a particular confidence level. To make the problem tractable, the probability distribution of a line feature represented in the acoustic image will be approximated to a bivariate Gaussian distribution on its ρ and θ parameters (see Figure 6.5. An additional example justifying that this approximation is suitable can be found in Section 6.2.4). Therefore, the process to estimate the feature uncertainty consists of determining the Gaussian which best fits the segmented data representing a probability distribution for a given confidence level.

A simple description of this process is shown in Algorithm 1. After the detection of a line feature with the voting algorithm, the uncertainty estimation process begins with the assignment of a feasible confidence coefficient to the imprint left after

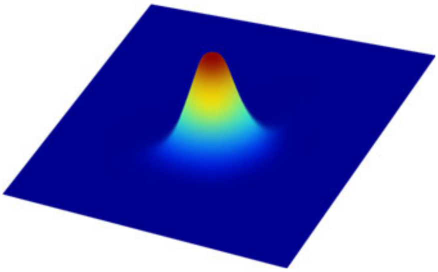

(a) Gaussian distribution representing an uncertain ρ-θ line in a polar space.

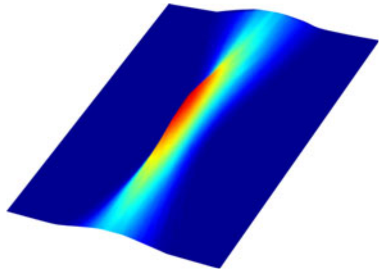

(b) The same uncertain line represented in a cartesian space.

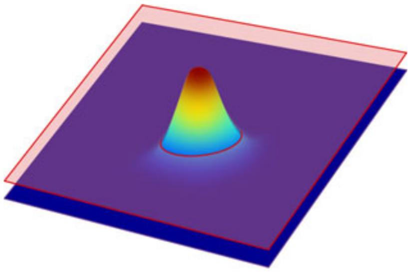

(c) Elliptic section resulting from the definition of a particular confidence interval.

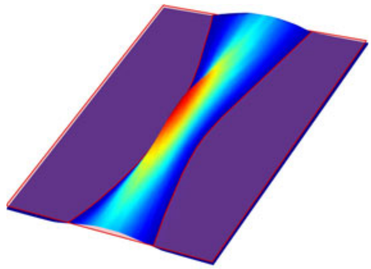

(d) The confidence interval defined in the cartesian representation

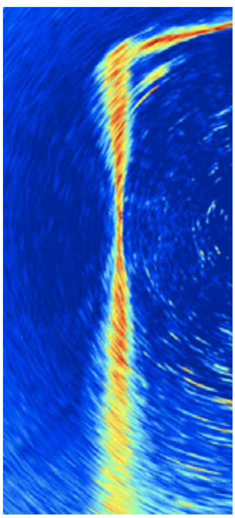

(e) The intensities in a cartesian acoustic image are related with the probability of the existence of a line feature.

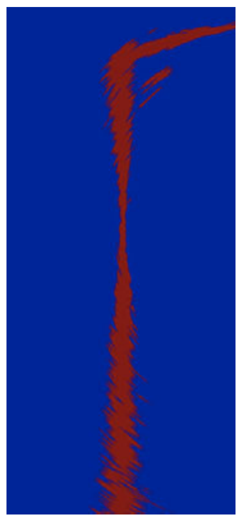

(f) The segmented image resembles the zone defined by the confidence interval in Figure 6.5(d)

Fig. 6.5 Relating a segmented acoustic image with a Gaussian probability distribution.

the segmentation (for instance, it is realistic to assume that the segmented data in Figure 6.2(b) will contain the real feature in 95% of cases). Since the winning candidate line has received a considerable number of votes, it must be one of the lines contained within the confidence interval defined by the segmented imprint. The next step of the process consists of finding a number of compatible lines belonging to the neighborhood of the winning candidate which overlap the segmented data in the same way. The objective of this is to obtain a set of line realizations representative of the population contained within the defined confidence interval (i.e. a set of lines that "fill" the segmented area).

Estimating the Gaussian distribution from a set of lines is not straightforward, however. It is worth noting that lines described by its ρ and θ parameters can also be represented as points in a polar ρ-θ space. Representing the set of lines in such a space will result in a cloud of points (the lines are similar) with an elliptic form. This particular elliptic disposition of the ρ-θ points suggests that the approximation of the line feature to a Gaussian distribution is correct. Although the space has changed, the set still represents a population of lines within the previously defined confidence interval. This fact is used to estimate the uncertainty of the line feature. It is achieved by approximating the area occupied by the set of points to the area enclosed inside the ellipse that a bivariate Gaussian distribution would generate at the same given confidence. By knowing the confidence coefficient, the major and minor axis of the ellipse and its orientation, it is possible to recover the covariance matrix. Moreover, the mean value of the ρ-θ pair defining the line feature can also be obtained from the center of the ellipse.

Figure 6.6 illustrates the different steps involved in the process of estimating the feature uncertainty. The image in Figure 6.6(a) reproduces a voting space which has just obtained a winning candidate (marked with the small box). The corresponding sonar measurements appear in Figure 6.6(b) and are represented in the same B-based polar space as the Hough space. Since the data is represented in polar, the line feature appears as an arc whose thickness is related to its uncertainty. Note that the ρ-θ pair, representing the winning candidate line in the Hough space, can also be represented in this space. In fact, to parametrize the line, its point with the smallest distance to the origin is used (again, represented with the same small box in the figure). Applying a threshold and assigning a confidence coefficient to the segmented data results in the space represented in Figure 6.6(c). At this point, and using the winning candidate line as a paradigm, the search for lines contained within the segmented imprint is performed. The resulting set of lines is contained inside the bounds represented as black arcs, while the representation of the place occupied by their ρ and θ pairs is represented as a black shape at the apex of the arc. The final step of the procedure consists of finding the ellipse containing this area and extracting the covariance matrix given the predefined confidence coefficient. Finally, Figure 6.6(d) represents the estimated feature over a cartesian representation of the scan sector. The line in the center corresponds to the ρ-θ mean value while the lines at the sides represent the uncertainty bounds at 95% confidence.

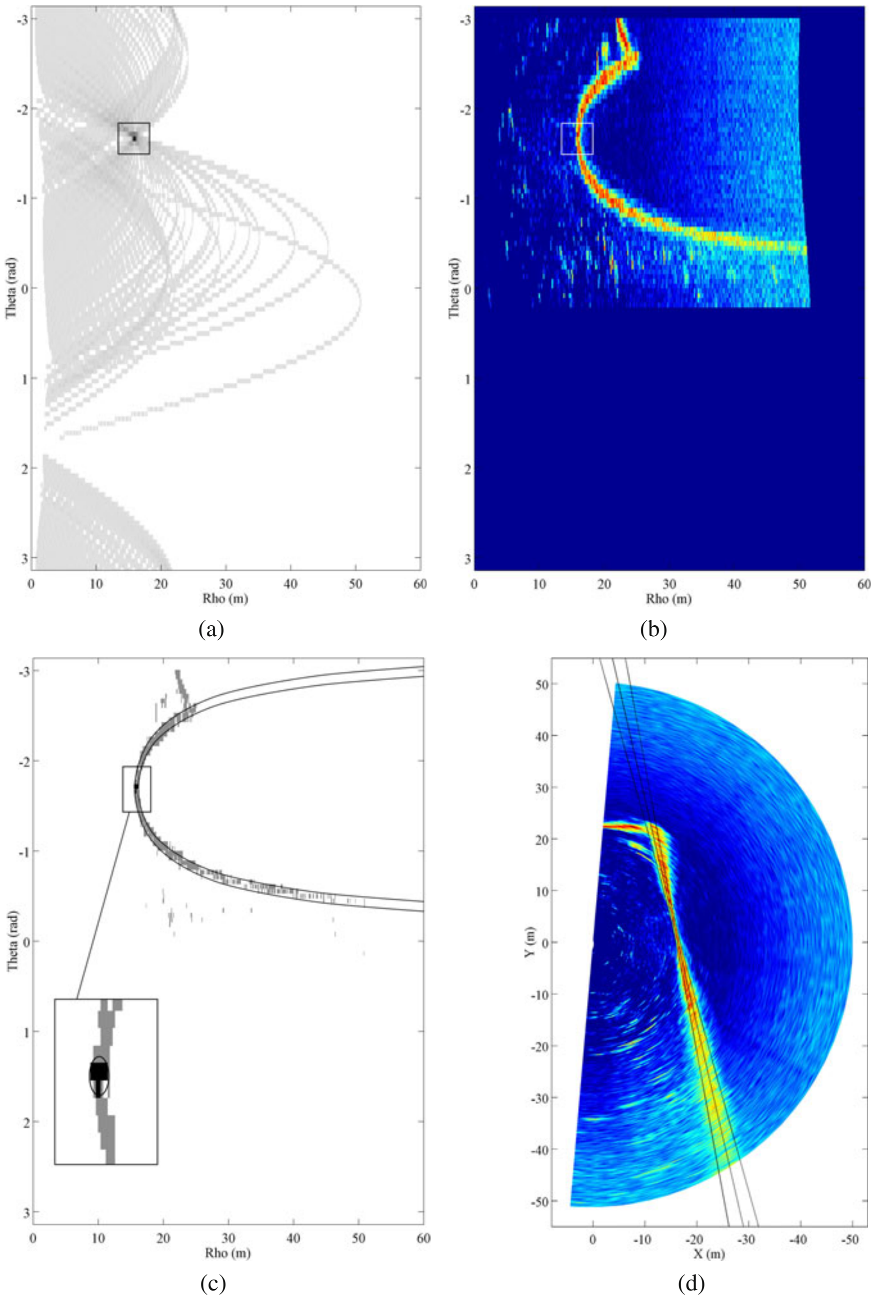

Fig. 6.6 Process for uncertainty estimation. (a) Winning candidate in the Hough space. (b) Polar representation of the sonar data. (c) Segmented data with the zone occupied by line features inside the confidence level. (d) Resulting uncertainty estimate represented over the scan sector.

Algorithm 1. $get\_measurements([\rho_c, \theta_c], \text{scan}, \text{confidence\_level})$

```
/* Initialization of the polar grid space that will
   contain the segmented sonar data                                  */
```
boolean last180scan $[\rho_{resolution}, \theta_{resolution}]$;
$[\text{last180scan}] = init\_scan(\text{scan})$;

```
/* Set the paradigm with the candidate line from the
   voting                                                            */
```
$[\eta_c] = get\_overlap\_ratio([\rho_c, \theta_c], \text{last180scan})$;

```
/* Search for compatible lines                                       */
```
$\text{lines2check} = \{[\rho_c, \theta_c]\}$;
$\text{accepted} = \emptyset$;
$\text{rejected} = \emptyset$;
while $\text{lines2check} \neq \emptyset$ **do**
  $[\rho_i, \theta_i] = get\_candidate(\text{lines2check})$;
  $[\eta_i] = get\_overlap\_ratio([\rho_i, \theta_i], \text{last180scan})$;
  if $accept\_line(\eta_c, \eta_i)$ **then**
    $\text{accepted} = \text{accepted} \cup \{[\rho_i, \theta_i]\}$;
    $\text{lines2check} = \text{lines2check} \setminus \{[\rho_i, \theta_i]\}$;
    $\text{lines2check} =$
    $\text{lines2check} \cup \{neighbour8connectivity([\rho_i, \theta_i]) \cap \overline{\{\text{rejected} \bigcup \text{accepted}\}}\})$
  else
    $\text{rejected} = \text{rejected} \cup \{[\rho_i, \theta_i]\}$;
    $\text{lines2check} = \text{lines2check} \setminus \{[\rho_i, \theta_i]\}$;

```
/* Given the set of lines, determine the ellipse that
   contains the area where they exist                                */
```
$[major\_axis, minor\_axis, \rho_{mean}, \theta_{mean}, \alpha] = get\_ellipse(accepted)$;

```
/* Given the ellipse and the confidence level related to
   the segmentation, find the mean and covariance                    */
```
$\mathbf{z}^V = [\rho_{mean}, \theta_{mean}]$;
$\mathbf{R} = get\_covariance(major\_axis, minor\_axis, \rho_{mean}, \theta_{mean}, conf\_level)$
return $\left[\mathbf{z}^V, \mathbf{R}\right]$;

6.2.3 Correlations in the Extracted Features

The method presented for extracting line features relies on odometry motion to compensate for the distortion affecting the sonar measurements. When motion estimates from the EKF are introduced in the voting, correlations with past vehicle states are introduced to any observed line. From a theoretical point of view, these correlations should be taken into account when performing the update by, for example, using an augmented state EKF to represent position data for the accumulated scan sector. However, this approach has a substantial computational cost because of the large number of vehicle states involved. On the other hand, these correlations have been shown to have a small influence on the proposed SLAM algorithm. For this reason, we have chosen to deal with the problem by adopting a pessimistic uncertainty model which assures that the possible correlations are included in the uncertainty of the estimated measurement. Although this approach is sub-optimal, it has been shown to work satisfactorily in the tested scenarios.

6.2.4 Validation of the Feature Extraction Algorithm

In order to validate the feature extraction algorithm, several tests with both synthetic and real data have been carried out. By generating synthetic data we have two objectives. The first is to justify the use of a bivariate ρ-θ Gaussian distribution to represent the uncertain features present in the acoustic images. The second is to have a way of comparing the output from the algorithm with the paradigm which makes it possible to confirm the correctness of the estimation. To obtain the synthetic data, a large population of ρ-θ pairs was generated following a given probability distribution. Then, the lines represented by each pair were projected into a polar space analogous to those produced by the measurements from an MSIS. Each cell from this space represents a bin and its echo intensity value is assigned according to the number of lines that cross its area. The resulting synthetic dataset is represented in polar and cartesian coordinates in Figures 6.7(a) and 6.7(d). In spite of the large uncertainty assigned in the example to make the estimation process more clear, the synthetic data has sufficient points in common with the real acoustic images to consider this model as valid. It can be observed how the high intensity zone in the center corresponds with the major concentration of lines, while the dispersion at the sides, caused by the angular uncertainty, produces an effect similar to the loss of intensity and precision affecting the beams with large incidence angles. Figures 6.7(b) and 6.7(c) illustrate the voting and the uncertainty estimation process. The elliptic shaped zone representing the population of compatible lines reflects the Gaussianity of the estimated feature. As can be observed in Figure 6.7(d), the estimated line feature is a good representation of what appears in the synthetic data.

Additional verification of the method can be seen in Figure 6.8, where the cloud of ρ-θ pairs initially used to generate the synthetic data is plotted together with an ellipse representing the original Gaussian distribution (dashed line) and another representing that estimated with the proposed method (solid line). When comparing the two ellipses, it can be appreciated that they are almost coincident except for a small angular misalignment. It is important to note that correlated data, like the one in this example, has turned out to be the most difficult scenario for the proposed uncertainty estimation method and therefore one could expect even better estimates when working with less correlated data.

A second set of tests was carried out with real data acquired with the Ictineu AUV. Under real working conditions, it is not possible to obtain reliable references to test the performance of the method. Therefore, only the direct visualization of the estimated line feature represented over the acoustic images can be used as an indicator. The first example in Figure 6.9(a) shows the features extracted from a dataset obtained in a real application scenario; in particular, in the same marina environment which served as the testbed for the SLAM algorithm. The second example is

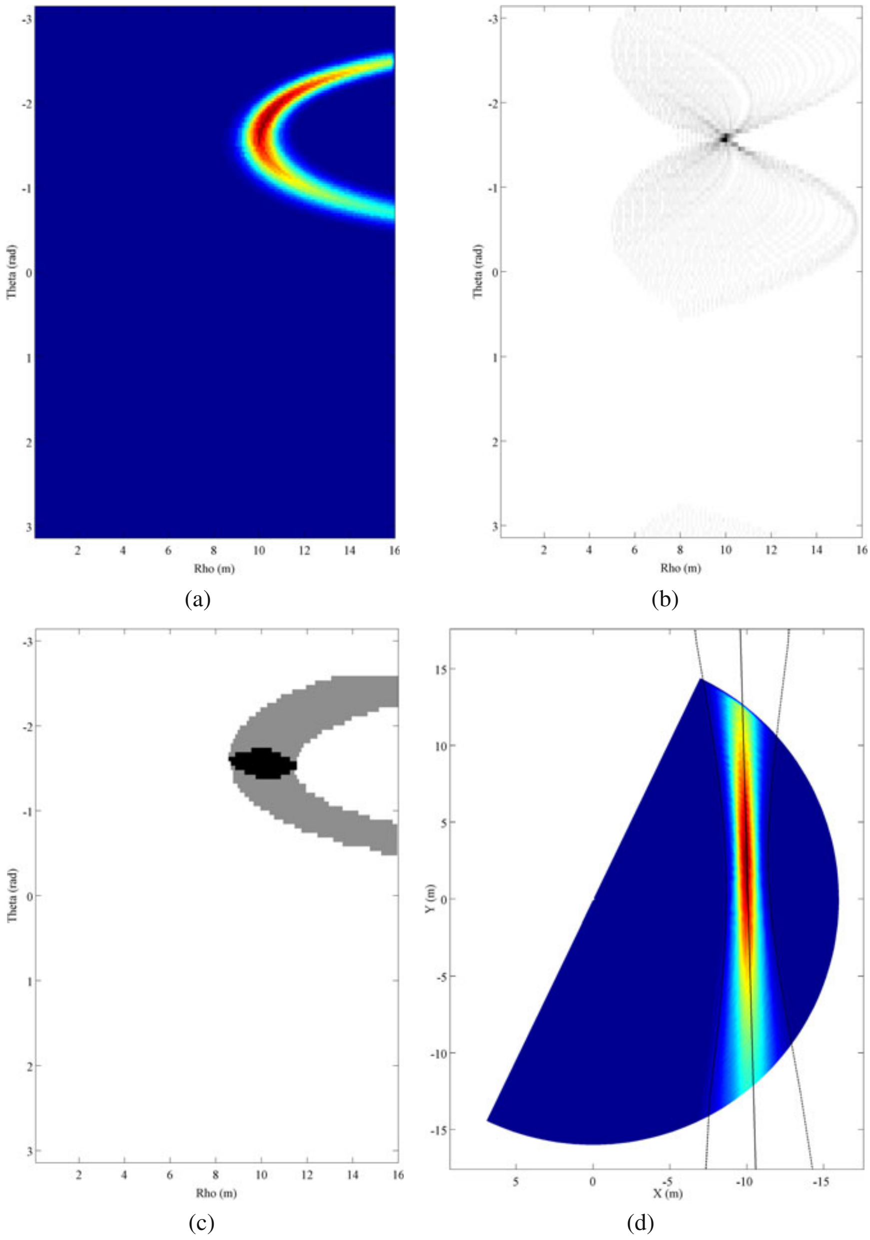

Fig. 6.7 Testing the algorithm with synthetic data. (a) Raw sensor data generated from ρ and θ given a normally distributed uncertainty. Some correlation affects the two variables increasing the difficulty of the test. (b) The voting space clearly identifies the line. (c) Uncertainty estimation using the segmented data. The black elliptic shape corresponds to the lines with compatible overlapping and represents the uncertainty of ρ and θ. (d) The estimated line feature fits almost perfectly with the synthetic one.

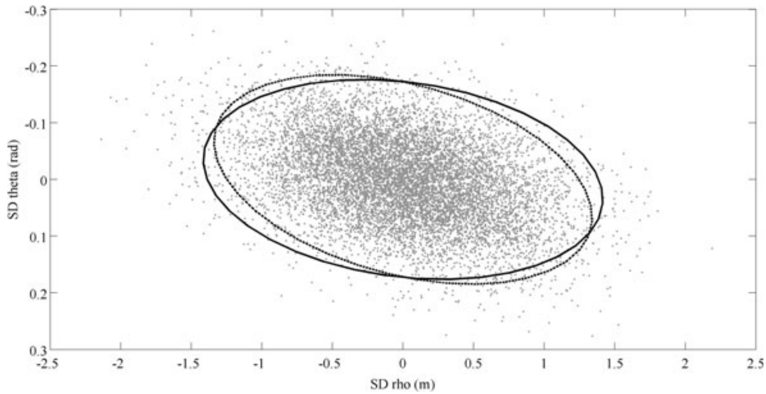

Fig. 6.8 Comparison between the bivariate Gaussian distribution used to produce the synthetic data and the output from the algorithm. The ellipse with the dashed line represents the Gaussian distribution at 95% confidence while the solid line is the output of the algorithm at the same confidence level.

represented in Figure 6.9(b). It corresponds to an experiment performed in the water tank of the Underwater Robotics Research Center at the University of Girona. This confined environment with highly reflective concrete walls produces noisy data with many reflections and phantoms. The results in both cases are consistent with the representation of the walls in the acoustic images and, moreover, the method shows reliable behavior when working with noisy data, filtering linear features from shapeless phantoms.

6.3 Obtaining Segments

The last step in the process of acquiring features from acoustic images is to determine the line segments. This method takes advantage of the same segmented data used during the uncertainty estimation process as well as the mean value of the estimated line parameters. The process consists basically of determining the overlap of the estimated line over the thresholded data and finding the line segments which are placed over high intensity areas. Then a process equivalent to the *dilation* and *erosion* morphological operations for image processing is applied to the obtained segments in order to group and remove short segments and to produce a more compact representation. Finally, the resulting segment endpoints are referenced as distances, measured along the line, from the point represented by the ρ-θ parameters (the point at which the line is closest to the coordinate reference frame) and stored for their posterior use. It is worth noting that these segments are produced for representation purposes only. The segment endpoints are not introduced in the state vector and hence they are not estimated in any way.

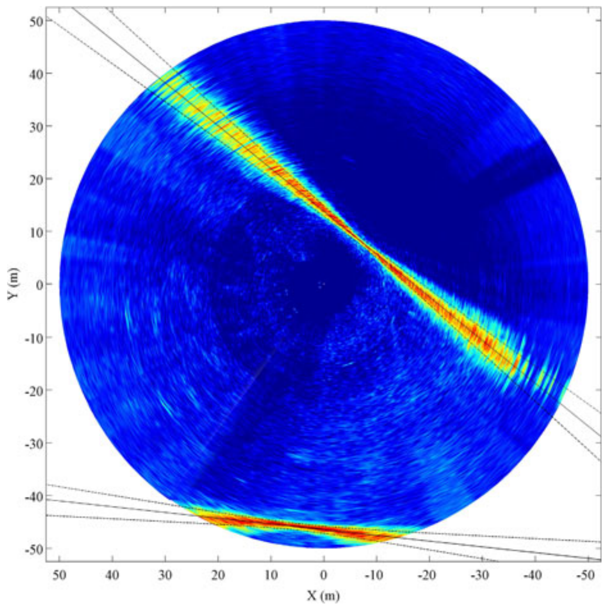

(a)

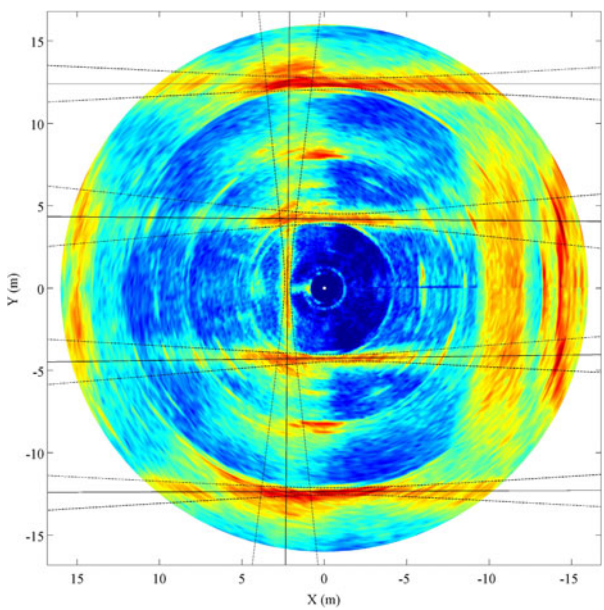

(b)

Fig. 6.9 Testing the algorithm with real data. (a) Line features extracted from acoustic data gathered in a marina environment. (b) Line features obtained from acoustic data gathered in a small water tank. The lines on the right side are not estimated as they are split between the start and the end of the scan.

6.4 EKF-Based SLAM

An EKF integrates the vehicle's navigation sensors to provide an estimate of its position and retain the estimates of the previously observed features in order to build a map. This filter is an implementation of the stochastic map [115] in which the estimate of the position of both the vehicle $\mathbf{x}_V$ and the set of map features $F = \{\mathbf{x}_1 \ldots \mathbf{x}_n\}$ are stored in the state vector $\hat{\mathbf{x}}$.

$$\hat{\mathbf{x}}(k) = [\hat{\mathbf{x}}_V(k) \;\; \hat{\mathbf{x}}_1(k) \; \ldots \; \hat{\mathbf{x}}_n(k)]^T$$

The covariance matrix $\mathbf{P}$ describes the covariance of the vehicle and the features as well as their respective cross correlations:

$$\mathbf{P}(k) = E([\mathbf{x}(k) - \hat{\mathbf{x}}(k)][\mathbf{x}(k) - \hat{\mathbf{x}}(k)]^T | Z(k))$$

The vehicle's state $\hat{\mathbf{x}}_V$ has dimension 9, which defines the minimum size of the state vector $\hat{\mathbf{x}}$ at the beginning of the execution. The features are represented in polar coordinates and therefore the state will be increased by 2 with each new incorporation in the map.

6.4.1 Map Initialization

When creating a new stochastic map at step 0, a base local reference frame L must be selected (Figure 6.10). In this approach, the initial vehicle position is chosen to set this base location and thus is initialized with perfect knowledge. The vehicle's state $\mathbf{x}_V$ is represented as:

$$\mathbf{x}_V = \left[x \; y \; z \; \psi \; u \; v \; w \; r \; \psi_{L_0}\right]^T$$

where $[x \; y \; z \; \psi]$ represent the position and heading of the vehicle in the local reference frame L while $[u \; v \; w \; r]$ are their corresponding linear and angular velocities in the vehicle's coordinate frame V. As can be seen, the vehicle's state vector is exactly the same as that presented in Section 5.3, except for the term ψ_{L_0} which represents the angle between the initial vehicle heading at step 0 (orientation of L) and magnetic north in the earth global frame E. This term works as a sensor bias and allows us to initialize the vehicle heading ψ in the local frame L , making it possible to use compass measurements (angle to the north in the E frame) for its estimation as shown in Section 6.4.3. Assuming that the vehicle is not moving at step 0, the state is initialized as:

$$\hat{\mathbf{x}}(0) = \hat{\mathbf{x}}_V(0) = \left[0\;0\;0\;0\;0\;0\;0\;0\;\hat{\psi}_{L_0}\right]^T; \quad \mathbf{P}(0) = \mathbf{P}_V(0) = \begin{bmatrix} \mathbf{0}_{8\times 8} & \mathbf{0}_{8\times 1} \\ \mathbf{0}_{1\times 8} & \sigma^2_{\psi_{L_0}} \end{bmatrix}$$

where $\hat{\psi}_{L_0}$ takes its value from the first available compass measurement and $\sigma^2_{\psi_{L_0}}$ is initialized according to the sensor's precision. It is worth noting that at the beginning

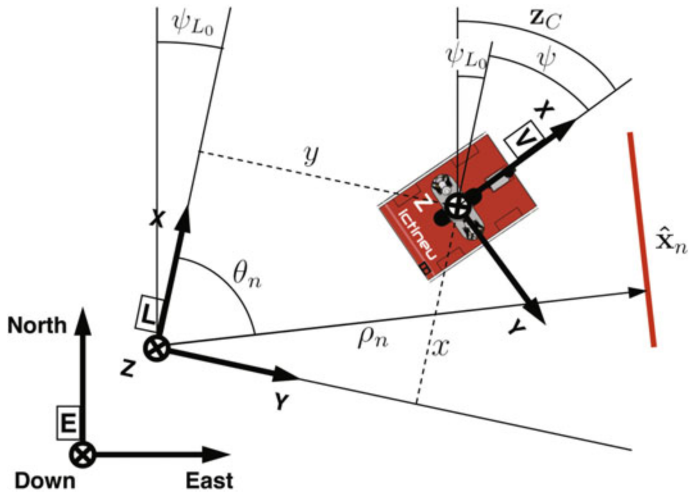

Fig. 6.10 Representation of the different reference coordinate frames.

of the execution, the map does not contain any feature and hence the state $\hat{\mathbf{x}}$ contains only the vehicle's state $\hat{\mathbf{x}}_V$.

6.4.2 Prediction

Again, the previously introduced constant velocity kinematics model is used to predict the state of the vehicle (see Section 5.3.4). The new term ψ_{L_0} has been added and modeled as constant since the original orientation of the local map does not change with time:

$$\mathbf{x}_V(k) = f(\mathbf{x}_V(k-1), \mathbf{n}(k-1)),$$

$$\begin{bmatrix} x \\ y \\ z \\ \psi \\ u \\ v \\ w \\ r \\ \psi_{L_0} \end{bmatrix}_{(k)} = \begin{bmatrix} x+(uT+n_u\frac{T^2}{2})cos(\psi)-(vT+n_v\frac{T^2}{2})sin(\psi) \\ y+(uT+n_u\frac{T^2}{2})sin(\psi)+(vT+n_v\frac{T^2}{2})cos(\psi) \\ z+wT+n_w\frac{T^2}{2} \\ \psi+rT+n_r\frac{T^2}{2} \\ u+n_uT \\ v+n_vT \\ w+n_wT \\ r+n_rT \\ \psi_{L_0} \end{bmatrix}_{(k-1)}.$$

The noise model is also the same, with $\mathbf{n} = [n_u\ n_v\ n_w\ n_r]^T$ representing an acceleration white noise additive in the velocity terms which has a zero mean and covariance $\mathbf{Q}$. On the other hand, as features correspond to fixed objects from the environment, we can assume they are stationary. Hence, the whole state can be predicted as:

$$\hat{\mathbf{x}}(k|k-1) = [f(\hat{\mathbf{x}}_V(k-1)) \quad \hat{\mathbf{x}}_1(k-1) \ \ldots \ \hat{\mathbf{x}}_n(k-1)]^T$$

and its covariance matrix updated as:

$$\mathbf{P}(k|k-1) = \begin{bmatrix} \mathbf{F}_V(k) & \mathbf{0}_{9\times 2n} \\ \mathbf{0}_{2n\times 9} & \mathbf{I}_{2n\times 2n} \end{bmatrix} \mathbf{P}(k-1) \begin{bmatrix} \mathbf{F}_V(k) & \mathbf{0}_{9\times 2n} \\ \mathbf{0}_{2n\times 9} & \mathbf{I}_{2n\times 2n} \end{bmatrix}^T + \begin{bmatrix} \mathbf{W}_V(k) \\ \mathbf{0}_{2n\times 4} \end{bmatrix} \mathbf{Q} \begin{bmatrix} \mathbf{W}_V(k) \\ \mathbf{0}_{2n\times 4} \end{bmatrix}^T$$

where $\mathbf{F}_V$ and $\mathbf{W}_V$ are the Jacobian matrices of partial derivatives of the non-linear model function f with respect to the state $\mathbf{x}_V$ and the noise $\mathbf{n}$ respectively:

$$\mathbf{F}_V = \frac{\partial f}{\partial \mathbf{x}_V}(\hat{\mathbf{x}}_V(k), \mathbf{0}) = \begin{bmatrix} 1 & 0 & 0 & -\hat{u}T\sin\hat{\psi} - \hat{v}T\cos\hat{\psi} & T\cos\hat{\psi} & -T\sin\hat{\psi} & 0 & 0 & 0 \\ 0 & 1 & 0 & \hat{u}T\cos\hat{\psi} - \hat{v}T\sin\hat{\psi} & T\sin\hat{\psi} & T\cos\hat{\psi} & 0 & 0 & 0 \\ 0 & 0 & 1 & 0 & 0 & 0 & T & 0 & 0 \\ 0 & 0 & 0 & 1 & 0 & 0 & 0 & T & 0 \\ 0 & 0 & 0 & 0 & 1 & 0 & 0 & 0 & 0 \\ 0 & 0 & 0 & 0 & 0 & 1 & 0 & 0 & 0 \\ 0 & 0 & 0 & 0 & 0 & 0 & 1 & 0 & 0 \\ 0 & 0 & 0 & 0 & 0 & 0 & 0 & 1 & 0 \\ 0 & 0 & 0 & 0 & 0 & 0 & 0 & 0 & 1 \end{bmatrix},$$

$$\mathbf{W}_V = \frac{\partial f}{\partial \mathbf{n}}(\hat{\mathbf{x}}_V(k), \mathbf{0}) = \begin{bmatrix} \frac{T^2}{2}\cos\hat{\psi} & \frac{-T^2}{2}\sin\hat{\psi} & 0 & 0 \\ \frac{T^2}{2}\sin\hat{\psi} & \frac{T^2}{2}\cos\hat{\psi} & 0 & 0 \\ 0 & 0 & \frac{T^2}{2} & 0 \\ 0 & 0 & 0 & \frac{T^2}{2} \\ T & 0 & 0 & 0 \\ 0 & T & 0 & 0 \\ 0 & 0 & T & 0 \\ 0 & 0 & 0 & T \\ 0 & 0 & 0 & 0 \end{bmatrix}.$$

6.4.3 Sensor Updates

The measurements from the DVL, the pressure sensor and the compass are treated as described in Section 5.3.5. However, the measurement model equations should be adapted to deal with the changes introduced in the state vector as follows:

Velocity: The velocity measurements provided by the DVL are integrated as direct observations of the vehicle's velocities in the state. The observation matrix $\mathbf{H}$ is adapted to the dimension of the state vector as:

$$\mathbf{H}_D = \begin{bmatrix} \mathbf{0}_{3\times 4} & \mathbf{I}_{3\times 3} & \mathbf{0}_{3\times 2} & \mathbf{0}_{3\times 2n} \end{bmatrix},$$

while the covariance matrix for the measurement noise (see Appendix B) remains as:

$$\mathbf{R}_D = \begin{bmatrix} \sigma_{Du}^2 & \sigma_{Duv} & \sigma_{Duw} \\ \sigma_{Dvu} & \sigma_{Dv}^2 & \sigma_{Dvw} \\ \sigma_{Dwu} & \sigma_{Dwv} & \sigma_{Dw}^2 \end{bmatrix}.$$

Depth: The pressure sensor measurements are also integrated as a direct observation of the vehicle's depth (position in the Z axis). The adapted $\mathbf{H}$ matrix is:

$$\mathbf{H}_P = \begin{bmatrix} 0 \; 0 \; 1 \; 0 \; 0 \; 0 \; 0 \; 0 \; 0 \; \mathbf{0}_{1\times 2n} \end{bmatrix}.$$

The variance of the depth measurement will be represented by:

$$\mathbf{R}_P = \sigma_P^2.$$

Heading: Working in a local map makes modifying the measurement model to update the vehicle's heading necessary. As can be observed in Figure 6.10, the compass measurement $\mathbf{z}_C$ corresponds to the addition of the heading of the vehicle ψ with respect to the local reference frame L and the orientation of this frame ψ_{L_0}. The resulting measurement model is:

$$\mathbf{H}_C = \begin{bmatrix} 0 \; 0 \; 0 \; 1 \; 0 \; 0 \; 0 \; 0 \; 1 \; \mathbf{0}_{1\times 2n} \end{bmatrix}.$$

The measurement noise $\mathbf{R}_C$ is represented by the variance of the compass:

$$\mathbf{R}_C = \sigma_C^2.$$

Again, the measurements from the different sensors will be integrated as soon as they are acquired using the classical Kalman filter update equations for linear measurement models. In order to deal with simultaneously arriving measurements, a reconfigurable composed form of the $\mathbf{H}$ matrix equivalent to the one presented in Section 5.3.5 is used. The same is applicable in the case of the use of bottom and/or water tracking velocities from the DVL.

6.4.4 About the Use of a Compass in SLAM

Working with compass data can be a difficult task in some situations. The effect of electromagnetic fields like those produced by the thrusters, and the presence of large structures with ferromagnetic materials can considerably distort compass measurements and render them unusable. Nowadays, there are alternative technologies such as Fiber Optic Gyro (FOG) and Ring Laser Gyro (RLG) which offer perturbation-free high precision measurements [63]. However, these devices are very expensive and their use is not viable for low-cost vehicles. Although it is almost impossible to completely avoid the effect of perturbations on compasses, taking certain precautions such as performing calibrations before each mission and avoiding operating close to walls (generally, 1-2 m is sufficient) can provide measurements of sufficient quality. Moreover, a compass is an especially useful sensor for SLAM because it provides *absolute* orientation measurements, unlike the dead reckoning sensors

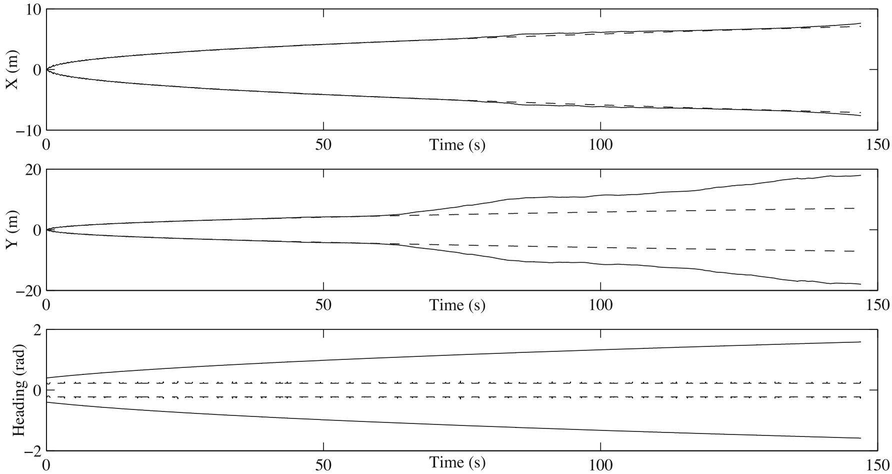

Fig. 6.11 Estimated position covariance plots represented within 2σ bounds. This data corresponds to the first minutes of the abandoned marina experiment executing the EKF with the updates from the dead-reckoning sensors. The results using a cheap inaccurate gyro sensor are represented with a solid line, while those using absolute data from a compass are indicated with a dashed line.

normally used in SLAM such as wheel encoders, gyros or, in our case, the DVL. The effect of using a compass is threefold:

1. The error in vehicle orientation will *not* increase during the SLAM process.
2. Vehicle orientation introduces nonlinearity in the SLAM problem, so loss of precision because of linearization effects will also be limited.
3. Vehicle orientation errors in a certain step become position errors in future steps. Bounding the errors in orientation will also result in a reduction in the rate of increase of vehicle position errors.

Figure 6.11 shows the evolution of the vehicle's position and orientation using the DVL velocity data together with the rate of turn measurements from gyros (solid line) and using *absolute* attitude information from the compass (dashed line). We can see that the error in orientation remains constant. There is also a reduction in the rate of increase of the error in the direction transverse to the vehicle's direction of motion.

6.4.5 Map Building Process

The Tritech Miniking imaging sonar produces beams at a 10-30Hz rate depending on the settings of the sensor. Each new beam is stored together with the current vehicle position estimate from the filter in the data buffer and fed to the feature extraction algorithm as shown in Section 6.1. Eventually, the information added by a new beam arrival is sufficient to produce a line feature detection. In this case, the ρ - θ pair obtained is represented in the B frame which is placed in the current position of the sonar head. For the sake of simplicity, let us assume that the transformation between B and the vehicle's coordinate system is known. Hence, we could represent a new measurement i with respect to the vehicle's frame V as $\mathbf{z}_i^V = [\rho_i^V \ \theta_i^V]^T$. Of course, the same transformation should be applied to the covariance matrix obtained from the uncertainty estimation method. This transformation will result in the covariance matrix $\mathbf{R}_i$. The next step is to solve the data association problem. Thit is to determine if the measured line $\mathbf{z}_i^V$ corresponds to any of the features $F_j, j = 1 \dots n$ already existing in the map and should be used to update the system or, on the contrary, it is new and has to be incorporated into the map. The result of the data association process is a hypothesis $\mathscr{H} = \mathtt{j}_i$ associating the measurement $\mathbf{z}_i^V$ with one of the map features F_j ($\mathtt{j}_i = 0$ indicates that $\mathbf{z}_i^V$ has no correspondence with the existing features). Finding the correct hypothesis is a process involving the analysis of the discrepancy between the actual line measurement and its prediction. This prediction is obtained from the nonlinear measurement function h_j, which relates the i measurement with the state vector $\mathbf{x}(k)$ containing the locations of the vehicle and the j feature:

$$\begin{aligned}
\mathbf{z}_i^V(k) &= h_j(\mathbf{x}(k), \mathbf{s}_i), \\
\begin{bmatrix} \rho_i^V \\ \theta_i^V \end{bmatrix} &= \begin{bmatrix} \rho_j - x\cos\theta_j - y\sin\theta_j \\ \theta_j - \psi \end{bmatrix} + \mathbf{s}_i,
\end{aligned}$$

where $\mathbf{s}_i$, the noise affecting the line feature observation, is a zero-mean white noise with covariance $\mathbf{R}_i$. To calculate the discrepancy between the measurement and its prediction, the innovation term ν_{ij} and its associate covariance matrix $\mathbf{S}_{ij}$ are obtained as:

$$\begin{aligned}
\boldsymbol{\nu}_{ij}(k) &= \mathbf{z}_i^V(k) - h_j(\hat{\mathbf{x}}(k|k-1)), \\
\mathbf{S}_{ij}(k) &= \mathbf{H}_j(k)\mathbf{P}(k|k-1)\mathbf{H}(k)_j^T + \mathbf{R}_i,
\end{aligned}$$

where $\mathbf{H}_j$ represents the Jacobian matrix which linearizes the nonlinear measurement function h_j around the best available estimation of the state $\hat{\mathbf{x}}(k|k-1)$:

$$\begin{aligned}
\mathbf{H}_j &= \frac{\partial h_j}{\partial \mathbf{x}}(\hat{\mathbf{x}}(k|k-1), \mathbf{0}) \\
&= \begin{bmatrix} -\cos\theta_j & -\sin\theta_j & 0 & 0 & 0 & 0 & 0 & 0 & 0 & \cdots & 1 & x\sin\theta_j - y\cos\theta_j & \cdots & 0 & 0 \\ 0 & 0 & 0 & -1 & 0 & 0 & 0 & 0 & 0 & \cdots & 0 & 1 & \cdots & 0 & 0 \end{bmatrix}.
\end{aligned}$$

To determine if the correspondence is valid, an individual compatibility (IC) test using the Mahalanobis distance is carried out:

$$D_{ij}^2 = \boldsymbol{\nu}_{ij}(k)^T \mathbf{S}_{ij}(k)^{-1} \boldsymbol{\nu}_{ij}(k) < \chi^2_{d,\alpha},$$

where $d = \dim(\mathbf{h}_j)$ and α is the desired confidence level. It is possible for a multiple hypothesis relating the measurement with different map features to satisfy the IC test. Then, in order to select the best candidate, the nearest neighbor (NN) criterion is applied (in situations where clutter or vehicle uncertainty are high, more complex data association algorithms such as JCBB [90] can be used). Finally, after the correspondence has been decided, it is used to update the state estimate by means of the EKF update equations.

$$\begin{aligned}
\mathbf{K}_{ij}(k) &= \mathbf{P}(k|k-1)\mathbf{H}_j(k)^T\mathbf{S}_{ij}(k)^{-1},\\
\hat{\mathbf{x}}(k) &= \hat{\mathbf{x}}(k|k-1)+\mathbf{K}_{ij}(k)\boldsymbol{\nu}_{ij}(k),\\
\mathbf{P}(k) &= (\mathbf{I}-\mathbf{K}_{ij}(k)\mathbf{H}_j(k))\mathbf{P}(k).
\end{aligned}$$

In case there is no valid hypothesis relating the measured line with any of the features from the map (i.e. $\mathscr{H}=0$), this measurement can be added to the current state vector as a new feature. However, this cannot be done directly because this new feature needs to be represented in the map reference frame. The change of reference is done by compounding (see Appendix C) the line feature with the current vehicle position as follows:

$$\hat{\mathbf{x}}(k) = \begin{bmatrix} \hat{\mathbf{x}}_V(k) \\ \hat{\mathbf{x}}_1(k) \\ \vdots \\ \hat{\mathbf{x}}_n(k) \end{bmatrix} \quad \Rightarrow \quad \hat{\mathbf{x}}(k)^+ = \begin{bmatrix} \hat{\mathbf{x}}_V(k) \\ \hat{\mathbf{x}}_1(k) \\ \vdots \\ \hat{\mathbf{x}}_n(k) \\ \hat{\mathbf{x}}_V(k) \oplus \mathbf{z}_i^V(k) \end{bmatrix}.$$

Augmenting the state vector also requires updating the estimated error covariance matrix as:

$$\mathbf{P}(k) = \mathbf{D}(k)\mathbf{P}(k)\mathbf{D}(k)^T + \mathbf{G}(k)\mathbf{R}_i\mathbf{G}(k)^T,$$

$$\mathbf{D}(k) = \begin{bmatrix} \mathbf{I} & 0 \dots 0 \\ \vdots & \vdots \dots \vdots \\ 0 & 0 \dots \mathbf{I} \\ \mathbf{J}_{1\oplus} & 0 \dots 0 \end{bmatrix}, \quad \mathbf{G}(k) = \begin{bmatrix} 0 \\ \vdots \\ 0 \\ \mathbf{J}_{2\oplus} \end{bmatrix},$$

where $\mathbf{J}_{1\oplus}$ and $\mathbf{J}_{2\oplus}$ are the Jacobian matrices of the compounding transformation.

6.5 SLAM with Local Maps

In recent years, many different authors have proposed methods to carry out SLAM by building sequences of local maps [71, 117, 131, 73, 6, 95, 7, 33, 21, 96]. The main advantages of building sequences of local maps are the limitation of the cost associated with the update of a full covariance matrix [52] and the improvement of the system's consistency [17, 55]. In the present case, an additional advantage is obtained with using local maps. The parametrization of line features using polar coordinates is the most suitable approach for our type of sensor (polar). However, it is not the best choice for referencing the features in a large map. Some issues appear when an observation of a new feature is translated from the sensor frame to the map base frame, particularly in those situations where the map base and the sensor base are far from each other, since a small variation in the θ parameter of a feature with a large ρ value translates into large changes in Cartesian coordinates. Using local maps overcomes this issue as their area is smaller and hence the reference changes are less critical.

An important restriction of such methods is that the local maps must be statistically independent (no information can be shared between them) to avoid introducing inconsistency when recovering the global map. As a consequence, vehicle states such as velocities or estimated sensor biases cannot be transferred between maps. Recently, [104] presented a technique which overcomes this limitation and makes sharing information between local maps possible, while remaining conditionally independent. This is especially useful in our case because it allows information about the vehicle's state to be kept. This method has been chosen to implement the local map sequencing in the present work. Although this section summarizes the main characteristics of our particular implementation of the algorithm, a more detailed presentation of the method can be found in the bibliographic reference mentioned.

6.5.1 Local Map Building

The local map building process relies on defining a set of state variables which are common to two consecutive maps. This commonality serves as a link to transmit the information from one map to the other while maintaining their conditional independence. In the application at hand, this link makes it possible to use the estimates of the vehicle's velocities and the compass bias obtained at the end of a map to initialize the next local map. Moreover, after new measurements modify the estimate of these terms, it is also possible to update their estimated values in the previous map through back-propagation.

The procedure to build the local maps begins by initializing the filter presented in Section 6.4. Then, the vehicle moves through the scenario acquiring sensor information regarding its own state and the position of existing features. After a certain time period, the state vector $\hat{\mathbf{x}}$ will contain the current estimate of the states of the vehicle $\hat{\mathbf{x}}_V$ as well as the position of several map features $F = \{\mathbf{x}_1 \ldots \mathbf{x}_n\}$. At a given instant k, the current local map is finished and a new one is initialized by defining a new state $\hat{\mathbf{x}}$ containing only the current vehicle state $\hat{\mathbf{x}}_V$ as follows:

$$\hat{\mathbf{x}}(k) = [\hat{\mathbf{x}}_V(k) \;\; \mathbf{T}\hat{\mathbf{x}}_V(k)]^T ,$$

where the first term is a clone of the vehicle's state that will serve as a link between the two local maps, and the second term represents the initialization of the vehicle's state in the new map after performing a change of the base reference defined by the linear transformation function $\mathbf{T}$:

$$\mathbf{T}\hat{\mathbf{x}}_V(k) = \begin{bmatrix} 0 \; 0 \; 0 \; 0 \; u \;\; v \;\; w \;\; r \;\; \psi + \psi_{L_0} \end{bmatrix}^T ,$$

$$\mathbf{T} = \begin{bmatrix} \mathbf{0}_{4\times4} & \mathbf{0}_{4\times4} & \mathbf{0}_{4\times1} \\ \mathbf{0}_{4\times4} & \mathbf{I}_{4\times4} & \mathbf{0}_{4\times1} \\ 0\,0\,0\,1 & \mathbf{0}_{1\times4} & 1 \end{bmatrix}.$$

This transformation sets the current vehicle location as the base reference of the new local map, while its velocity estimates (represented by the vehicle's frame) are preserved. It is important to note that the term of the compass bias is also updated to make integrating compass measurements with respect to the new base possible. The resulting state vector has a dimension of 18. To complete the initialization process, the state covariance matrix $\mathbf{P}$ has to be set accordingly:

$$\mathbf{P}(k) = \begin{bmatrix} \mathbf{P}_V(k) & \mathbf{P}_V(k)\mathbf{T}^T \\ \mathbf{T}\mathbf{P}_V(k) & \mathbf{T}\mathbf{P}_V(k)\mathbf{T}^T \end{bmatrix},$$

where $\mathbf{P}_V$ is the submatrix corresponding to the vehicle's state from the full covariance matrix of the first map. At this point, the filter is ready to begin the estimation of the new local map using the equations presented in Section 6.4. Of course, those equations should be adapted to the presence of the common state variables representing the link between the maps.

6.5.2 Local Map Joining

The map building procedure will result in a sequence of local maps with the form:

$$\mathscr{M}_i = (\hat{\mathbf{x}}^i, \mathbf{P}^i); \quad \text{with} \quad \hat{\mathbf{x}}^i = \left[\hat{\mathbf{x}}_V^{i-1}\ \hat{\mathbf{x}}_1^i \ldots \hat{\mathbf{x}}_n^i\ \hat{\mathbf{x}}_V^i\right]^T. \tag{6.1}$$

Each local map $\mathscr{M}_i$ contains the term $\hat{\mathbf{x}}_V^{i-1}$, a copy of the vehicle's state at the end of the previous map $\mathscr{M}_{i-1}$ which represents the common part connecting the two maps. It also contains a set of features $\{\hat{\mathbf{x}}_1^i \ldots \hat{\mathbf{x}}_n^i\}$ which have been added to the state vector during the generation of the map and, finally, the term $\hat{\mathbf{x}}_V^i$, which represents the estimate of the vehicle's state throughout the creation of the map and whose final value will serve to initialize the $\mathscr{M}_{i+1}$ local map.

The process of joining local maps into a single global map is described here using a notation similar to that presented in [104]. Consider two consecutive local maps defined as:

$$\mathscr{M}_A = \left(\begin{bmatrix} \hat{\mathbf{x}}_A \\ \hat{\mathbf{x}}_{Ca} \end{bmatrix}, \begin{bmatrix} \mathbf{P}_A & \mathbf{P}_{ACa} \\ \mathbf{P}_{CaA} & \mathbf{P}_{Ca} \end{bmatrix} \right),$$
$$\mathscr{M}_B = \left(\begin{bmatrix} \hat{\mathbf{x}}_{Cb} \\ \hat{\mathbf{x}}_B \end{bmatrix}, \begin{bmatrix} \mathbf{P}_{Cb} & \mathbf{P}_{CbB} \\ \mathbf{P}_{BCb} & \mathbf{P}_B \end{bmatrix} \right).$$

The part common to both maps is represented by $\hat{\mathbf{x}}_{Ca}$, which corresponds to the state of the vehicle at the end of $\mathscr{M}_A$, and $\hat{\mathbf{x}}_{Cb}$, which is initialized as an exact clone of $\hat{x}_{Ca}$ during the creation of the $\mathscr{M}_B$ map but evolves because of the updates propagated through the correlation terms during the generation of $\mathscr{M}_B$. The rest of the information stored in the maps is represented by $\hat{\mathbf{x}}_A$ and $\hat{\mathbf{x}}_B$. According to the general form described in (6.1), $\hat{\mathbf{x}}_A$ will contain the common term representing the link with a previous map and all the features in $\mathscr{M}_A$, while $\hat{\mathbf{x}}_B$ will contain the features in $\mathscr{M}_B$ and the estimate of the vehicle's state at the end of the map.

The objective of the map joining process is to obtain a single global map containing the information from all the local maps. In this example, the global map is represented by:

$$\mathscr{M}_{AB} = \left(\begin{bmatrix} \hat{\mathbf{x}}'_A \\ \hat{\mathbf{x}}_{Cb} \\ \hat{\mathbf{x}}_B \end{bmatrix}, \begin{bmatrix} \mathbf{P}'_A & \mathbf{P}'_{ACb} & \mathbf{P}'_{AB} \\ \mathbf{P}'_{CbA} & \mathbf{P}_{Cb} & \mathbf{P}_{CbB} \\ \mathbf{P}'_{BA} & \mathbf{P}_{BCb} & \mathbf{P}_B \end{bmatrix} \right)$$

The last two blocks of the global map coincide exactly with $\mathscr{M}_B$ (they are up to date). Therefore, only the terms related to $\mathbf{x}_A$ need to be updated (a tilde is used to denote these terms). This is because the first map has only been updated with its own measurements but does not contain any information obtained during the generation of the second map. In order to transmit the effect of these measurements to the estimates in the $\mathscr{M}_A$ map, a back-propagation procedure is carried out:

$$\begin{aligned} \mathbf{K} &= \mathbf{P}_{ACa}\mathbf{P}_{Ca}^{-1} \\ \mathbf{P}'_{ACb} &= \mathbf{K}\mathbf{P}_{Cb} \\ \mathbf{P}'_A &= \mathbf{P}_A + \mathbf{K}(\mathbf{P}'_{CbA} - \mathbf{P}_{CaA}) \\ \hat{\mathbf{x}}'_A &= \hat{\mathbf{x}}_A + \mathbf{K}(\hat{\mathbf{x}}_{Cb} - \hat{\mathbf{x}}_{Ca}) \end{aligned}$$

Moreover, in order to recover the full covariance matrix of the global map, it is necessary to calculate the correlation term relating the two local maps:

$$\begin{aligned} \mathbf{P}'_{AB} &= \mathbf{P}'_{ACb}\mathbf{P}_{Cb}^{-1}\mathbf{P}_{CbB} \\ &= \mathbf{K}\mathbf{P}_{CbB} \end{aligned}$$

At this point, all the elements in $\mathscr{M}_{AB}$ have been determined. It is important to note that this map joining procedure is applicable to sequences of more than two local maps. After each union, the resulting map still contains the common elements that serve as a link with the adjacent ones, therefore the same procedure can be applied.

Each element from the resulting global map is still represented in the base frame of its respective local maps. Moreover, it is possible that some features could have been observed from different local maps and therefore they are repeated. The final part of this procedure consists of transforming all the features to a common coordinate frame (see the operators described in Appendix C). Data association can be carried out and, after obtaining the correspondences, the global map can be updated to produce a better estimate. In the context of this work, the Joint Compatibility Branch and Bound (JCBB) data association algorithm has been used [90] to obtain the hypothesis relating features from different local maps. Then, an implicit measurement equation representing the equivalence between paired features is used to perform the update [18].

6.6 Experimental Results

This section presents two experiments used to test the proposed SLAM approach. The first corresponds to the same CIRS water tank test previously used in Chapter 5 to test various localization algorithms, while the second is an experiment performed in an abandoned marina environment.

6.6.1 Water Tank

The CIRS water tank is a difficult scenario in which to perform SLAM. The reduced dimensions and the reflectivity of the surfaces make it difficult for the DVL to operate correctly and, as a consequence, the sensor produced a substantial number of erroneous velocity measurements. As mentioned in Section 5.3.7, both bottom and water velocities are integrated in order to improve the estimate of the vehicle's motion. The compass is also sensitive to the presence of nearby structures. Although the vehicle was operated at a distance from the walls (about 1 meter) it is not possible to ensure that the heading measurements are free of perturbations. However, the pessimistic uncertainty model for the vehicle's heading seem to cope with this problem. The operation of the MSIS is not simple, either. The confined space produces noisy measurements and, although the range of the sensor was set to avoid phantom reflections from the boundary walls, there are still some sonar artifacts affecting the data. Also, the tank has a particular geometry with two inclined planes (ramps) at each side. As can be seen in Figure 6.12, those planes appear as wide stripes in the acoustic image. The width of these zones is related with the slant angle of the surfaces. The more slanted the ramps are, the wider the stripes become. Moreover, this increase in the inclination is usually associated to a decrease in the measured intensity, especially when compared with the values produced by a vertical wall. Another characteristic of these ramps is that the position of the stripes will change with the depth of the vehicle, making them an unreliable landmark for a SLAM system. In this test, however, the vehicle moved at a constant depth and the inclination of the ramps produced sufficiently narrow stripes. For these reasons, they have been used as landmarks. It is worth noting that, if necessary, these types of features can be discarded by either selecting a higher threshold value or setting a larger value for the "minimum distance between them" criterion that filters high intensity bins in the sonar data segmentation process (see Section 6.1.2.1).

Figure 6.13 represents the resulting trajectory (red line) and the six line features composing the map (black). Because of the reduced dimensions of the test scenario, it was not necessary to create local maps. The dimensions match those of the real water tank (8 by 16 meters) and, as can be seen, the features corresponding to the ramps are correctly placed at each side of the tank, symmetrically and at equal distance from the center. It is important to note that the line segments are longer than the actual dimensions of the walls. This is mainly because of the sonar reflections that may occur at the corners of the water tank, which extend the high intensity zones beyond the limits of the walls (see the example in Figure 6.12(b)). It was not possible to establish a ground truth for the vehicle's location during the experiment.

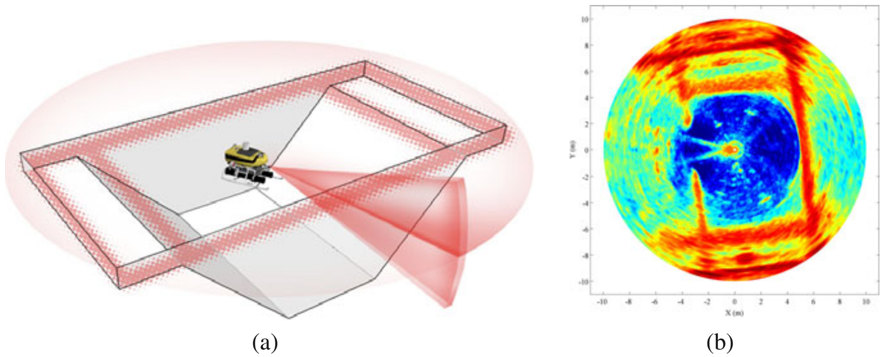

Fig. 6.12 Acquisition of MSIS data in the CIRS water tank. (a) Schematic representation of the scenario. The highlighted zones correspond to the places where high intensity bins are expected. (b) The resulting acoustic image of the tank.

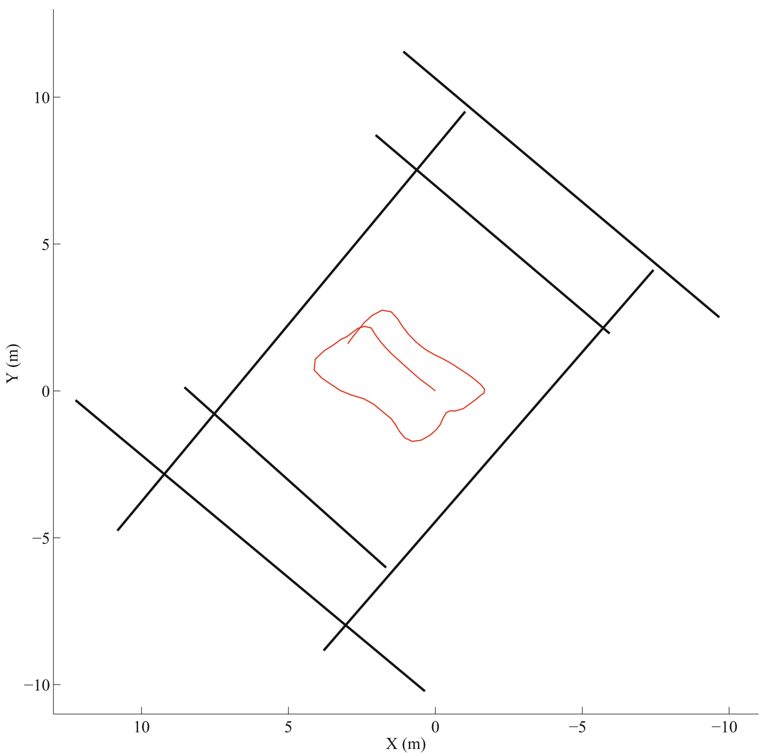

Fig. 6.13 The SLAM trajectory (red) and the resulting map (black) for the CIRS water tank dataset.

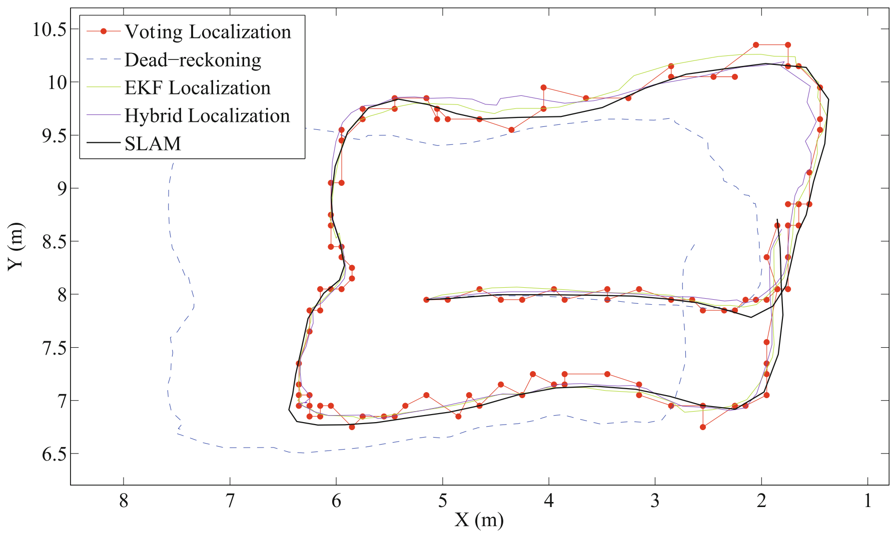

Fig. 6.14 Comparison between the SLAM trajectory and those obtained with the presented localization methods .

However, we can compare the output of the SLAM algorithm with the trajectories estimated with the different localization methods presented in Chapter 5. This is shown in Figure 6.14. As expected, the resulting trajectory is very similar to the reference ones and, again, the approach avoids the drift caused by the use of dead-reckoning sensors.

6.6.2 Marina Environment

In order to test the reliability of the proposed algorithm in a real application scenario, an experiment was carried out in an abandoned marina situated near St. Pere Pescador on the Costa Brava (Spain) [47]. The Ictineu AUV gathered a data set along a 600 m operated trajectory which included a small loop around the larger water area and a 200 m straight path through an outgoing canal (see Figure 6.15). The vehicle moved at about 0.2 m/s and the experiment lasted 50 min. The data set included measurements from the DVL, the compass and the imaging sonar, which was set to a range of 50 m, with a resolution of 0.1 m and 1.8°. For validation purposes, the vehicle was operated close to the surface attached to a GPS equipped buoy used for registering the trajectory. In the test scenario, only the boundary walls contain ferromagnetic elements, while the bottom is natural. The vehicle always moved at a considerable distance from these walls and hence we can assume that there is little distortion affecting the compass. However, this cannot be confirmed since no ground truth is available for the angle measurements. On the other hand, the DVL measurements were much more reliable than those obtained in the water tank. Only 3% of the bottom tracking velocities received a bad status indicator from the sensor.

(a) (b)

Fig. 6.15 Experiment in the abandoned marina. (a) Ortophotomap of the test area. (b) The Ictineu AUV equipped with a surface buoy during the experiment.

Therefore, it was not necessary to rely on water velocities during the execution. The configuration parameters of the SLAM algorithm for this dataset are the same as those used in the water tank test. Only the threshold value for the segmentation of the sonar data has been adapted because the gain setting of the MSIS was different in the two experiments. In the water tank, the gain was too high, which resulted in more saturated images, while during the current experiment it was set to a more suitable value.

Figure 6.16 represents the trajectory obtained during the generation of the different submaps (solid black line), which is a good approximation to the one measured with the GPS (dashed). As mentioned on before, one of the benefits of working with small local maps is that it improves the behavior of line features represented in polar coordinates. For this reason, a distance from the origin of 75 meters was set as the condition to initialize a new local map (the limits are represented by circles in the figure). It is worth noting the sudden position change that appears in the estimated trajectory at approximately [-40, 25]. This correction is a consequence of re-observing, in the second local map and after performing a small loop, the features at the beginning of the long canal. Given the shape and dimensions of the scenario and the range setting of the sonar, the few places where a loop closure could occur are limited to the principal area. The path followed towards the top part of this area is split between the two first local maps. Therefore, the only place where a loop closure could occur is in the lower part of the area, when the features at each side go out of sight. In these loop-closing situations, a discontinuity is introduced in the trajectory stored in the sonar data buffer. It is, however, uncommon for such strong position corrections to affect the feature extraction process. The update that produces this discontinuity generally takes place just after the complete observation of a feature and during the initial moments of the next one. Therefore, the majority of the new bins introduced into the buffer will usually be obtained on the already corrected track. It can also be observed how the discrepancy with the GPS data increases when the vehicle moves through the canal. This is caused mainly by the

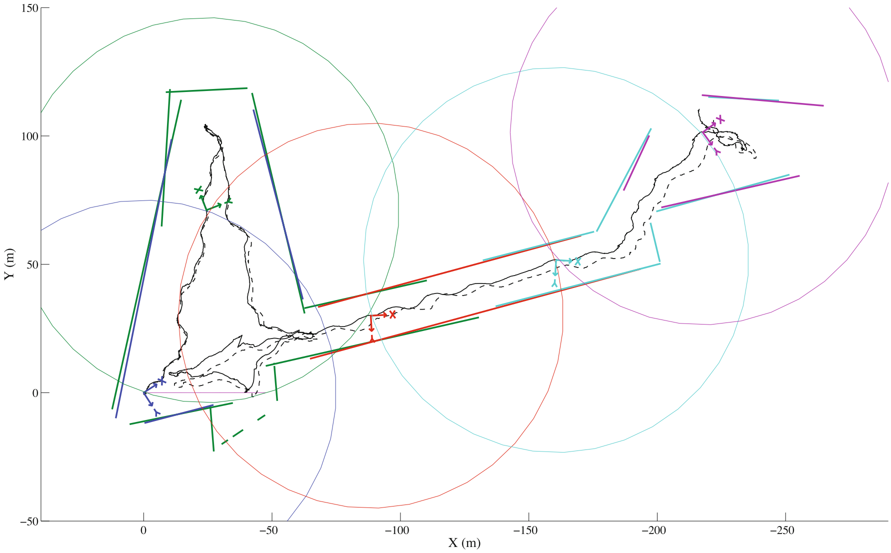

Fig. 6.16 Sequence of local maps. The SLAM trajectory is represented with a solid line and the DGPS with a dashed line. Different colors represent each one of the local maps, their boundaries and base frames.

absence of features situated perpendicular to the direction of the canal axis, which makes it difficult to correct the errors accumulating in this direction.

The global map and the estimated trajectory (solid line) obtained after the joining are plotted in Figure 6.17 layered over a satellite image. For comparison, the GPS trajectory (dashed line) and a dead-reckoning trajectory (dot-dashed line), obtained by executing the filter with only the measurements from the DVL and the compass, are also represented. As can be observed, the dead-reckoning data suffers from an appreciable drift (even causing it to go outside the canal), while the SLAM estimated trajectory follows the GPS track with considerable precision. The resulting map is also a good approximation, matching almost perfectly with the real position of the marina's boundaries. A problem with the position of a feature is observed in the upper-left part of the map. This effect is due to the similarity between the two intersecting lines. The small intersection angle makes it difficult for the feature extraction to discern between the two lines and, eventually, they are interpreted as a single (slightly distorted) one. Of course, this also affects the measurement of the segment endpoints, as it makes it difficult to determine the overlapping with the thresholded data and tends to make longer segments. Some minor problems with the measurement of the segment endpoints are also observed in the small channel entrance in the lower-left part of the map. They mainly appear because of the polar parametrization used in the line features which, in some particular situations, produces a misplacement of the segment endpoints.

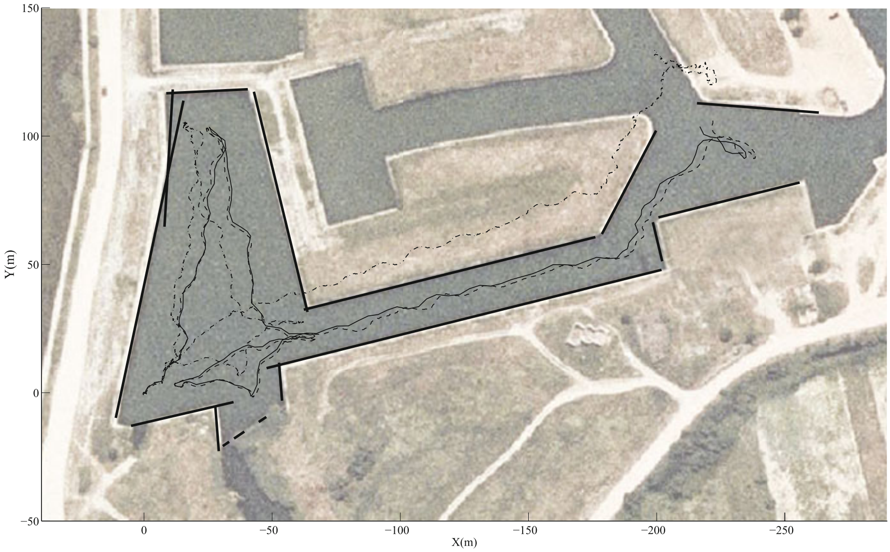

Fig. 6.17 The resulting global map together with the dead-reckoning (dash-dotted line), GPS (dashed line) and SLAM (solid line) trajectories represented over a satellite image of the scenario.

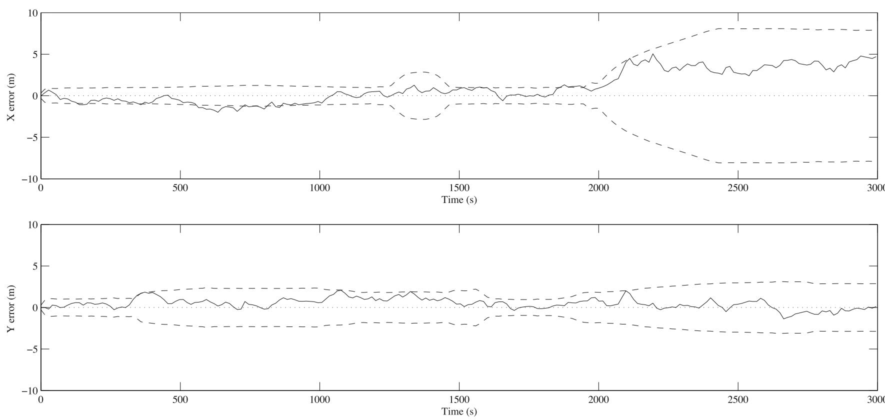

Fig. 6.18 Error plots (2σ bounds) for the resulting estimated trajectory after the local map joining. The DGPS data has been used as ground truth.

Figure 6.18 represents the error plots for the resulting estimated trajectory obtained after producing the local map. The GPS data has been used as the ground truth. As can be seen, the error is contained within the 2σ limits, confirming the correct operation of the SLAM.

Additional results validating the algorithm are shown in Figure 6.19, which reproduces two acoustic images generated by placing the sonar measurements from

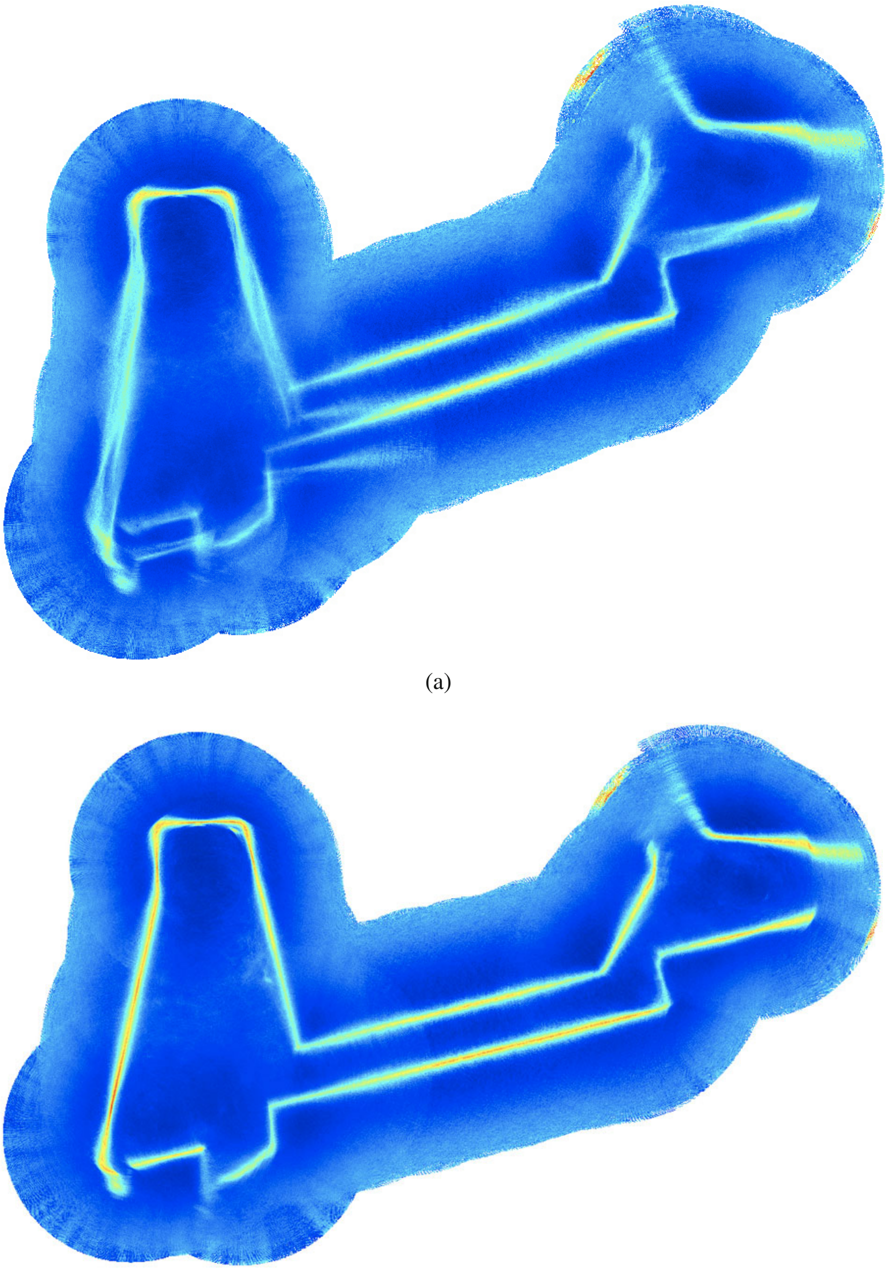

Fig. 6.19 Acoustic maps obtained after an averaged composition of the sonar readings along different trajectories. (a) The filter executed with only the input from the dead-reckoning sensors. (b) SLAM estimated trajectory.

the complete dataset according to the dead-reckoning and the SLAM estimated trajectories. An averaged representation of all the overlapping scans has been used; therefore, one can expect the diffuse appearance shown in the dead-reckoning image as a result of the dispersion induced by the erroneous trajectory. On the other hand, using the SLAM trajectory provides a more accurate placement of the measurements resulting in a sharper image.

Only the acquisition of the sensor data was performed in real time by the computers onboard the Ictineu. This SLAM approach was implemented on Matlab and executed off-line on an ordinary desktop computer. The execution time is shorter than the duration of the real experiment. Therefore, it is not unrealistic to assume that a more optimized implementation should be able to operate onboard.

Chapter 7
Conclusion

This concluding chapter summarizes the thesis by reviewing the contents described in each chapter. The significant research contributions are then listed. The objectives still to be accomplished and interesting future research issues are discussed in the future work section. The research framework for the thesis is then described. Finally, the publications related to this work are listed.

7.1 Summary

One of the most crucial problems that needs to be addressed to obtain truly autonomous vehicles is that of navigation. The SLAM approach represents the ultimate navigation solution since it makes it possible to localize a vehicle and simultaneously map its environment without the need of external devices or previous knowledge of the scenario.

Chapter 2 of the thesis presents the fundamental principles behind the SLAM solution and briefly overviews its research history and recent developments. The chapter focuses on the use of SLAM systems in underwater environments, introducing the various sensorial options based on available acoustic devices, and then reviews the most remarkable work done in the field. This review leads to interesting observations such as the tendency to use vehicles equipped with high cost systems such as electronically scanned devices, or the fact that the majority of works revolve around the possible application of SLAM systems in natural underwater environments. In contrast, the work presented throughout this dissertation is centered on the use of mechanically scanned sonars and the exploration of new application domains such as those found in man-made environments. Chapter 3 presents the Ictineu AUV, the research vehicle developed during the course of this thesis and employed for the experimental work. The structure, the sensor suite and the software architecture are described as well as plans for future upgrades. The introductory part of this document ends with Chapter 4, where the principles of operation of the MSIS in relation to the generation and interpretation of acoustic images are explained. The principal issues related with the use of this type of sensor are described and identified as problems to be addressed by the proposed navigation algorithms.

D. Ribas et al.: Underwater SLAM for Structured Environments, STAR 65, pp. 113–119.
springerlink.com © Springer-Verlag Berlin Heidelberg 2010

The second part of this work presents different approaches for navigating in man-made underwater environments endorsed by many experiments carried out with real sensor data. Chapter 5 describes three localization methods of increasing complexity relying on different sensors and an *a priori map* of the environment. The first is based on the use of an adapted version of the Hough transform to vote for the vehicle's position using the measurements from an MSIS and the heading from a compass. The second introduces a Kalman filter and the use of a DVL sensor to estimate the vehicle's velocities. The measurements from the MSIS are individually contrasted with the map to perform position updates. Finally, the third method combines the other two by setting up a Kalman filter which receives updates from an improved version of the Hough-based voting scheme. The experimental demonstration includes a comparison of the methods with a test performed in the CIRS water tank. An additional example is presented to show the performance of the first approach when used as the navigation system for the Ictineu AUV during the SAUC-E competition. Chapter 6 culminates this work with the proposal of a SLAM system for navigation in structured environments composed of rectilinear walls. This system presents a line feature extraction algorithm capable of dealing with the issues associated with the operation of MSISs. It uses a voting scheme to look for new features and analyzes the imprint left in the acoustic images to determine its uncertainty. The SLAM consists of an EKF-based implementation of the stochastic map. A constant velocity kinematics model predicts the vehicle's motion while the measurements from a DVL, a compass and a pressure sensor update the estimate. The observations from the line feature extraction algorithm are incorporated into the map building process and, as a consequence, the vehicle's position estimate is improved. In addition, the problems associated with dealing with large scenarios have been addressed and solved through the implementation of a local map building procedure. The final part of the chapter proves the capacity of the proposal with two different tests. The first evaluates the performance of the SLAM approach in comparison with the previously proposed localization methods by means of the CIRS water tank experiment. The second experiment is more ambitious and realistic. A long run performed in an abandoned marina serves as a test not only of the SLAM approach but also the local map building method.

7.2 Contributions

This thesis work has accomplished the proposed goal of developing a SLAM approach for an AUV to achieve localization in man-made underwater environments using an MSIS as the principal sensor. In the development of this goal, various research contributions were achieved. These contributions are listed below.

Application domain: Most of the works published on underwater SLAM present systems operating in natural environments and use point features to build the map. To the best of the author's knowledge, the approach presented here is the first work on underwater SLAM focused on operation in man-made structured environments and the use of line features for the representation of underwater scenarios. This contribution opens the door to the use of SLAM systems in new application domains.

Localization with an *a priori* map: Three different methods for localization with an *a priori* map have been developed and tested. Although the use of Kalman filters and voting schemes in localization is not new, the particular treatment given to the MSIS data and its application in man-made underwater environments adds value to the approach and represents a contribution to the field.

Feature extraction from MSIS data: An important contribution of this work is the development of a method to extract features from acoustic underwater images acquired with an MSIS. The method deals with the continuous arrival of measurements, undistorts the data affected by the vehicle's motion and determines the uncertainty of the observed features from the imprint left in the acoustic images. This method makes it possible to use MSIS for SLAM as a lower cost alternative to electronically scanned sonars.

Simultaneous localization and mapping: The number of published SLAM approaches for submersibles operating in underwater environments is still small. For this reason, developing a new algorithm for an unattempted application domain and demonstrating its operation with real sensor data constitutes an important contribution of this thesis.

Dataset acquisition: Producing a dataset is not an easy task when operating with underwater vehicles. The sensors and equipment are expensive and the working conditions are difficult. Moreover, obtaining ground truth data to validate the navigation algorithms is not common. An additional contribution of this thesis is making the abandoned marina dataset publicly available to the research community. The dataset can be downloaded from [107].

7.3 Future Work

During the development of this research work, new problems and topics of interest for future research have arisen. The following points have been identified as the most logical lines for continuing this research.

Development of the localization systems: Although the proposed localization techniques have shown promising results, further work needs to be done to obtain a system reliable enough to be implemented in the real vehicle. The current methods are suitable only for planar environments or those composed only of vertical walls which have a constant section independent of the vehicle's depth. Producing a tridimensional *a priori* map of the scenario would make it possible to define the characteristics of the voting space depending on a particular operational depth estimated through pressure sensor measurements. A second issue to be addressed is to guarantee the safe operation of the vehicle in the absence of reliable sensor measurements particularly while operating very close to walls (strong compass distortions) or near the bottom (DVL is unable to produce velocity measurements). Of course, the integration of better (and more expensive) sensors such as fiber optic gyros can solve most of these problems. However, exploring alternatives based on the introduction of the vehicle's dynamics in the prediction part of the filter would be interesting and inexpensive.

Representation of line features: The line feature extraction algorithm for the proposed SLAM system provides polar observations (ρ and θ parameters) which are referenced to the sensor base frame. The author believes that this representation is the most appropiate given the characteristics of the sensor and the measurement estimation process. However, this is not so true when the features are introduced into the map. Their base reference frame is changed from that of in the sensor to that in which the map is represented. When the reference frame is placed far from the current position of a particular line segment (large ρ value), even the smallest correction in the angle (θ value) may produce large displacements in the segment position and hence an awkward representation of the map. Although this is sufficient while operating in scenarios of reduced dimensions, at the present time and having testing in larger environments in mind, this has become one of the principal weak points of the proposed SLAM approach. Although the use of a smaller local map has shown potential for mitigating this effect, it would be preferable to implement a better method to represent the line features. The plans to improve the SLAM algorithm shortly after the presentation of this work include the implementation of the SP map [18] as a worthwhile candidate for solving this problem.

Extended feature typology: Line features are characteristic of man-made environments. Although the use of lines has been shown to be sufficient for the test scenarios presented, introducing new types of features can offer a better and richer representation of the environment. The proposed feature extraction algorithm can be easily adapted to other types of features as long as a suitable parametrization is possible. One of the simplest options is the detection of corners at the intersection of two walls. The detection of curves or planes are other candidates, although their parametrization requirements would entail the use of higher-dimensional voting spaces. This can even lead to obtaining tridimensional map representations of the explored spaces.

New scenarios: Better and improved algorithms should be tested in new and more challenging scenarios. Operating in real scenarios populated with moored boats, piers, breakwaters and other common elements may offer the possibility of producing new types of features but may also generate new problems. For instance, the presence of traffic in a harbor-like scenario would require more sophisticated data association techniques to discriminate static elements from moving boats.

7.4 Research Framework

The results and conclusions presented in this thesis were made possible after the carrying out of countless tests and experiments, which were the fruit of numerous efforts made in the development of the different research vehicles and the necessary software and equipment. All the work done during the evolution of this thesis is summarized here with references to the most relevant research publications produced by the author. The complete list of publications can be consulted in the next section.

At the beginning of this thesis in the year 2003, there were two research platforms in the Underwater Robotics laboratory at the University of Girona. The first was the URIS AUV [AMI'04], a robot of reduced dimensions designed to operate under laboratory conditions in a small tank. The second was the GARBI AUV, a larger vehicle for operation in real environments which at the time was undergoing an intense remodeling and upgrade process. One of the new systems to be installed in the GARBI was the recently purchased Argonaut DVL sensor. In [WESIC'03], it was presented with preliminary work towards the development of an EKF-based navigation system to integrate the different DVL measurements with the predictions of a dynamic model. In parallel to the long development period of the GARBI, many works were carried out with the URIS vehicle and particularly with a localization system developed for the small experimental tank [IBPRIA'03]. The system comprised a down-looking camera mounted on the robot and a coded pattern placed on the bottom of the tank. The incorporation of an EKF to improve its position estimates was also studied [MCMC'03]. A similar EKF was later implemented on an image mosaicking approach tested with the same URIS vehicle over a staged underwater scenario [IROS'03]. In mid-2004, many datasets were acquired on the Costa Brava, near Colera (Spain), in the context of a new research line on underwater SLAM. Unfortunately, the upgrading of the GARBI had still not been completed at the time. For this reason, different sensors (including a GPS, the DVL and a new sensor, the MSIS) had to be mounted on a metallic structure and attached to a small boat to perform the experiments. The analysis of the resulting datasets and the development of the first SLAM system relying on natural features was completed during a research stay at the University of Zaragoza, under the supervision of Prof. Jose Neira. The result of this work was presented in [MASTER'05]. In 2006, the GARBI was operative and the new installations at the CIRS were completely functional. This same year, a group of students entered the SAUCE 06 competition and, in a short period of time, developed the Ictineu AUV [CCIA'06]. The author acted as team leader and took part in the construction of the new prototype, as well as in the design of different localization approaches for the competition [MCMC'06, ICRA'07], which were later improved with a new proposal [CAMS'07]. Simultaneously, the work on SLAM continued with the development of a system for structured environments which was tested in the CIRS water tank [IROS'06]. The following year, a new approach for feature extraction was developed [IBPRIA'07, IAV'07] and a new dataset was acquired in the abandoned marina scenario using the Ictineu AUV. These results served to demonstrate an improved SLAM approach [IROS'07, MARTECH'07]. Later, the introduction of a strategy for building sequences of local maps improved the final results [JFR'08].

7.5 Related Publications

7.5.0.1 Simultaneous Localization and Mapping

[JFR'08] D. Ribas, P. Ridao, J.D. Tardós and J. Neira. Underwater SLAM in man made structured environments. Journal of Field Robotics, *accepted for publication*, 2008.

[MARTECH'07] D. Ribas, P. Ridao, J. Neira and J.D. Tardós. Underwater SLAM for man-made environments. 2nd Congrés Internacional sobre Tecnologia Marina (Martech'07), Vilanova i la Geltrú, Spain, November 2007.

[IROS'07] D. Ribas, P. Ridao, J.D. Tardós and, J. Neira. Underwater SLAM in a marina environment. IEEE/RSJ International Conference on Intelligent Robots and Systems, San Diego, USA, October 2007.

[IROS'06] D. Ribas, J. Neira, P. Ridao and J.D. Tardós. SLAM using an imaging sonar for partially structured environments. IEEE/RSJ International Conference on Intelligent Robots and Systems, Beijing, China, October 2006.

[MASTER'05] D. Ribas. Towards Simultaneous Localization & Mapping for an AUV using an imaging sonar. Master thesis, University of Girona, Spain, 2005.

7.5.0.2 Feature Extraction from Sonar Images

[IAV'07] D. Ribas, P. Ridao, J. Neira and J.D. Tardós. A method for extracting lines and their uncertainty from acoustic underwater images for SLAM. 6th IFAC Symposium on Intelligent Autonomous Vehicles, Toulouse, France, September 2007.

[IBPRIA'07] D. Ribas, P. Ridao, J. Neira and J.D. Tardós. Line extraction from mechanically scanned imaging sonar. 3rd Iberian Conference on Pattern Recognition and Image Analysis. Lecture Notes in Computer Science, 4477:322–329, 2007.

7.5.0.3 Localization

[CAMS'07] G. García de Marina, D. Ribas and P. Ridao. A global localization system for structured environments using an imaging sonar. IFAC Conference on Control in Marine Systems, Bol, Croatia, September 2007.

[ICRA'07] D. Ribas, N. Palomeras, P. Ridao, M. Carreras and E. Hernàndez. Ictineu AUV wins the first SAUC-E competition. IEEE International Conference on Robotics and Automation, Roma, Italy, April 2007.

[CCIA'06] E. Hernàndez, P. Ridao, M. Carreras, D. Ribas and N. Palomeras. Ictineu AUV, un Robot per a Competir. 9th Congrés Català d'Intel.ligència Artificial, Perpignan, France, October 2006.

[MCMC'06] D. Ribas, J. Neira, P. Ridao and J.D. Tardós. AUV localization in structured underwater environments using an a priori map. 7th IFAC Conference on Manoeuvring and Control of Marine Crafts, Lisboa, Portugal, September 2006.

[IBPRIA'03] M. Carreras, P. Ridao, J. Batlle, and D. Ribas. High-accuracy localization of an underwater robot in a structured environment using computer vision. 2nd Iberian Conference on Pattern Recognition and Image Analysis. Lecture Notes in Computer Science, 2652:150–157, 2003.

[IROS'03] R. García, T. Nicosevici, P. Ridao, and D. Ribas. Towards a real-time vision-based navigation system for a small-class UUV. IEEE/RSJ International Conference on Intelligent Robots and Systems, Las Vegas, USA, October 2003.

[MCMC'03] D. Ribas, P. Ridao, M. Carreras, and X. Cufí. An EKF vision-based navigation of an UUV in a structured environment. 6th IFAC Conference on Manoeuvring and Control of Marine Crafts, Girona, Spain, September 2003.

[WESIC'03] D. Ribas, P. Ridao, X. Cufí, and A. El-fakdi. Towards a DVL-based navigation system for an underwater robot. 4th Workshop on European Scientific and Industrial Collaboration, Miskolc, Hungary, May 2003.

7.5.0.4 Related Work in Underwater Robotics

[IJC'07] M. Carreras, N. Palomeras, P. Ridao, and D. Ribas. Design of a mission control system for an AUV. International Journal of Control, 80(7):993–1007, July 2007.

[OCEANS'04] P. Ridao, E. Batlle, D. Ribas, and M. Carreras. NEPTUNE: A HIL simulator for multiple UUVs. Oceans 04 MTS/IEEE, Kobe, Japan, November 9-12 2004.

[WAF'04] P. Ridao, D. Ribas, E. Batlle, and E. Hernàndez. Simulation of physical agents. An application to underwater robots. V Workshop on Physical Agents, Girona, Spain, March 2004.

[ISCCSP'04] P. Ridao, M. Carreras, D. Ribas, and A. El-Fakdi. Graphical simulators for AUV development. First International Symposium on Control, Communications and Signal Processing, Hammamet, Tunisia, March 2004.

[AMI'04] J. Batlle, P. Ridao, R. García, M. Carreras, X. Cufí, A. El-Fakdi, D. Ribas, T. Nicosevici, E. Batlle, G. Oliver, A. Ortiz and J. Antich. URIS: Underwater Robotic Intelligent System. Automation for the Maritime Industries, chapter 11, pages 177–203. Instituto de Automática Industrial, Consejo Superior de Investigaciones Científicas, first edition, 2004.

Appendix A
The Kalman Filter

The Kalman filter is a recursive data processing algorithm which addresses the problem of estimating the state of a stochastic system. Generally, this state is composed of some system variables of interest whose value is unknown and cannot be directly measured. The Kalman filter makes it possible to determine the value of these parameters by combining knowledge of the system dynamics and its initial conditions, a set of sensor measurements and their relation with system parameters, and a statistical representation of the system noises, measurement errors and model uncertainties.

An important advantage of the Kalman filter is its recursive nature which, unlike other estimation strategies, does not require storing all previous data for reprocessing every time a new sensor measurement is obtained. It performs a sequential processing by calculating, at time k, a new estimate of the state given the previous estimate and a measurement obtained at the same time k.

In addition to this, the Kalman filter is also an optimal Bayesian estimator which minimizes the quadratic error of the state $\mathbf{x}$ defined by the cost function:

$$C(\mathbf{x} - \hat{\mathbf{x}}) = \|\mathbf{x} - \hat{\mathbf{x}}\|^2.$$

The optimality of the filter is possible as long as some basic conditions are met:

- The system and measurement noises are *white*, which means that noise values are not correlated in time and that the system has the same power at all frequencies.
- The noises are *Gaussian*.
- The system dynamics can be described through a *linear* model.

Although these conditions may seem restrictive, they can be accepted as reasonable approximations for many real systems. For instance, white noise is only a theoretical construction which makes the filter mathematics tractable. It cannot physically exist because having power at all frequencies would require a signal with infinite power. However, within the frequency bandpass in which a system can respond, a wideband noise with constant power will look similar to a white one and hence it can be taken as a good approximation. Moreover, applying a small "shaping" filter to a white noise input it is possible to generate time correlated noises and even noises whose power level is not constant over all frequencies.

The second condition refers to the *Gaussianity* of the noises. Generally, the perturbations affecting a system are originated by multiple sources. It can be mathematically demonstrated that the sum of small noise sources, regardless of the shape of their individual densities, can be approximated to a Gaussian probability density [110].

With respect to the third condition, it is not always possible to represent the system at hand by an adequate linear model. In such cases, a linearization of a nonlinear model can be relied on to run the filter. Although suboptimal, this approach, known as Extended Kalman filter, has been proven valid for most situations.

The objective of this appendix is to briefly introduce the equations for the linear and non-linear formulations of the Kalman filter. Mathematical demonstrations and a more detailed description on this topic can be found in [125, 85, 61].

A.1 The Linear Kalman Filter

A.1.1 Linear System Models

The state vector $\mathbf{x}$ to be estimated describes the state of a discrete-time controlled process governed by a linear stochastic difference equation. This equation is generally denominated as the process model:

$$\mathbf{x}(k) = \mathbf{A}\mathbf{x}(k-1) + \mathbf{B}\mathbf{u}(k-1) + \mathbf{n}(k-1),$$

where $\mathbf{A}$ is a matrix that relates the state at $k-1$ to the actual state at time k, $\mathbf{B}$ is a matrix determining the effect that the control input $\mathbf{u}$ produces on the evolution to the actual state and finally, $\mathbf{n}$ is a noise representing the process uncertainty which is assumed independent, white, and with a Gaussian probability distribution of covariance $\mathbf{Q}$:

$$\begin{aligned} E\left[\mathbf{n}(k)\right] &= \mathbf{0}, \\ E\left[\mathbf{n}(k)\mathbf{n}(j)^T\right] &= \delta_{kj}\mathbf{Q}(k), \end{aligned}$$

At discrete intervals, the sensors provide observations of the system's state. This process is described with the measurement model:

$$\mathbf{z}(k) = \mathbf{H}\mathbf{x}(k) + \mathbf{m}(k),$$

where $\mathbf{H}$ is a matrix relating measurement $\mathbf{z}$ to state $\mathbf{x}$ and $\mathbf{m}$ is an independent white Gaussian noise with covariance $\mathbf{R}$ that represents the measurement's uncertainty.

$$\begin{aligned} E\left[\mathbf{m}(k)\right] &= \mathbf{0}, \\ E\left[\mathbf{m}(k)\mathbf{m}(j)^T\right] &= \delta_{kj}\mathbf{R}(k). \end{aligned}$$

The initial state of the system $\mathbf{x}(0)$ will be a random Gaussian variable, independent of the noises $\mathbf{n}$ and $\mathbf{m}$ (for any k), with known mean $\hat{\mathbf{x}}(0)$ and covariance $\mathbf{P}(0)$.

A.1.2 The Discrete Kalman Filter Equations

The objective of the filter is to obtain an estimate of the system's state represented by the mean $\hat{\mathbf{x}}$ and the variance $\mathbf{P}$ of the state distribution. The state is estimated recursively using the knowledge of the process dynamics, the measurement model and a set of measurements.

The estimate of the state $\mathbf{x}$ at time k given all the observations obtained up to time $k-1$ is represented as $\hat{\mathbf{x}}(k|k-1)$. This estimate is equivalent to the conditional mean of the state at time $k-1$ and the sequence of observations $\mathbf{Z}^{k-1}$:

$$\hat{\mathbf{x}}(k|k-1) = E[\mathbf{x}(k)|\mathbf{Z}^{k-1}].$$

Consequently, the propagation of the estimated state covariance matrix is:

$$\mathbf{P}(k|k-1) = E[(\mathbf{x}(k)-\hat{\mathbf{x}}(k|k-1))(\mathbf{x}(k)-\hat{\mathbf{x}}(k|k-1))^T|\mathbf{Z}^{k-1}].$$

The recursive estimation process of the Kalman filter is divided into two parts: the prediction and the correction. The prediction step projects the estimates of the state vector and its error covariances ahead in time by means of the stated process model. The equations responsible for this are:

$$\begin{aligned}\hat{\mathbf{x}}(k|k-1) &= \mathbf{A}\mathbf{x}(k-1)+\mathbf{B}\mathbf{u}(k-1),\\ \mathbf{P}(k|k-1) &= \mathbf{A}\mathbf{P}(k-1)\mathbf{A}^T+\mathbf{Q},\end{aligned}$$

where $[\hat{\mathbf{x}}(k|k-1), \mathbf{P}(k|k-1)]$ is the estimated prediction of the current state $\mathbf{x}$(k) obtained from the estimate at time k, the control input $\mathbf{u}(k-1)$ and the model defined by $\mathbf{A}$ and $\mathbf{B}$. The increment of the estimated uncertainty inherent in a prediction process is reflected with the addition of the term $\mathbf{Q}$ that corresponds to the covariance of the noise in the process model. The next step is to update this estimate by adding the information provided by a sensor measurement $\mathbf{z}(k)$. This is achieved with the measurement update equations of the Kalman filter:

$$\begin{aligned}\hat{\mathbf{x}}(k) &= \hat{\mathbf{x}}(k|k-1)+\mathbf{K}\boldsymbol{\nu},\\ \mathbf{P}(k) &= (\mathbf{I}-\mathbf{K}\mathbf{H})\mathbf{P}(k|k-1),\end{aligned}$$

where

$$\begin{aligned}\boldsymbol{\nu} &= \mathbf{z}(k)-\mathbf{H}\hat{\mathbf{x}}(k|k-1),\\ \mathbf{S} &= \mathbf{H}\mathbf{P}(k|k-1)\mathbf{H}^T+\mathbf{R},\\ \mathbf{K} &= \mathbf{P}(k|k-1)\mathbf{H}^T\mathbf{S}^{-1}.\end{aligned}$$

The term $\boldsymbol{\nu}$ represents the discrepancy between the actual sensor measurement $\mathbf{z}$ and the prediction of this same measurement obtained with the measurement model $\mathbf{H}\hat{\mathbf{x}}$, $\mathbf{S}$ being its corresponding covariance. This is necessary to calculate $\mathbf{K}$, the Kalman gain, which is chosen to correct the estimate and minimize the error covariance $\mathbf{P}$ after the update.

A.2 The Extended Kalman Filter

A.2.1 Non-linear System Models

The extended Kalman filter is a version of the Kalman filter that can deal with systems governed by non-linear stochastic difference equations. In this situation, a non-linear process model is defined as:

$$\mathbf{x}(k) = f(\mathbf{x}(k-1), \mathbf{u}(k-1), \mathbf{n}(k-1)),$$

while a non-linear measurement model is represented as:

$$\mathbf{z}(k) = h(\mathbf{x}(k), \mathbf{m}(k)),$$

$\mathbf{n}$ and $\mathbf{m}$ being analogous to the process and measurement noises defined in the linear version of the filter in Section A.1.1.

A.2.2 The Discrete Extended Kalman Filter Equations

The extended Kalman filter deals with the non-linearities of the system by performing linearizations for the current mean and covariance. The equations for the two-step recursive estimation process are similar to those of the Kalman filter:

$$\begin{aligned}
\hat{\mathbf{x}}(k|k-1) &= f(\hat{\mathbf{x}}(k-1), \mathbf{u}(k-1), 0), \\
\mathbf{P}(k|k-1) &= \mathbf{F}(k)\mathbf{P}(k-1)\mathbf{F}^T(k) + \mathbf{W}(k)\mathbf{Q}\mathbf{W}^T(k).
\end{aligned}$$

The $\mathbf{F}$ and $\mathbf{W}$ Jacobian matrices are responsible for the linearization. They contain the partial derivatives of the f function with respect to the state $\mathbf{x}$ and the process noise $\mathbf{n}$:

$$\begin{aligned}
\mathbf{F}(k) &= \frac{\partial f}{\partial \mathbf{x}}(\hat{\mathbf{x}}(k|k-1), \mathbf{u}(k-1), \mathbf{0}) \\
\mathbf{W}(k) &= \frac{\partial f}{\partial \mathbf{n}}(\hat{\mathbf{x}}(k|k-1), \mathbf{u}(k-1), \mathbf{0})
\end{aligned}$$

The measurement update equations are also adapted to the use of non-linear measurement equations:

$$\begin{aligned}
\hat{\mathbf{x}}(k) &= \hat{\mathbf{x}}(k|k-1) + \mathbf{K}\boldsymbol{\nu}, \\
\mathbf{P}(k) &= (\mathbf{I} - \mathbf{K}\mathbf{H}(k))\mathbf{P}(k|k-1),
\end{aligned}$$

where

$$\begin{aligned}
\boldsymbol{\nu} &= \mathbf{z}(k) - h(\hat{\mathbf{x}}(k|k-1), 0), \\
\mathbf{S} &= \mathbf{H}(k)\mathbf{P}(k|k-1)\mathbf{H}^T(k) + \mathbf{V}(k)\mathbf{R}\mathbf{V}^T(k), \\
\mathbf{K} &= \mathbf{P}(k|k-1)\mathbf{H}^T(k)\mathbf{S}^{-1}.
\end{aligned}$$

Again, the Jacobians $\mathbf{H}$ and $\mathbf{V}$ are necessary to linearize the measurement function h:

$$\begin{aligned}
\mathbf{H}(k) &= \frac{\partial h}{\partial \mathbf{x}}(\hat{\mathbf{x}}(k|k-1), \mathbf{0}), \\
\mathbf{V}(k) &= \frac{\partial h}{\partial \mathbf{m}}(\hat{\mathbf{x}}(k|k-1), \mathbf{0}).
\end{aligned}$$

Appendix B
Correlations in DVL Measurements

To estimate the vehicle's velocity, a DVL measures the projection of this velocity onto the axis of each transducer. Generally, these axes do not form an orthogonal frame and hence a transformation is necessary to represent this velocity in a Cartesian reference (see Figure B.1). As a result of the transformation, a correlation appears between the velocity components of this new representation which should be taken into account when integrating the measurements into a Kalman filter. In [8] the equations behind this transformation are described for a DVL with four transducers (also known as the *Janus configuration*). Here, similar equations will be presented for a DVL equipped with three transducers.

The speed measured by a transducer is the component of the vehicle's velocity that is parallel to the direction of the acoustic signal's propagation. This

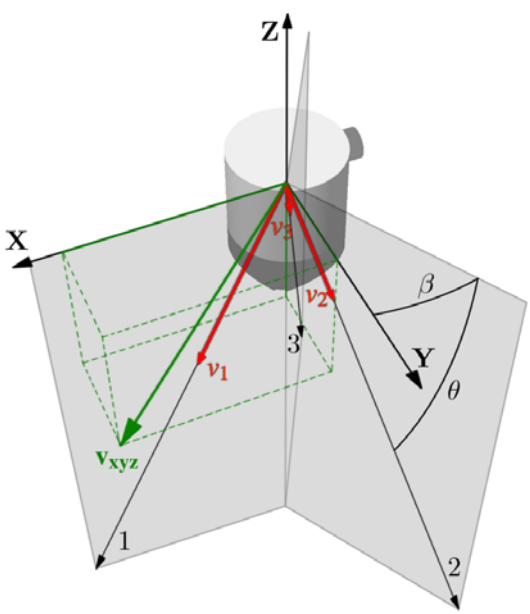

Fig. B.1 Different reference frames on a DVL with three transducers. The XYZ labels mark the Cartesian body frame while the numbered axes correspond to the transducer's beam reference frame.

propagation is described by a unit vector referenced to the sensor body frame and aligned with the transducer axis. The unit vector defines the relation between these two velocities as:

$$v_i = \mathbf{e_i} \cdot \mathbf{v_{xyz}},$$

where v_i is a scalar value representing the velocity measured by the i transducer, $\mathbf{e_i}$ is the unit vector corresponding to the same transducer and $\mathbf{v_{xyz}}$ represents the vehicle's velocity in the sensor body frame:

$$\mathbf{v_{xyz}} = \begin{bmatrix} v_x & v_y & v_z \end{bmatrix}. \tag{B.1}$$

In a three transducer configuration the unit vectors are defined as:

$$\begin{aligned}
\mathbf{e_1} &= \begin{bmatrix} \cos\theta & 0 & -\sin\theta \end{bmatrix} \\
\mathbf{e_2} &= \begin{bmatrix} -\cos\theta\sin\beta & \cos\theta\cos\beta & -\sin\theta \end{bmatrix} \\
\mathbf{e_3} &= \begin{bmatrix} -\cos\theta\sin\beta & -\cos\theta\cos\beta & -\sin\theta \end{bmatrix}.
\end{aligned} \tag{B.2}$$

Then, the velocities measured at each beam can be obtained by substituting the unit vectors in B.2 into equation B.1:

$$\begin{aligned}
\mathbf{v_1} &= v_x\cos\theta - v_z\sin\theta \\
\mathbf{v_2} &= -v_x\cos\theta\sin\beta + v_y\cos\theta\cos\beta - v_z\sin\theta \\
\mathbf{v_3} &= -v_x\cos\theta\sin\beta - v_y\cos\theta\cos\beta - v_z\sin\theta
\end{aligned}$$

Finally, these three equations can be used to determine the three unknown components of the vehicle's velocity:

$$\begin{aligned}
v_x &= \frac{v_1}{\cos\theta} + \frac{v_3 + v_2 + 2v_1\sin\beta}{-2\cos\theta - 2\cos\theta\sin\beta} \\
v_y &= \frac{v_2 - v_3}{2\cos\theta\cos\beta} \\
v_z &= \frac{v_3 + v_2 + 2v_1\sin\beta}{-2\sin\theta - 2\sin\theta\sin\beta}
\end{aligned}$$

The Sontek Argonaut DVL (see Section3.6.2) has 3 transducers spaced at 120° ($\beta =$ 30°) and depressed from the horizontal 65° ($\theta = 65°$). Therefore, these equations can be solved for our particular device:

$$\begin{aligned}
v_x &= 1.58v_1 - 0.79v_2 - 0.79v_3 \\
v_y &= 1.37v_2 - 1.37v_3 \\
v_z &= -0.37v_1 - 0.37v_2 - 0.37v_3
\end{aligned}$$

Since this is a linear operation, it can be written in matrix form:

$$\mathbf{v_{xyz}} = \mathbf{T}_{DVL} \begin{bmatrix} v_1 \\ v_2 \\ v_3 \end{bmatrix}$$

$$\mathbf{T}_{DVL} = \begin{bmatrix} 1.58 & -0.79 & -0.79 \\ 0 & 1.37 & -1.37 \\ -0.37 & -0.37 & -0.37 \end{bmatrix}$$

Given the transformation $\mathbf{T}_{DVL}$ and assuming that the covariances of the velocities measured in the beams are known, the correlations of the velocities represented in the sensor frame can be calculated as:

$$\mathbf{R}_D = \mathbf{T}_{DVL} \begin{bmatrix} \sigma_{v_1}^2 & 0 & 0 \\ 0 & \sigma_{v_2}^2 & 0 \\ 0 & 0 & \sigma_{v_3}^2 \end{bmatrix} \mathbf{T}_{DVL}^T$$

$$\mathbf{R}_D = \begin{bmatrix} 2.49\sigma_{v_1}^2 + 0.62(\sigma_{v_2}^2 + \sigma_{v_3}^2) & 1.08(\sigma_{v_3}^2 - \sigma_{v_2}^2) & 0.29(\sigma_{v_2}^2 + \sigma_{v_3}^2) - 0.58\sigma_{v_1}^2 \\ 1.08(\sigma_{v_3}^2 - \sigma_{v_2}^2) & 1.87(\sigma_{v_2}^2 + \sigma_{v_3}^2) & 0.50(\sigma_{v_3}^2 - \sigma_{v_2}^2) \\ 0.29(\sigma_{v_2}^2 + \sigma_{v_3}^2) - 0.58\sigma_{v_1}^2 & 0.50(\sigma_{v_3}^2 - \sigma_{v_2}^2) & 0.13(\sigma_{v_2}^2 + \sigma_{v_3}^2 - \sigma_{v_1}^2) \end{bmatrix}$$

Appendix C
Transformations in 2D

In [115] two operations were presented representing the most frequently encountered spatial relationships in stochastic mapping applications. These are the inversion and compounding transformations, represented by the operators $\ominus$ and $\oplus$:

$$
\begin{aligned}
\mathbf{x}_C^A &= \mathbf{x}_B^A \oplus \mathbf{x}_C^B, \\
\mathbf{x}_C^A &= \ominus \mathbf{x}_A^C.
\end{aligned}
$$

Here, these operators will be described together with two additional compounding operators for transforming the references of point and line features.

C.1 Inversion

Given a spatial transformation (location of a reference B relative to reference A):

$$
\mathbf{x}_B^A = \begin{bmatrix} x_1 \\ y_1 \\ \phi_1 \end{bmatrix}.
$$

The location of A relative to B can be described by the inversion operation $\ominus$:

$$
\mathbf{x}_A^B = \ominus \mathbf{x}_B^A = \begin{bmatrix} -x_1 \cos\phi_1 - y_1 \sin\phi_1 \\ x_1 \sin\phi_1 - y_1 \cos\phi_1 \\ -\phi_1 \end{bmatrix}.
$$

The Jacobian of the inversion operation is:

$$
\mathbf{J}_\ominus = \begin{bmatrix} -\cos\phi_1 & -\sin\phi_1 & x_1 \sin\phi_1 - y_1 \cos\phi_1 \\ \sin\phi_1 & -\cos\phi_1 & x_1 \cos\phi_1 + y_1 \sin\phi_1 \\ 0 & 0 & -1 \end{bmatrix}.
$$

Therefore, given the estimated mean and covariance of the spatial transformation:

$$E\left[\mathbf{x}_B^A\right] = \hat{\mathbf{x}}_B^A,$$
$$E\left[(\mathbf{x}_B^A - \hat{\mathbf{x}}_B^A)(\mathbf{x}_B^A - \hat{\mathbf{x}}_B^A)^T\right] = \mathbf{P}_B^A.$$

The estimated location of A relative to B can be described as the inversion:

$$\hat{\mathbf{x}}_A^B = \ominus\hat{\mathbf{x}}_B^A,$$

With associated covariance calculated as:

$$\mathbf{P}_A^B \simeq \mathbf{J}_\ominus \mathbf{P}_B^A \mathbf{J}_\ominus^T.$$

C.2 Composition

Given two spatial transformations (reference B relative to reference A and reference C relative to reference B):

$$\mathbf{x}_B^A = \begin{bmatrix} x_1 \\ y_1 \\ \phi_1 \end{bmatrix}, \quad \mathbf{x}_C^B = \begin{bmatrix} x_2 \\ y_2 \\ \phi_2 \end{bmatrix}.$$

The location of C relative to A can be described by the composition operation as:

$$\mathbf{x}_C^A = \mathbf{x}_B^A \oplus \mathbf{x}_C^B = \begin{bmatrix} x_1 + x_2\cos\phi_1 - y_2\sin\phi_1 \\ y_1 + x_2\sin\phi_1 + y_2\cos\phi_1 \\ \phi_1 + \phi_2 \end{bmatrix}.$$

Two Jacobian matrices are necessary to linearize the composition with respect to each one of the two spatial transformations $\mathbf{x}_B^A$ and $\mathbf{x}_C^B$:

$$\mathbf{J}_{1\oplus} = \begin{bmatrix} 1 & 0 & -x_2\sin\phi_1 - y_2\cos\phi_1 \\ 0 & 1 & x_2\cos\phi_1 - y_2\sin\phi_1 \\ 0 & 0 & 1 \end{bmatrix},$$
$$\mathbf{J}_{2\oplus} = \begin{bmatrix} \cos\phi_1 & -\sin\phi_1 & 0 \\ \sin\phi_1 & \cos\phi_1 & 0 \\ 0 & 0 & 1 \end{bmatrix}.$$

So, given the estimated mean and covariance of the spatial transformations $(\hat{\mathbf{x}}_B^A, \mathbf{P}_B^A)$ and $(\hat{\mathbf{x}}_C^B, \mathbf{P}_C^B)$, the estimated location of C relative to A can be described as the composition of:

$$\hat{\mathbf{x}}_C^A = \hat{\mathbf{x}}_B^A \oplus \hat{\mathbf{x}}_C^B.$$

with associated covariance approximated as:

$$\mathbf{P}_C^A \simeq \mathbf{J}_{1\oplus} \mathbf{P}_B^A \mathbf{J}_{1\oplus}^T + \mathbf{J}_{2\oplus} \mathbf{P}_C^B \mathbf{J}_{2\oplus}^T.$$

C.3 Composition of Point Features

Given the location of point feature P relative to reference B:

$$\mathbf{x}_P^B = \begin{bmatrix} x_2 \\ y_2 \end{bmatrix}.$$

In a similar manner as mentioned before, the location of P relative to reference A can be described by the composition operation for a point:

$$\mathbf{x}_P^A = \mathbf{x}_B^A \oplus \mathbf{x}_P^B = \begin{bmatrix} x_1 + x_2 \cos\phi_1 - y_2 \sin\phi_1 \\ y_1 + x_2 \sin\phi_1 + y_2 \cos\phi_1 \end{bmatrix}.$$

The Jacobians of this transformation are:

$$\mathbf{J}_{1\oplus} = \begin{bmatrix} 1 & 0 & -x_2 \sin\phi_1 - y_2 \cos\phi_1 \\ 0 & 1 & x_2 \cos\phi_1 - y_2 \sin\phi_1 \end{bmatrix},$$

$$\mathbf{J}_{2\oplus} = \begin{bmatrix} \cos\phi_1 & -\sin\phi_1 \\ \sin\phi_1 & \cos\phi_1 \end{bmatrix}.$$

Again, given the estimated mean and covariance of the spatial transformation $(\hat{\mathbf{x}}_B^A, \mathbf{P}_B^A)$ and the point $(\hat{\mathbf{x}}_P^B, \mathbf{P}_P^B)$, the estimated location of P relative to A can be described as the composition:

$$\hat{\mathbf{x}}_P^A = \hat{\mathbf{x}}_B^A \oplus \hat{\mathbf{x}}_P^B$$

and its associated covariance as:

$$\mathbf{P}_P^A \simeq \mathbf{J}_{1\oplus} \mathbf{P}_B^A \mathbf{J}_{1\oplus}^T + \mathbf{J}_{2\oplus} \mathbf{P}_P^B \mathbf{J}_{2\oplus}^T$$

C.4 Composition of Line Features

Given the location of line feature L represented in polar coordinates with respect to reference B:

$$\mathbf{x}_L^B = \begin{bmatrix} \rho_2 \\ \theta_2 \end{bmatrix}.$$

In a similar manner, as mentioned before, the location of L in polar coordinates relative to reference A can be described by the composition operation for a line:

$$\mathbf{x}_L^A = \mathbf{x}_B^A \oplus \mathbf{x}_L^B = \begin{bmatrix} x_1 \cos(\phi_1 + \theta_2) + y_1 \sin(\phi_1 + \theta_2) + \rho_2 \\ \phi_1 + \theta_2 \end{bmatrix}.$$

The Jacobians of this transformation are:

$$\mathbf{J}_{1\oplus} = \begin{bmatrix} \cos(\phi_1 + \theta_2) & \sin(\phi_1 + \theta_2) & -x_1 \sin(\phi_1 + \theta_2) + y_1 \cos(\phi_1 + \theta_2) \\ 0 & 0 & 1 \end{bmatrix},$$

$$\mathbf{J}_{2\oplus} = \begin{bmatrix} 1 & -x_1 \sin(\phi_1 + \theta_2) + y_1 \cos(\phi_1 + \theta_2) \\ 0 & 1 \end{bmatrix}.$$

Again, given the estimated mean and covariance of the spatial transformation $(\hat{\mathbf{x}}_B^A, \mathbf{P}_B^A)$ and the line $(\hat{\mathbf{x}}_L^B, \mathbf{P}_L^B)$, the estimated polar parameters of L relative to A can be described as the composition transformation:

$$\hat{\mathbf{x}}_L^A = \hat{\mathbf{x}}_B^A \oplus \hat{\mathbf{x}}_L^B,$$

and its associated covariance as:

$$\mathbf{P}_L^A \simeq \mathbf{J}_{1\oplus} \mathbf{P}_B^A \mathbf{J}_{1\oplus}^T + \mathbf{J}_{2\oplus} \mathbf{P}_L^B \mathbf{J}_{2\oplus}^T.$$

References

1. Arkin, R.C.: Behavior-Based Robotics. The MIT Press, Cambridge (1998)
2. Bailey, T., Durrant-Whyte, H.F.: Simultaneous localization and mapping (SLAM): Part II, state of the art. IEEE Robotics and Automation Magazine 13(3), 108–117 (2006)
3. Bailey, T., Nebot, E.M., Rosenblatt, J.K., Durrant-Whyte, H.F.: Data association for mobile robot navigation: A graph theoretic approach. In: Proceedings of the IEEE International Conference on Robotics and Automation, San Francisco, CA, USA, pp. 2512–2517 (2000)
4. Ballard, D.H.: Generalizing the Hough transform to detect arbitrary shapes. Morgan Kaufmann Publishers Inc., San Francisco (1987)
5. Batlle, J., Nico, T., García, R., Carreras, M.: ROV-aided dam inspection: Practical results. In: Proceedings of the 6th IFAC Conference on Manoeuvring and Control of Marine Crafts, Girona, Spain (2003)
6. Bosse, M., Newman, P., Leonard, J., Soika, M., Feiten, W., Teller, S.: An Atlas framework for scalable mapping. In: Proceedings of the IEEE International Conference on Robotics and Automation, Taipei, Taiwan, pp. 1899–1906 (2003)
7. Bosse, M., Newman, P., Leonard, J.J., Teller, S.: SLAM in large-scale cyclic environments using the Atlas framework. International Journal of Robotics Research 23(12), 1113–1139 (2004)
8. Brokloff, N.A.: Matrix algorithm for doppler sonar navigation. In: Proceedings of the Oceans MTS/IEEE, Brest, France, vol. 3, pp. 378–383 (1994)
9. Burgard, W., Fox, D., Hennig, D., Schmidt, T.: Estimating the absolute position of a mobile robot using position probability grids. In: Proceedings of the 14th National Conference on Artificial Intelligence (1996)
10. Caccia, M., Bruzzone, G., Veruggio, G.: Sonar-based guidance of unmanned underwater vehicles. Advanced Robotics 15(5), 551–573 (2001)
11. Carpenter, R.N.: Concurrent mapping and localization with FLS. In: Workshop on Autonomous Underwater Vehicles, Cambridge, MA, USA, pp. 133–148 (1998)
12. Carreras, M., Batlle, J., Ridao, P.: Hybrid coordination of reinforcement learning-based behaviors for AUV control. In: Proceedings of the IEEE/RSJ International Conference on Intelligent Robots and Systems, Maui, Hawaii, USA (2001)
13. Carreras, M., Palomeras, N., Ridao, P., Ribas, D.: Design of a mission control system for an AUV. International Journal of Control 80(7), 993–1007 (2007)
14. Carreras, M., Ridao, P., Garcia, R., Nicosevici, T.: Vision-based localization of an underwater robot in a structured environment. In: Proceedings of the IEEE International Conference on Robotics and Automation, Taipei, Taiwan (2003)

15. Carreras, M., Yuh, J., Batlle, J., Ridao, P.: A behavior-based scheme using reinforcement learning for autonomous underwater vehicles. IEEE Journal of Oceanic Engineering 30(2), 416–427 (2005)
16. Castellanos, J., Montiel, J., Neira, J., Tardós, J.: The SPmap: a probabilistic framework for simultaneous localization and map building. IEEE Transactions on Robotics and Automation 15(5), 948–953 (1999)
17. Castellanos, J.A., Neira, J., Tardós, J.D.: Limits to the consistency of EKF-based SLAM. In: Proceedings of the 5th IFAC Symposium on Intelligent Autonomous Vehicles, Lisbon, Portugal (2004)
18. Castellanos, J.A., Tardós, J.D.: Mobile Robot Localization and Map Building: A Multisensor Fusion Approach. Kluwer Academic Publishers, Boston (1999)
19. Chatila, R., Laumond, J.P.: Position referencing and consistent world modeling for mobile robots. In: Proceedings of the IEEE International Conference on Robotics and Automation, pp. 138–143 (1985)
20. Choset, H.: Sensor based motion planning: The hierarchical generalized voronoi graph. Ph.D. thesis, California Institute of Technology (1996)
21. Clemente, L., Davison, A.J., Reid, I.D., Neira, J., Tardós, J.D.: Mapping large loops with a single hand-held camera. In: Proceedings of Robotics Science and Systems, Atlanta, GA, USA (2007)
22. Cox, I.J.: Blanche - an experiment in guidance and navigation of an autonomous robot vehicle. IEEE Transactions on Robotics and Automation 7(2), 193–204 (1991)
23. Csorba, M.: Simultaneous localisation and map building. Ph.D. thesis, University of Oxford (1997)
24. Daniel, S., Leannec, F.L., Roux, C., Soliman, B., Maillard, E.P.: Side-scan sonar image matching. IEEE Journal of Oceanic Engineering 23(3), 245–259 (1998)
25. Davison, A.J., Cid, Y.G., Kita, N.: Real-time 3D SLAM with wide-angle vision. In: Proceedings of the 5th IFAC Symposium on Intelligent Autonomous Vehicles, Lisbon, Portugal (2004)
26. Dissanayake, G., Newman, P., Clark, S., Durrant-Whyte, H.F., Csorba, M.: A solution to the simultaneous localization and map building (SLAM) problem. IEEE Transactions on Robotics and Automation 17(3), 229–241 (2001)
27. DSTL: Student Autonomous Underwater Challenge - Europe, SAUC-E (2006), `http://www.dstl.gov.uk/news_events/competitions/sauce/index.php` (accessed July 12, 2007)
28. Duda, R.O., Hart, P.E.: Use of the Hough transformation to detect lines and curves in pictures. Communications of the ACM 15(1), 11–15 (1972)
29. Durrant-Whyte, H.F.: Uncertain geometry in robotics. IEEE Journal of Robotics and Automation 4(1), 23–31 (1988)
30. Durrant-Whyte, H.F., Bailey, T.: Simultaneous localization and mapping (SLAM): Part I, the essential algorithms. IEEE Robotics and Automation Magazine 13(2), 99–108 (2006)
31. Durrant-Whyte, H.F., Rye, D., Nebot, E.: Localisation of automatic guided vehicles. In: Proceedings of the 7th International Symposium on Robotics Research, pp. 613–625 (1995)
32. Elfes, A.: Sonar-based real-world mapping and navigation. IEEE Journal of Robotics and Automation 3(3), 249–265 (1987)
33. Estrada, C., Neira, J., Tardós, J.D.: Hierarchical SLAM: real-time accurate mapping of large environments. IEEE Transactions on Robotics 21(4), 588–596 (2005)
34. Eustice, R., Pizarro, O., Singh, H.: Visually augmented navigation in an unstructured environment using a delayed state history. In: Proceedings of the IEEE International Conference on Robotics and Automation, New Orleans, USA (2004)

35. Eustice, R., Singh, H., Leonard, J., Walter, M., Ballard, R.: Visually navigating the RMS titanic with SLAM information filters. In: Proceedings of Robotics Science and Systems, Cambridge, MA, USA (2005)
36. Fairfield, N., Jonak, D., Kantor, G.A., Wettergreen, D.: Field results of the control, navigation, and mapping systems of a hovering AUV. In: Proceedings of the 15th International Symposium on Unmanned Untethered Submersible Technology, Durham, NH, USA (2007)
37. Fairfield, N., Kantor, G., Wettergreen, D.: Real-time SLAM with octree evidence grids for exploration in underwater tunnels. Journal of Field Robotics 24, 3–21 (2007b)
38. Ferrer, J., Elibol, A., Delaunoy, O., Gracias, N., García, R.: Large-area photo-mosaics using global alignment and navigation data. In: Proceedings of the Oceans MTS/IEEE, Vancouber, Canada (2007)
39. Fischler, M.A., Bolles, R.C.: Random sample consensus: a paradigm for model fitting with applications to image analysis and automated cartography. Communications of the ACM 24(6), 381–395 (1981)
40. Fleischer, S.: Bounded-error vision-based navigation of autonomous underwater vehicles. Ph.D. thesis, Stanford University (2000)
41. Folkesson, J., Jensfelt, P., Christensen, H.: Vision SLAM in the measurement subspace. In: Proceedings of the IEEE International Conference on Robotics and Automation, Barcelona, Spain, pp. 30–35 (2005)
42. Fossen, T.I.: Guidance and Control of Ocean Vehicles. John Wiley & Sons Ltd., Chichester (1994)
43. Fox, D., Burgard, W., Dellaert, F., Thrun, S.: Monte carlo localization: Efficient position estimation for mobile robots. In: Proceedings of the 16th National Conference on Artificial Intelligence (1999)
44. Fox, D., Burgard, W., Thrun, S.: Active markov localization for mobile robots. Robotics and Autonomous Systems 25(3-4), 195–207 (1998)
45. García, R., Nicosevici, T., Ridao, P., Ribas, D.: Towards a real-time vision-based navigation system for a small-class UUV. In: Proceedings of the IEEE/RSJ International Conference on Intelligent Robots and Systems, Las Vegas, USA, vol. 1, pp. 818–823 (2003)
46. García, R., Puig, J., Ridao, P., Cufí, X.: Augmented state Kalman filtering for AUV navigation. In: Proceedings of the IEEE International Conference on Robotics and Automation, Washington DC, USA, pp. 4010–4015 (2002)
47. Google Maps: Abandoned marina, St. Pere Pescador, Spain (2008), `http://maps.google.es/maps?hl=es&ie=UTF8&ll=42.202645,3.10662&spn=0.005182,0.008862&t=h&z=17` (accessed May 3, 2008)
48. Gracias, N.R., van der Zwaan, S., Bernardino, A., Santos-Victor, J.: Mosaic-based navigation for autonomous underwater vehicles. IEEE Journal of Oceanic Engineering 28(4), 609–624 (2003)
49. Griffiths, G., McPhail, S., Rogers, R., Meldrum, D.: Leaving and returning to harbour with an autonomous underwater vehicle. In: Proceedings of the Oceanology International, Brighton, UK (1998)
50. Grimson, W.E.L.: Object Recognition by Computer: The Role of Geometric Constraints. The MIT Press, Cambridge (1990)
51. Grisetti, G., Tipaldi, G.D., Stachniss, C., Burgard, W., Nardi, D.: Fast and accurate slam with rao-blackwellized particle filters. Robotics and Autonomous Systems 55(1), 30–38 (2007)
52. Guivant, J.E., Nebot, E.M.: Optimization of the simultaneous localization and map-building algorithm for real-time implementation. IEEE Transactions on Robotics and Automation 17(3), 242–257 (2001)

53. Gutmann, J.S., Konolige, K.: Incremental mapping of large cyclic environments. In: Proceedings of the International Symposium on Computational Intelligence in Robotics and Automation, pp. 318–325 (1999)
54. Heckman, D.B., Abbot, R.C.: An acoustic navigation technique. In: Proceedings of the Oceans MTS/IEEE, pp. 591–595 (1973)
55. Huang, S., Dissanayake, G.: Convergence and consistency analysis for extended Kalman filter based SLAM. IEEE Transactions on Robotics 23(5), 1036–1049 (2007)
56. Hunt, M., Marquet, W., Moller, D., Peal, K., Smith, W., Spindel, R.: An acoustic navigation system. Tech. Rep. WHOI-74-6, Woods Hole Oceanographic Institution (1974)
57. Ictineu: Ictineu AUV performance during the SAUC-E 06 final run. Video attachment of [109] (2007), `http://ieeexplore.ieee.org/iel5/4209048/4209049/1248.MM.zip` (accessed August 8, 2007)
58. Illingworth, J., Kittler, J.: A survey of the Hough transform. Computer Vision, Graphics, and Image Processing 44(1), 87–116 (1988)
59. Imagenex technology corp.: Sonar theory and applications (2002), `http://www.imagenex.com/sonar_theory.pdf` (accessed September 12, 2007)
60. Iovenittl, L., Venturi, M., Albano, G., Touisi, E.: Submarine pipeline inspection: the 12 years experience of transmed and future developments. In: Proceedings of the 13th International Conference on Offshore Mechanics and Arctic Engineering, Houston, TX, USA, pp. 149–161 (1994)
61. Kalman, R.E.: A new approach to linear filtering and prediction problems. Transactions of the ASME, Journal of Basic Engineering 82(Series D), 35–45 (1960)
62. Kim, J.H., Sukkarieh, S.: Airborne simultaneous localisation and map building. In: Proceedings of the IEEE International Conference on Robotics and Automation, Taipei, Taiwan, pp. 406–411 (2003)
63. Kinsey, J., Eustice, R., Whitcomb, L.: A survey of underwater vehicle navigation: Recent advances and new challenges. In: Proceedings of the 7th IFAC Conference on Manoeuvring and Control of Marine Crafts, Lisbon, Portugal (2006)
64. Knight, J., Davison, A.J., Reid, I.: Towards constant time SLAM using postponement. In: Proceedings of the IEEE/RSJ International Conference on Intelligent Robots and Systems, Maui, Hawaii, USA, pp. 406–412 (2001)
65. Kondo, H., Maki, T., Ura, T., Sakamaki, T.: AUV navigation based on multi-sensor fusion for breakwater observation. In: Proceedings of the 23rd International Symposium on Autonomous Robotics in Construction, Tokyo, Japan, pp. 72–77 (2006)
66. Kuipers, B., Byun, Y.T.: A robot exploration and mapping strategy based on a semantic hierarchy of spatial representations. Journal of Robotics and Autonomous Systems 8, 47–63 (1991)
67. Kuritsky, M.M., Goldstein, M.S.: Inertial navigation. In: Autonomous robot vehicles, pp. 96–116. Springer, New York (1990)
68. Leonard, J.J., Carpenter, R.N., Feder, H.J.S.: Stochastic mapping using forward look sonar. Robotica 19(5), 467–480 (2001)
69. Leonard, J.J., Durrant-Whyte, H.F.: Mobile robot localization by tracking geometric beacons. IEEE Transactions on Robotics and Automation 7(3), 376–382 (1991)
70. Leonard, J.J., Durrant-Whyte, H.F.: Directed Sonar Sensing for Mobile Robot Navigation. Kluwer Academic Publishers, Norwell (1992)
71. Leonard, J.J., Feder, H.: Decoupled stochastic mapping. IEEE Journal of Oceanic Engineering 26(4), 561–571 (2001)

72. Leonard, J.J., Feder, H.J.S.: A computationally efficient method for large-scale concurrent mapping and localization. In: Koditschek, D., Hollerbach, J. (eds.) Proceedings of the 9th International Symposium on Robotics Research, pp. 169–176. Springer, Snowbird (2000)
73. Leonard, J.J., Newman, P.M.: Consistent, convergent and constant-time SLAM. In: Proceedings of the International Joint Conference on Artificial Intelligence, Acapulco, Mexico (2003)
74. Leonard, J.J., Rikoski, R.J.: Incorporation of delayed decision making into stochastic mapping. In: Proceedings of the International Symposium on Experimental Robotics, vol. 271, pp. 533–542 (2000)
75. Leonard, J.J., Rikoski, R.J., Newman, P.M., Bosse, M.C.: Mapping partially observable features from multiple uncertain vantage points. International Journal of Robotics Research 21(10-11), 943–975 (2002)
76. Lim, J.H., Leonard, J.J.: Mobile robot relocation from echolocation constraints. IEEE Transactions on Pattern Analysis and Machine Intelligence 22(9), 1035–1041 (2000)
77. Lu, F., Milios, E.: Globally consistent range scan alignment for environment mapping. Autonomous Robots 4, 333–349 (1997)
78. Lucas, B.D., Kanade, T.: An iterative image registration technique with an application to stereo vision. In: Proceedings of the 7th International Joint Conference on Artificial Intelligence, pp. 674–679 (1981)
79. Lucido, L., Opderbecke, J., Rigaud, V., Deriche, R., Zhang, Z.: A terrain referenced underwater positioning using sonar bathymetric profiles and multiscale analysis. In: Proceedings of the Oceans MTS/IEEE, Fort Lauderdale, FL, USA (1996)
80. Mahalanobis, P.C.: On the generalized distance in statistics. Proceedings of the National Institute of Science of India 12, 49–55 (1936)
81. Maki, T., Kondo, H., Ura, T., Sakamaki, T.: Navigation of an autonomous underwater vehicle for photo mosaicing of shallow vent areas. In: Proceedings of the Oceans Asia Pacific, Singapore (2006)
82. Maki, T., Kondo, H., Ura, T., Sakamaki, T.: Photo mosaicing of Tagiri shallow vent area by the AUV Tri-Dog 1 using SLAM based navigation scheme. In: Proceedings of the Oceans MTS/IEEE, Boston, MA, USA (2006b)
83. Martins, A., Matos, A., Cruz, N., Pereira, F.L.: IES an open system for underwater inspection. In: Proceedings of the Oceans MTS/IEEE, Seattle, USA, vol. 2, pp. 549–554 (1999)
84. May, M.B.: Gravity navigation. In: Record of the 1978 Position Location and Navigation Symposium, San Diego, CA, USA, pp. 212–218 (1978)
85. Maybeck, P.: Stochastic models, estimation and control, vol. 1. Academic Press, London (1982)
86. Milne, P.H.: Underwater Acoustic Positioning System. Gulf Publishing Company, Houston (1983)
87. Montemerlo, M., Thrun, S., Koller, D., Wegbreit, B.: FastSLAM: A factored solution to the simultaneous localization and mapping problem. In: Proceedings of the AAAI National Conference on Artificial Intelligence, Edmonton, Canada (2002)
88. Moravec, H.: Sensor fusion in certainty grids for mobile robots. AI Magazine 9(2), 61–74 (1988)
89. Negahdaripour, S., Xun, X.: Mosaic-based positioning and improved motion-estimation methods for automatic navigation of submersible vehicles. IEEE Journal of Oceanic Engineering 27(1), 79–99 (2002)
90. Neira, J., Tardós, J.D.: Data association in stochastic mapping using the joint compatibility test. IEEE Transactions on Robotics and Automation 17(6), 890–897 (2001)

91. Neira, J., Tardós, J.D., Castellanos, J.A.: Linear time vehicle relocation in SLAM. In: Proceedings of the IEEE International Conference on Robotics and Automation, Taipei, Taiwan, pp. 427–433 (2003)
92. Newman, P., Leonard, J., Tardós, J.D., Neira, J.: Explore and return: Experimental validation of real-time concurrent mapping and localization. In: Proceedings of the IEEE International Conference on Robotics and Automation, pp. 1802–1809. IEEE, Los Alamitos (2002)
93. Newman, P.M.: On the structure and solution of the simultaneous localisation and map building problem. Ph.D. thesis, Australian Centre for Field Robotics. The University of Sydney (1999)
94. Newman, P.M., Leonard, J.J.: Pure range-only sub-sea SLAM. In: Proceedings of the IEEE International Conference on Robotics and Automation, Taipei, Taiwan, vol. 2, pp. 1921–1926 (2003)
95. Newman, P.M., Leonard, J.J., Rikoski, R.J.: Towards constant-time SLAM on an autonomous underwater vehicle using synthetic aperture sonar. In: Proceedings of the 11th International Symposium on Robotics Research, Sienna, Italy (2003)
96. Ni, K., Steedly, D., Dellaert, F.: Tectonic SAM: Exact, out-of-core, submap-based SLAM. In: Proceedings of the IEEE International Conference on Robotics and Automation, Rome, Italy (2007)
97. Nie, J., Yuh, J., Kardash, E., Fossen, T.: On-board sensor-based adaptative control of small UUVs in very shallow water. In: Control Applications in Marina Systems (1998)
98. Olson, E., Leonard, J.J., Teller, S.: Robust range-only beacon localization. In: Autonomous Underwater Vehicles, pp. 66–75 (2004)
99. Paglia, J.G., Wyman, W.F.: DARPA's autonomous minehunting and mapping technologies (AMMT) program: An overview. In: Proceedings of the Oceans MTS/IEEE, Fort Lauderdale, FL, USA, vol. 2, pp. 794–799 (1996)
100. Palomeras, N., Carreras, M., Ridao, P., Hernàndez, E.: Mission control system for dam inspection with an AUV. In: Proceedings of the IEEE/RSJ International Conference on Intelligent Robots and Systems, Beijing, China, pp. 2551–2556 (2006)
101. Pavlidis, T.: Algorithms for graphics and image processing. Computer Science Press (1982)
102. Paz, L.M., Piniés, P., Neira, J., Tardós, J.D.: Global localization in SLAM in bilinear time. In: Proceedings of the IEEE/RSJ International Conference on Intelligent Robots and Systems, Edmonton, Canada, pp. 2820–2826 (2005)
103. Petillot, Y., Reed, S., Bell, J.: Real time AUV pipeline detection and tracking using side scan sonar and multi-beam echo-sounder. In: Proceedings of the Oceans MTS/IEEE, Biloxi, MS, USA, vol. 1, pp. 217–222 (2002)
104. Piniés, P., Tardós, J.: Scalable SLAM building conditionally independent local maps. In: Proceedings of the IEEE/RSJ International Conference on Intelligent Robots and Systems, San Diego, CA, USA, pp. 3466–3471 (2007)
105. Reed, S., Bell, J., Petillot, Y.: Unsupervised segmentation of object shadow and highlight using statistical snakes. In: Proceedings of the Generic Oceanographic Array Technology Systems (GOATS) Conference, La Spezia, Italy (2001)
106. Reed, S., Petillot, Y., Bell, J.: Automated approach to classification of mine-like objects in sidescan sonar using highlight and shadow information. In: Proceedings of the IEE Radar, Sonar and Navigation, vol. 151, pp. 48–56 (2004)
107. Ribas, D.: Dataset obtained in an abandoned marina, St. Pere Pescador (Spain) (2006), `http://eia.udg.es/%7Edribas` (accessed July 12, 2007)
108. Ribas, D., Neira, J., Ridao, P., Tardós, J.D.: SLAM using an imaging sonar for partially structured environments. In: Proceedings of the IEEE/RSJ International Conference on Intelligent Robots and Systems, Beijing, China, pp. 5040–5045 (2006)

109. Ribas, D., Palomer, N., Ridao, P., Carreras, M., Hernàndez, E.: Ictineu AUV wins the first SAUC-E competition. In: Proceedings of the IEEE International Conference on Robotics and Automation, Roma, Italy, pp. 151–156 (2007)
110. Rice, J.: Mathematical Statistics and Data Analysis, 2nd edn. Duxbury Press (1995)
111. Ridao, P., Batlle, E., Ribas, D., Carreras, M.: NEPTUNE: A HIL simulator for multiple UUVs. In: Proceedings of the Oceans MTS/IEEE, Kobe, Japan, vol. 1, pp. 524–531 (2004b)
112. Ridao, P., Tiano, A., El-Fakdi, A., Carreras, M., Zirilli, A.: On the identification of non-linear models of unmanned underwater vehicles. Control Engineering Practice 12(12), 1483–1499 (2004)
113. Rikoski, R.J., Leonard, J.J.: Trajectory sonar perception. In: Proceedings of the IEEE International Conference on Robotics and Automation, Taipei, Taiwan, vol. 1, pp. 963–970 (2003)
114. Roman, C., Singh, H.: Improved vehicle based multibeam bathymetry using sub-maps and SLAM. In: Proceedings of the IEEE/RSJ International Conference on Intelligent Robots and Systems, Edmonton, Canada, pp. 3662–3669 (2005)
115. Smith, R., Self, M., Cheeseman, P.: Estimating uncertain spatial relationships in robotics. In: Autonomous robot vehicles, pp. 167–193. Springer-Verlag New York, Inc., New York (1990)
116. Smith, R.C., Cheeseman, P.: On the representation and estimation of spatial uncertainty. International Journal of Robotics Research 5(4), 56–68 (1986)
117. Tardós, J.D., Neira, J., Newman, P., Leonard, J.: Robust mapping and localization in indoor environments using sonar data. International Journal of Robotics Research 21(4), 311–330 (2002)
118. Tena, I.: Enhanced concurrent mapping and localisation using forward-looking sonar. Ph.D. thesis, Heriot-Watt University (2001)
119. Tena, I., Lane, D., Chantler, M.J.: A comparison of inter-frame feature measures for robust object classification in sector scan sonar image sequences. IEEE Journal of Oceanic Engineering 24(4), 458–469 (1999)
120. Tena, I., Petillot, Y., Lane, D.M.: Improved AUV navigation using side-scan sonar. In: Proceedings of the Oceans MTS/IEEE, San Diego, CA, USA (2003a)
121. Tena, I., Petillot, Y., Lane, D.M., Salson, C.: Feature extraction and data association for AUV concurrent mapping and localisation. In: Proceedings of the IEEE International Conference on Robotics and Automation, Seoul, Korea, pp. 2785–2790 (2001)
122. Tena, I., de Raucourt, S., Petillot, Y., Lane, D.M.: Concurrent mapping and localization using sidescan sonar. IEEE Journal of Oceanic Engineering 29(2), 442–456 (2004)
123. Tena, I., Reed, S., Petillot, Y., Bell, J., Lane, D.M.: Concurrent mapping and localisation using side-scan sonar for autonomous navigation. In: Proceedings of the 13th International Symposium on Unmanned Untethered Submersible Technology, Durham, NH, USA (2003b)
124. Thrun, S.: A probabilistic online mapping algorithm for teams of mobile robots. International Journal of Robotics Research 20(5), 335–363 (2001)
125. Thrun, S., Burgard, W., Fox, D.: Probabilistic Robotics. The MIT Press, Cambridge (2005)
126. Thrun, S., Liu, Y., Koller, D., Ng, A.Y., Ghahramani, Z., Durrant-Whyte, H.F.: Simultaneous localization and mapping with sparse extended information filters. International Journal of Robotics Research 23(7-8), 693–716 (2004)
127. Tyren, C.: Magnetic anomalies as a reference for ground-speed and map-matching navigation. Journal of Navigation 35(2), 242–254 (1982)

128. Urick, R.J.: Principles of underwater sound, 3rd edn. Peninsula Publishing, Los Altos (1983)
129. VICOROB: Team VICOROB homepage (2006), `http://eia.udg.es/sauce` (accessed July 12, 2007)
130. Williams, S., Mahon, I.: Simultaneous localisation and mapping on the great barrier reef. In: Proceedings of the IEEE International Conference on Robotics and Automation, New Orleans, USA, vol. 2, pp. 1771–1776 (2004)
131. Williams, S.B., Dissanayake, G., Durrant-Whyte, H.F.: An efficient approach to the simultaneous localisation and mapping problem. In: Proceedings of the IEEE International Conference on Robotics and Automation, Washington DC, USA, pp. 406–411 (2002)
132. Williams, S.B., Newman, P.M., Rosenblatt, J., Dissanayake, G., Durrant-Whyte, H.: Autonomous underwater navigation and control. Robotica 19(5), 481–496 (2001)

Springer Tracts in Advanced Robotics

Edited by B. Siciliano, O. Khatib and F. Groen

Further volumes of this series can be found on our homepage: springer.com

Vol. 64: Vasquez Govea, A.D.
Incremental Learning for Motion Prediction of Pedestrians and Vehicles
153 p. 2010 [978-3-642-13641-2]

Vol. 63: Vanderborght, B.;
Dynamic Stabilisation of the Biped Lucy Powered by Actuators with Controllable Stiffness
281 p. 2010 [978-3-642-13416-6]

Vol. 62: Howard, A.; Iagnemma, K.; Kelly, A. (Eds.):
Field and Service Robotics
511 p. 2010 [978-3-642-13407-4]

Vol. 61: Mozos, Ó.M.
Semantic Labeling of Places with Mobile Robots
134 p. 2010 [978-3-642-11209-6]

Vol. 60: Zhu, W.-H.
Virtual Decomposition Control – Toward Hyper Degrees of Freedom Robots
443 p. 2010 [978-3-642-10723-8]

Vol. 59: Otake, M.
Electroactive Polymer Gel Robots – Modelling and Control of Artificial Muscles
238 p. 2010 [978-3-540-23955-0]

Vol. 58: Kröger, T.
On-Line Trajectory Generation in Robotic Systems – Basic Concepts for Instantaneous Reactions to Unforeseen (Sensor) Events
230 p. 2010 [978-3-642-05174-6]

Vol. 57: Chirikjian, G.S.; Choset, H.; Morales, M., Murphey, T. (Eds.)
Algorithmic Foundations of Robotics VIII – Selected Contributions of the Eighth International Workshop on the Algorithmic Foundations of Robotics
680 p. 2010 [978-3-642-00311-0]

Vol. 56: Buehler, M.; Iagnemma, K.; Singh S. (Eds.)
The DARPA Urban Challenge – Autonomous Vehicles in City Traffic
625 p. 2009 [978-3-642-03990-4]

Vol. 55: Stachniss, C.
Robotic Mapping and Exploration
196 p. 2009 [978-3-642-01096-5]

Vol. 54: Khatib, O.; Kumar, V.; Pappas, G.J. (Eds.)
Experimental Robotics: The Eleventh International Symposium
579 p. 2009 [978-3-642-00195-6]

Vol. 53: Duindam, V.; Stramigioli, S.
Modeling and Control for Efficient Bipedal Walking Robots
211 p. 2009 [978-3-540-89917-4]

Vol. 52: Nüchter, A.
3D Robotic Mapping
201 p. 2009 [978-3-540-89883-2]

Vol. 51: Song, D.
Sharing a Vision
186 p. 2009 [978-3-540-88064-6]

Vol. 50: Alterovitz, R.; Goldberg, K.
Motion Planning in Medicine: Optimization and Simulation Algorithms for Image-Guided Procedures
153 p. 2008 [978-3-540-69257-7]

Vol. 49: Ott, C.
Cartesian Impedance Control of Redundant and Flexible-Joint Robots
190 p. 2008 [978-3-540-69253-9]

Vol. 48: Wolter, D.
Spatial Representation and Reasoning for Robot Mapping
185 p. 2008 [978-3-540-69011-5]

Vol. 47: Akella, S.; Amato, N.; Huang, W.; Mishra, B.; (Eds.)
Algorithmic Foundation of Robotics VII
524 p. 2008 [978-3-540-68404-6]

Vol. 46: Bessière, P.; Laugier, C.; Siegwart R. (Eds.)
Probabilistic Reasoning and Decision Making in Sensory-Motor Systems
375 p. 2008 [978-3-540-79006-8]

Vol. 45: Bicchi, A.; Buss, M.;
Ernst, M.O.; Peer A. (Eds.)
The Sense of Touch and Its Rendering
281 p. 2008 [978-3-540-79034-1]

Vol. 44: Bruyninckx, H.; Přeučil, L.;
Kulich, M. (Eds.)
European Robotics Symposium 2008
356 p. 2008 [978-3-540-78315-2]

Vol. 43: Lamon, P.
3D-Position Tracking and Control
for All-Terrain Robots
105 p. 2008 [978-3-540-78286-5]

Vol. 42: Laugier, C.; Siegwart, R. (Eds.)
Field and Service Robotics
597 p. 2008 [978-3-540-75403-9]

Vol. 41: Milford, M.J.
Robot Navigation from Nature
194 p. 2008 [978-3-540-77519-5]

Vol. 40: Birglen, L.; Laliberté, T.; Gosselin, C.
Underactuated Robotic Hands
241 p. 2008 [978-3-540-77458-7]

Vol. 39: Khatib, O.; Kumar, V.; Rus, D. (Eds.)
Experimental Robotics
563 p. 2008 [978-3-540-77456-3]

Vol. 38: Jefferies, M.E.; Yeap, W.-K. (Eds.)
Robotics and Cognitive Approaches to
Spatial Mapping
328 p. 2008 [978-3-540-75386-5]

Vol. 37: Ollero, A.; Maza, I. (Eds.)
Multiple Heterogeneous Unmanned Aerial
Vehicles
233 p. 2007 [978-3-540-73957-9]

Vol. 36: Buehler, M.; Iagnemma, K.;
Singh, S. (Eds.)
The 2005 DARPA Grand Challenge – The Great
Robot Race
520 p. 2007 [978-3-540-73428-4]

Vol. 35: Laugier, C.; Chatila, R. (Eds.)
Autonomous Navigation in Dynamic
Environments
169 p. 2007 [978-3-540-73421-5]

Vol. 34: Wisse, M.; van der Linde, R.Q.
Delft Pneumatic Bipeds
136 p. 2007 [978-3-540-72807-8]

Vol. 33: Kong, X.; Gosselin, C.
Type Synthesis of Parallel
Mechanisms
272 p. 2007 [978-3-540-71989-2]

Vol. 30: Brugali, D. (Ed.)
Software Engineering for Experimental Robotics
490 p. 2007 [978-3-540-68949-2]

Vol. 29: Secchi, C.; Stramigioli, S.; Fantuzzi, C.
Control of Interactive Robotic Interfaces – A
Port-Hamiltonian Approach
225 p. 2007 [978-3-540-49712-7]

Vol. 28: Thrun, S.; Brooks, R.;
Durrant-Whyte, H. (Eds.)
Robotics Research – Results of the 12th
International Symposium ISRR
602 p. 2007 [978-3-540-48110-2]

Vol. 27: Montemerlo, M.; Thrun, S.
FastSLAM – A Scalable Method for the
Simultaneous Localization and Mapping
Problem in Robotics
120 p. 2007 [978-3-540-46399-3]

Vol. 26: Taylor, G.; Kleeman, L.
Visual Perception and Robotic Manipulation – 3D
Object Recognition, Tracking and Hand-Eye
Coordination
218 p. 2007 [978-3-540-33454-5]

Vol. 25: Corke, P.; Sukkarieh, S. (Eds.)
Field and Service Robotics – Results of the 5th
International Conference
580 p. 2006 [978-3-540-33452-1]

Vol. 24: Yuta, S.; Asama, H.; Thrun, S.;
Prassler, E.; Tsubouchi, T. (Eds.)
Field and Service Robotics – Recent Advances in
Research and Applications
550 p. 2006 [978-3-540-32801-8]

Vol. 23: Andrade-Cetto, J,; Sanfeliu, A.
Environment Learning for Indoor Mobile Robots
– A Stochastic State Estimation Approach
to Simultaneous Localization and Map Building
130 p. 2006 [978-3-540-32795-0]

Vol. 22: Christensen, H.I. (Ed.)
European Robotics Symposium 2006
209 p. 2006 [978-3-540-32688-5]

Vol. 21: Ang Jr., H.; Khatib, O. (Eds.)
Experimental Robotics IX – The 9th International
Symposium on Experimental Robotics
618 p. 2006 [978-3-540-28816-9]

Vol. 20: Xu, Y.; Ou, Y.
Control of Single Wheel Robots
188 p. 2005 [978-3-540-28184-9]

Vol. 19: Lefebvre, T.; Bruyninckx, H.;
De Schutter, J. Nonlinear Kalman Filtering
for Force-Controlled Robot Tasks
280 p. 2005 [978-3-540-28023-1]